CRYSTAL FIELD APPLICATIONS TO BIOCHEMICAL AND GEOCHEMICAL SYSTEMS: ELECTRONIC STRUCTURES OF BLUE COPPER PROTEINS AND IRON GROUP OLIVINES

Thesis by

Jeffrey W. Hare

In Partial Fulfillment of the Requirements

for the Degree of

Doctor of Philosophy

California Institute of Technology

Pasadena, California

1976

(Submitted December 10, 1975)

PREFACE

The existence of this thesis is due, primarily, to six people. My father stressed the importance of education from an early age and made it his goal to have both sons graduate from college. I regret he didn't live to see it fulfilled. I appreciate all the sacrifices my mother made so that goal could be achieved. My wife typed the text, but her love and encouragement through difficult times are a far more integral part.

I am indebted to George Rossman for rekindling my scientific interest and generously providing instruction in experimental techniques and research instruments from which a majority of the data reported within was derived; all in his cheerful, friendly manner.

I thank Edward Solomon for his friendship, for instilling in me a certain amount of self-confidence, for the long discussions concerning goals and assignments of this work, and for forcing me into a research area I had successfully avoided for five years.

Finally, I am grateful to Harry Gray for having patiently waited, far longer than he need have, for me to scientifically mature.

ABSTRACT OF THESIS

Part I, Chapter I

A helical secondary structure has been found to be associated with the metal site in bean plastocyanin. It is likely that such structure is also present in other blue copper proteins. This short section of helix is distorted by metal (copper or cobalt) incorporation, which is probably the result of coordination to an amide nitrogen or oxygen of the peptide backbone. The perturbed helical structure at the site remains conformationally rigid upon reduction of holoplastocyanin to the copper(I) derivative. Finally, a combination of known physical data leads to a picture of the metal site where copper(II) is bound by histidine-37, an amide nitrogen or oxygen or one or more of the following residues which make up the helix, and by cysteine-84 and histidine-87 which provide the final coordinating positions.

Part I, Chapter II

New low energy electronic transitions at ~10000 and 5000 cm^{-1} have been identified as ligand field bands of the blue site of the single copper proteins stellacyanin, plastocyanin and azurin from low temperature absorption as well as CD and MCD studies in the near-infrared. The well known visible series of

absorption bands are assigned as charge transfer transitions of π and σ character from sulfur to copper and of π character from deprotonated amide nitrogen to copper, based on comparison of visible absorption and CD intensities. Ligand field calculations have shown that the observed d-d excitation energies are consistent with a tetrahedral model distorted approximately 4 to 8° towards a square plane. A model of the blue site, which incorporates recent physical evidence for specific ligands, is presented. The reduction potentials have been shown to be influenced, but not dominated, by ligand field effects.

Part II

The absorption bands of iron, cobalt and nickel olivines have been separated with respect to metal site on the basis of previous assignments, the absorption spectra of synthetic and natural triphylites, and the polarized spectra of magnesium-nickel and magnesium-cobalt olivines. An effective C_{2v} site symmetry has been shown to adequately describe the band splittings, but it fails to completely describe the observed polarization properties particularly for Co(II). Ligand field calculations have resulted in values of B, Dq and the low symmetry radial parameters for both the M_1 and M_2 sites. Calculation of LFSE's and the ligand field

contribution to the distribution coefficients of the cation exchange reactions from these parameters and comparison to K_D's calculated from x-ray diffraction data has led to the conclusion that ligand field stabilization is the major driving force for cation ordering in olivine.

TABLE OF CONTENTS

I. SPECTRAL STUDIES OF THE BLUE SITE IN COPPER PROTEINS

CHAPTER 1

INFRARED SPECTRAL STUDIES OF METAL BINDING EFFECTS ON THE SECONDARY STRUCTURE OF BEAN PLASTOCYANIN

INTRODUCTION

The single metal binding blue copper proteins have been the object of several recent investigations concerning possible coordinating ligands and structure of the metal site. X-ray photoelectron spectra (XPS) have shown that copper is bound to sulfur[1], and resonance enhancement of Raman amide vibrations has suggested that copper is also bound to an amide nitrogen or oxygen[2]. This infrared study of French bean (Phaseolus vulgaris) plastocyanin was undertaken with the goal of learning more about the environment of the metal and the interactions between the metal and surrounding protein. Plastocyanin was chosen because its low molecular weight (10,000)[3] presented the best opportunity for observing metal site related vibrations.

The predominant features of biopolymer vibrational spectra have been assigned to motions of the basic structural unit, the amide linkage C_α-CONH-C'_α. The vibrational motions, based on the normal modes of N-methylacetamide have been designated as follows[4]: Amide A (ν_{NH}), Amide B ($2x\delta_{NH}$ in Fermi resonance with ν_{NH}), Amide I (ν_{CO}), Amide II ($\delta_{NH} + \nu_{CN}$), Amide III ($\nu_{CN} + \delta_{NH} + \nu_{CC_\alpha}$), Amide IV ($\delta_{OCN} + \nu_{CC_\alpha}$), Amide V ($\rho_{NH}$), Amide VI ($\rho_{CO}$), and Amide VII ($\tau$) ($\nu$ represents a stretching motion, δ in-plane bending, ρ out-of-plane

bending and τ the torsional motion of the CONH plane). The correlation of polymeric amino acid secondary structure to energies of the infrared active components of the Amide I-III motions has been extensively studied since the pioneering work of Elliott and Ambrose[5,6]. Following improvement in far-infrared spectrometers and techniques, the low energy backbone motions, including Amide IV-VI, were also shown to depend on secondary conformation[7-15]. A summary of infrared energies of helical polypeptides is given in Table I. Table II contains β sheet and random coil correlations. In recent years interest has shifted to the Raman vibrational spectra of polypeptides in both aqueous solution and the solid state[16-23]. Raman energies are listed in Table III for the major conformations and the polyglycine II helix.

Ambrose and Elliott extended their empirical correlation of Amide I frequency with secondary structure to fibrous proteins such as silk fibroin, keratins and collagen[24]. More complete infrared investigations on fibrous proteins and other proteins existing predominantly in one conformation have shown that the polypeptide correlations can be used to determine secondary structure in proteins[25,26]. However, extension of these observations to globular proteins has been difficult.

TABLE I

Infrared Frequencies for Amide I-VI Modes of Helical Polypeptides

Polypeptide	AmideI	AmideII	AmideIII	AmideIV	AmideV	AmideVI	Ref.
$(L\text{-Ala})_n$ α	1658	1548	1262,1330	528	610	658,686	16
$(L\text{-Leu})_n$ α	1656	1545	1260,1298	539	615	658,697	18
$(L\text{-norLeu})_n$ α	1654	1548	1242,1295	542	615	657,698	8
$(L\text{-norVal})_n$ α	1659	1549	1255,1290	522,540	616	658,699	8
$(\alpha\text{-aminobutyric acid})_n\alpha$	1656	1545	1276,1296	517,540	615	654,693	8
$(\gamma\text{-benzyl-L-Glu})_n$ α	1653	1550			615		13
$(\gamma\text{-isoamyl-L-Glu})_n$ α	1656	1550			615		13
$(\gamma\text{-ethyl-L-Glu})_n$ α	1658	1550			620		13
$(\gamma\text{-methyl-L-Glu})_n$ α	1658	1550			620		13
$(L\text{-Val-L-Ala-L-Ala})_n$ α				524,541	616	661	10
$(L\text{-Val-L-Ala})_n$ α				523,541		653	10
$(L\text{-Val-L-Val-L-Ala})_n$ α					610	660	10
$(L\text{-Ala-L-Gly})_n$ α				527			10
$(L\text{-Leu-L-Leu-L-Ala})_n$ α				527	609		10
$(L\text{-Leu-L-Ala})_n$ α				524			10
$(L\text{-Phe-L-Ala})_n$ α				525	622	668	10
$(L\text{-Phe-L-Ala-L-Ala})_n$ α				526	625		10
$(\beta\text{-benzyl-L-Asp})_n$L.H. α[a]	1662	1557			662,614		14
$(L\text{-Lys})_n$ α	1650,1652	1535,1516					50
$(Gly)_n$ PG II[b]	1644	1554	1249,1283	698	740	573	19

TABLE I Continued

Polypeptide	AmideI	AmideII	AmideIII	AmideIV	AmideV	AmideVI	Ref.
$(L\text{-Ala-Gly-Gly})_n$ PG II				672		559	10
$(Gly\text{-L-Pro-Gly})_n$ PLP II[c]				680		559	10
$(L\text{-Ala-L-Pro-Gly})_n$ PLP II				661		565	10
$(L\text{-Pro})_n$ PLP II	1650		1250	670		530	51
$(\gamma\text{-benzyl-L-Asp})_n$[d]	1675	1536			666,662		14
$(\gamma\text{-benzyl-DL-Glu})_n$[e]	1676	1532					15

[a] Left-handed α-helix

[b] polyglycine trigonal helix

[c] polyproline trigonal helix

[d] 4_{13} helix

[e] 4.4_{13} helix

TABLE II

Infrared Frequencies for Amide I-VI Modes of Sheet and Random Coil Polypeptides

Polypeptide	AmideI	AmideII	AmideIII	AmideIV	AmideV	AmideVI	Ref.
$(Gly)_n$ β	1636,1685	1517	1236,1214	589	708	628	19
$(L\text{-}Ala)_n$ β	1634,1695	1548	1224,1241	528	703	613,622	21
$(L\text{-}Val)_n$ β	1632,1699	1529			705	638	18
$(L\text{-}norVal)_n$ β	1629,1698	1526			704	640,605	8
$(L\text{-}norLeu)_n$ β	1629,1699	1529			705	638,616	8
$(L\text{-}Lys)_n$ β	1636,1685	1530					50
$(L\text{-}Ser)_n$ β	1621,1695	1537,1512	1235				18
$(\gamma\text{-methyl-}L\text{-}Glu)_n$ β	1629	1531			700		13
$(\gamma\text{-benzyl-}L\text{-}Glu)_n$ β	1629	1524					13
$(Na\ L\text{-}Glu)_n$ r.c.[a]	1655				650		13
$(L\text{-}Lys)_n$ r.c.	1656	1535					50
$(L\text{-}Ala\text{-}L\text{-}Ala\text{-}Gly)_n$ β					613		9
$(L\text{-}Ala\text{-}Gly)_n$ β				564	618		9
$(L\text{-}Ala\text{-}Gly\text{-}Gly)_n$ β				553	617		9
$(L\text{-}Val\text{-}L\text{-}Ala\text{-}L\text{-}Ala)_n$ β					637,617		9
$(L\text{-}Val\text{-}L\text{-}Ala)_n$ β					652,612		9

[a] random coil

TABLE III

Raman Frequencies for Amide I-VI Modes of Polypeptides

Polypeptide	AmideI	AmideII	AmideIII	AmideIV	AmideV	AmideVI	Ref.
$(L\text{-Ala})_n$ α	1654	1549	1265,1275 1283	662	756	610	16
$(\gamma\text{-benzyl-L-Glu})_n$ α	1652		1294	650	758		18
$(\gamma\text{-methyl-L-Glu})_n$ α	1656	1520,1570	1300,1250	635	695	595	52
$(L\text{-Leu})_n$ α	1652	1547	1261				18
$(L\text{-Lys})_n$ α	1647,1639	1537,1517					50
$(Gly)_n$ PG II[a]	1654		1244,1283	673	747,752	566	19
$(Gly)_n$ β	1674	1564,1515	1234		708	601	19
$(L\text{-Val})_n$ β	1671	1557	1229,1289				18
$(L\text{-Ala})_n$ β	1669	1552	1231				21
$(L\text{-Ser})_n$ β	1668	1531	1235				18
$(L\text{-Lys})_n$ β	1672	1535,1511					50
$(L\text{-Lys})_n$ r.c.[b]	1683,1665 1653	1565,1547 1521	1248				50
$(DL\text{-Ala})_n$ r.c.	1674		1247				22
$(DL\text{-Leu})_n$ r.c.	1658		1261				22
$(L\text{-Glu})_n$ r.c.	1656		1246				20
$(L\text{-ornithine})_n$ r.c.	1649		1245				20

[a] polyglycine II helix

[b] random coil

Since these proteins contain short lengths of different conformations, the amide absorptions observed are generally broadened over most of the frequency ranges found in homo- and copolypeptides. Only the Amide III mode in the Raman spectra of globular proteins has shown sufficient resolution to allow structure-frequency correlations[27-32].

In the energy region below 400 cm^{-1} in homo- and copolypeptide spectra, Itoh and coworkers have assigned IR bands attributable to α-helix and β-sheet structures at 376-369 and 265-235 cm^{-1}, respectively[8-11]. Since these vibrations are admixtures of backbone angle deformations and the amide bond torsion, allowed by specific coupling in an α-helix or β-sheet, they are found at much lower frequencies in monomeric amino acids and random coil structures[19,33]. Thus they represent unique frequencies for determining secondary structure in proteins. Previous infrared spectral studies on sperm whale myoglobin and collagen have demonstrated that conformationally dependent vibrations exist in proteins in this energy region[34]. A band observed at 376 cm^{-1} was assigned as the deformation of α-helix, which makes up almost 80% of the myoglobin structure, and an absorption at 345 cm^{-1} was attributed to a deformation of the collagen triple helix. Unfortunately, structure in this energy region in the Raman spectra of globular

proteins is generally obscured by backbone fluorescence and the broad Rayleigh scattering associated with large molecules.

EXPERIMENTAL SECTION

Solutions of holo-, reduced, apo- and cobalt(II)-substituted plastocyanin were prepared as previously described[35]. The buffer was removed from the solutions by anaerobic dialysis at 4° against triply-distilled water which had been treated with Chelex resin to remove any trace metal ions. The solutions were then lyophilized by quick freezing in liquid nitrogen and evacuating to 10^{-6} torr. Plastocyanin was heat denatured by dissolving lyophilized protein in triply-distilled water, millipore-filtering to remove any undissolved protein and heating at 75° over a steam bath for one hour. This sample was also quick frozen in liquid nitrogen and lyophilized. Acid denaturation was accomplished by dissolving 5 mg of plastocyanin in 1.5 ml of deoxygenated, triply-distilled water. The solution was transferred to a specially-designed pH cell, which was flushed with argon, and then concentrated hydrochloric acid was added until pH 2 was reached. After 30 minutes of stirring under argon at pH 2 in an ice bath, the solution was frozen and dried.

Samples for infrared spectral measurements were

prepared by lightly grinding approximately 2.5 mg of lyophilized protein with the minimum amount of Vaseline needed to form a mull. The mull was spread on a freshly-pressed cesium iodide pellet and covered with a second pellet. The sample was cooled to 77 or 12 K in a Cryogenics Technology, Inc. Model 20 Cryocooler equipped with cesium iodide windows and an adjustable temperature controller. Halocarbon grease mulls for the hydrocarbon IR regions were prepared in the same manner and spread between potassium bromide disks. All operations were performed in an argon- or nitrogen-filled glove bag to prevent protein oxidation and to minimize water and carbon dioxide absorption by the pellet material.

A thin film of plastocyanin was prepared by slow evaporation of a drop of concentrated, unbuffered protein solution on a silver bromide disk in a controlled-humidity dessicator at 4°. After the film had formed, a silicone rubber gasket and a second silver bromide disk were placed over it. This "sandwich" was then placed in the Cryocooler for comparative spectral measurements.

Cesium iodide pellets, containing approximately 1 mg of the various buffers and reducing agents employed, were prepared to test for interference from possible contaminants in critical energy regions.

Infrared spectra were measured using a Perkin-Elmer 180 grating spectrophotometer equipped with the far infrared option. A manual slit mode, set for 2-4 cm^{-1} resolution above 500 cm^{-1} and 4-6.5 cm^{-1} resolution below 500 cm^{-1}, was routinely used.

A 0.096 mM solution of bean plastocyanin in 0.05 M acetate buffer at pH 6 was millipore-filtered and placed in a 1 mm path length quartz cell. The circular dichroism (CD) spectrum of this solution was measured from 300 to 210 nm using a Cary 61 spectropolarimeter at a resolution of 1 nm and sensitivity of 0.1 degrees full scale.

RESULTS

The Vaseline mull infrared spectra (4000-200 cm^{-1}) of holo- (A), reduced (B), cobalt(II)-substituted (C), apo- (D), heat-denatured (E) and acid-denatured (F) bean plastocyanins, as well as thin film (G) and halocarbon mull (H) spectra of the holo protein are presented in Figures 1 and 2. The broad, intense peak at 3350 cm^{-1} and weaker absorption at 3050 cm^{-1} are assigned as the Amide A and Amide B modes, respectively. No significant changes in these bands are observed throughout the series of modified plastocyanins. The CH stretching region, masked in most spectra by Vaseline absorption, shows considerable structure in the halo-

FIGURE 1

Vaseline mull infrared spectra of holo (A), reduced (B), cobalt(II)-substituted (C), and apo (D) plastocyanins. Peaks marked # are due to the mulling agent and peaks marked ‡ are attributable to traces of buffer.

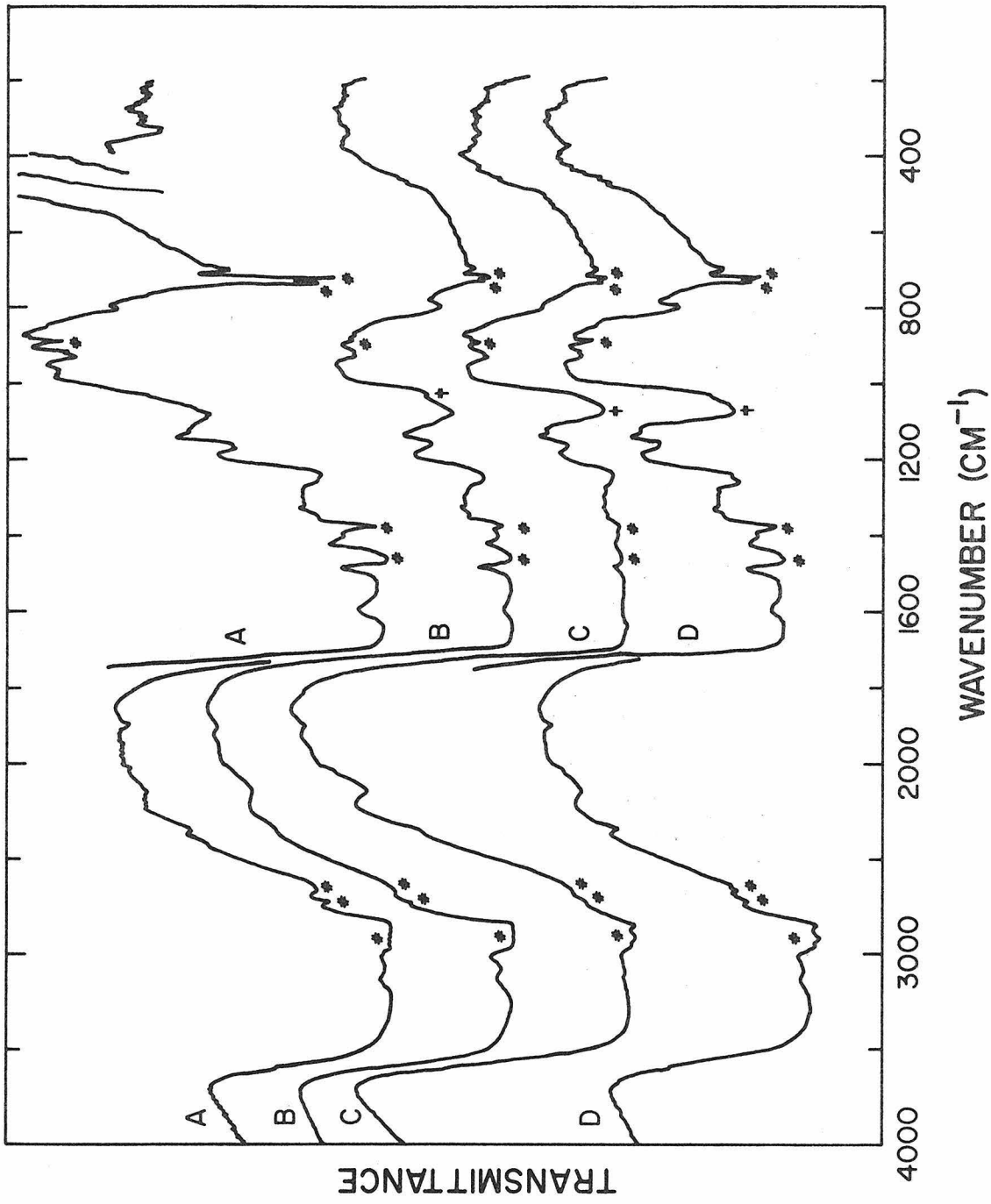
TRANSMITTANCE
WAVENUMBER (CM⁻¹)
4000
3000
2000
1600
1200
800
400
A
B
C
D
A
B
C
D

FIGURE 2

Vaseline mull infrared spectra of holo (A), heat-denatured (E), and acid-denatured (F) plastocyanins, as well as thin film (G) and halocarbon mull (H) spectra of holoplastocyanin. Peaks marked # are due to the mulling agent.

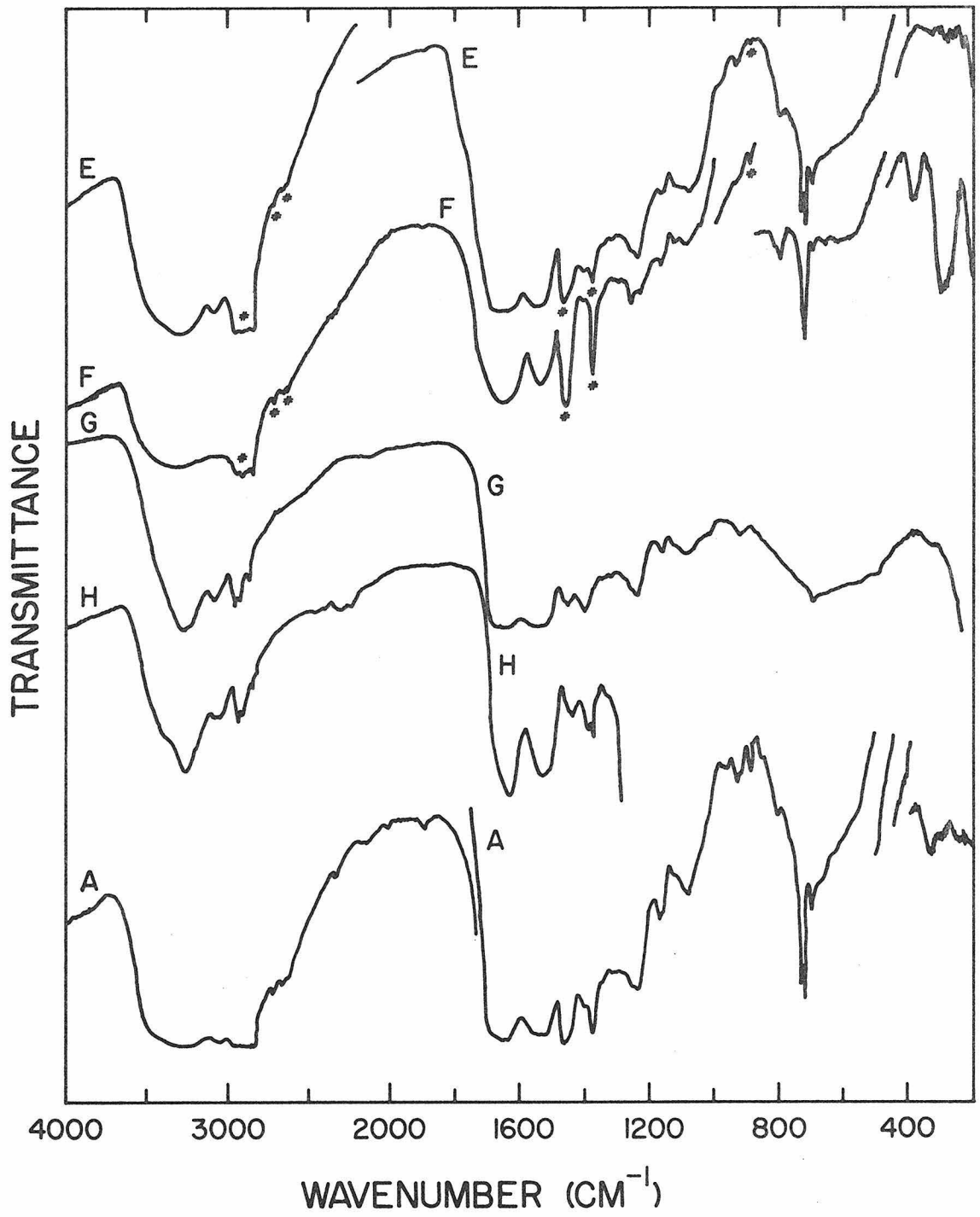
TRANSMITTANCE
E
F
G
H
A
4000
3000
2000
1600
1200
800
400
WAVENUMBER (CM⁻¹)

carbon mull and film spectra associated with the numerous aliphatic and aromatic side chains of the constituent amino acids. The Amide I and II bands at 1650 and 1540 cm^{-1}, respectively, are also broadened over most of the range observed in polypeptide spectra. The amide IV-VI region from 750 to 450 cm^{-1} contains discernable structure only at 700 cm^{-1}, with a shoulder appearing at 490 cm^{-1}. The Amide III region (1300-1230 cm^{-1}), however, shows distinct spectral features that are sensitive to protein modification at 1260 and 1240 cm^{-1}.

The low energy region (525-200 cm^{-1}) of the IR spectra of Vaseline mulls of holo- (AA), reduced (BB), cobalt(II)-substituted (CC), apo- (DD), heat-denatured (EE) and acid-denatured (FF) samples of bean plastocyanin is expanded in Figure 3. Each of the metal-bound proteins exhibits an absorption band at 345 cm^{-1} (AA, BB and CC), which shifts to 370 cm^{-1} (DD) when the metal is removed. Little residual intensity (<10%) remains at 345 cm^{-1} in apoplastocyanin. There is minimal absorption at either 345 or 370 cm^{-1} in the denatured sample (EE), although all higher frequency features are virtually identical to those of the metal-incorporated and apoprotein spectra. It is concluded that the 370 cm^{-1} band depends on protein conformation and further, is perturbed by the presence of a metal ion. Acidification to pH 2

FIGURE 3

Expanded low energy infrared spectra of holo-(AA), reduced (BB), cobalt(II)-substituted (CC), apo-(DD), heat-denatured (EE), and acid-denatured (FF) plastocyanins.

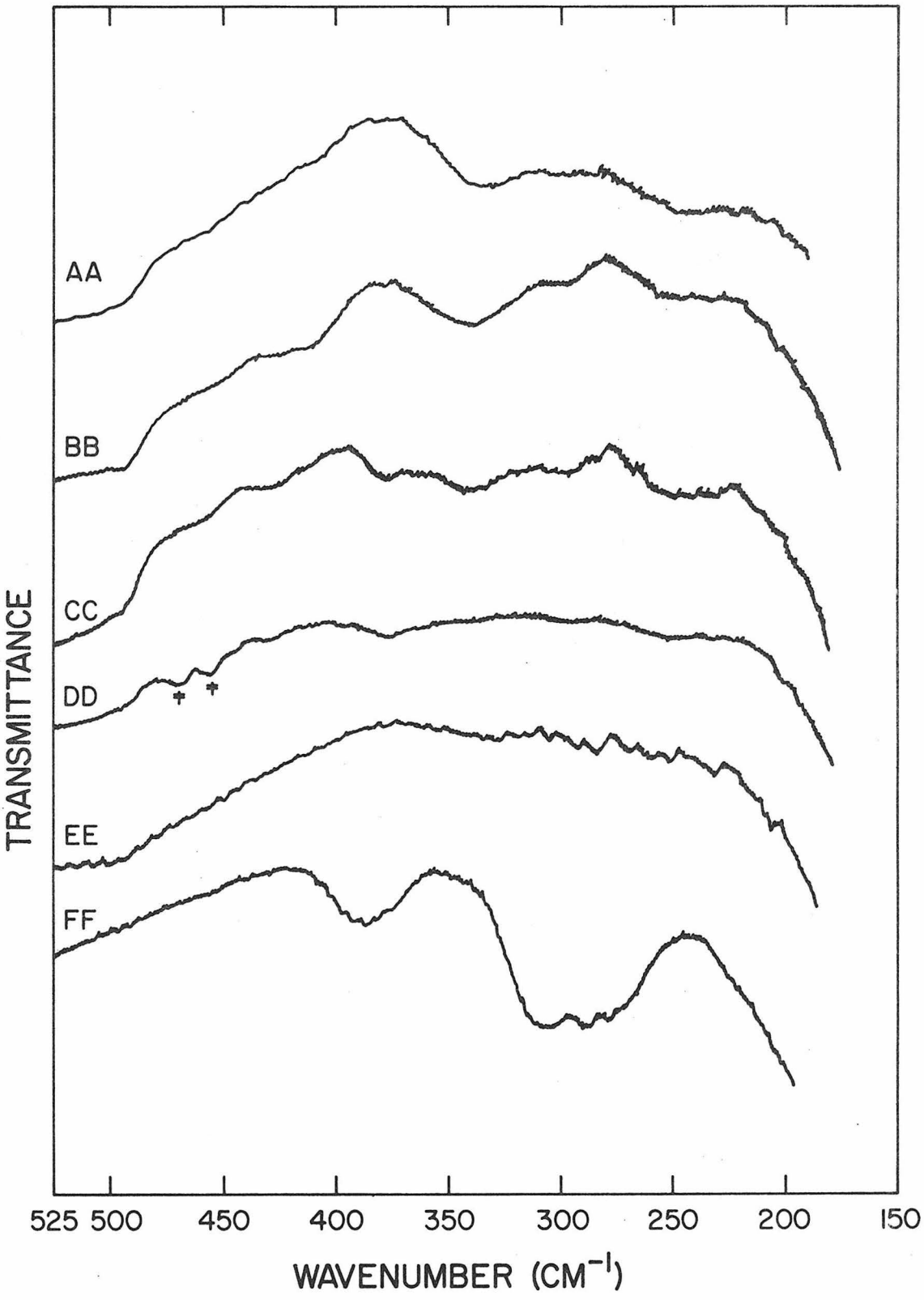
AA
BB
CC
DD
EE
FF
TRANSMITTANCE
525 500
450
400
350
300
250
200
150
WAVENUMBER (CM⁻¹)

completely destroys the blue color of holoplastocyanin, indicating a significant structural change in the protein. The infrared spectrum FF reflects a conformational change, as the low energy band shifts to 380 cm^{-1} and is enhanced in intensity.

The CD spectrum for the range 220 to 300 nm of holoplastocyanin is presented in Figure 4. The dashed curve represents the spectrum predicted for a protein containing 3% α-helix, 5% β-sheet and 92% random coil.

DISCUSSION

The 370 cm^{-1} band in apoplastocyanin matches the energy observed for the backbone deformation in polypeptides containing α-helices[9-11]. The shift observed upon metal incorporation probably is not the consequence of coordination of an appropriate side chain, as the potential ligands known to absorb at 370 cm^{-1} are aspartate and serine[36]. Since there are five aspartate and eight serine residues in the primary sequence[3], it seems extremely unlikely that only one or two of these units is vibrationally active. Those residues present in small enough numbers to be totally bound to the metal, cysteine, histidine and asparagine, do not absorb at 370 cm^{-1}. Complete absence of this low energy feature in the heat-denatured sample is also inconsistent with such an assignment.

FIGURE 4

The natural circular dichroism spectrum of holoplastocyanin (0.096 m$\underline{M}$ in 0.05 $\underline{M}$ acetate buffer, pH 6, 25°). The dashed line corresponds to the best fit spectrum calculated over the region 220 to 250 nm.

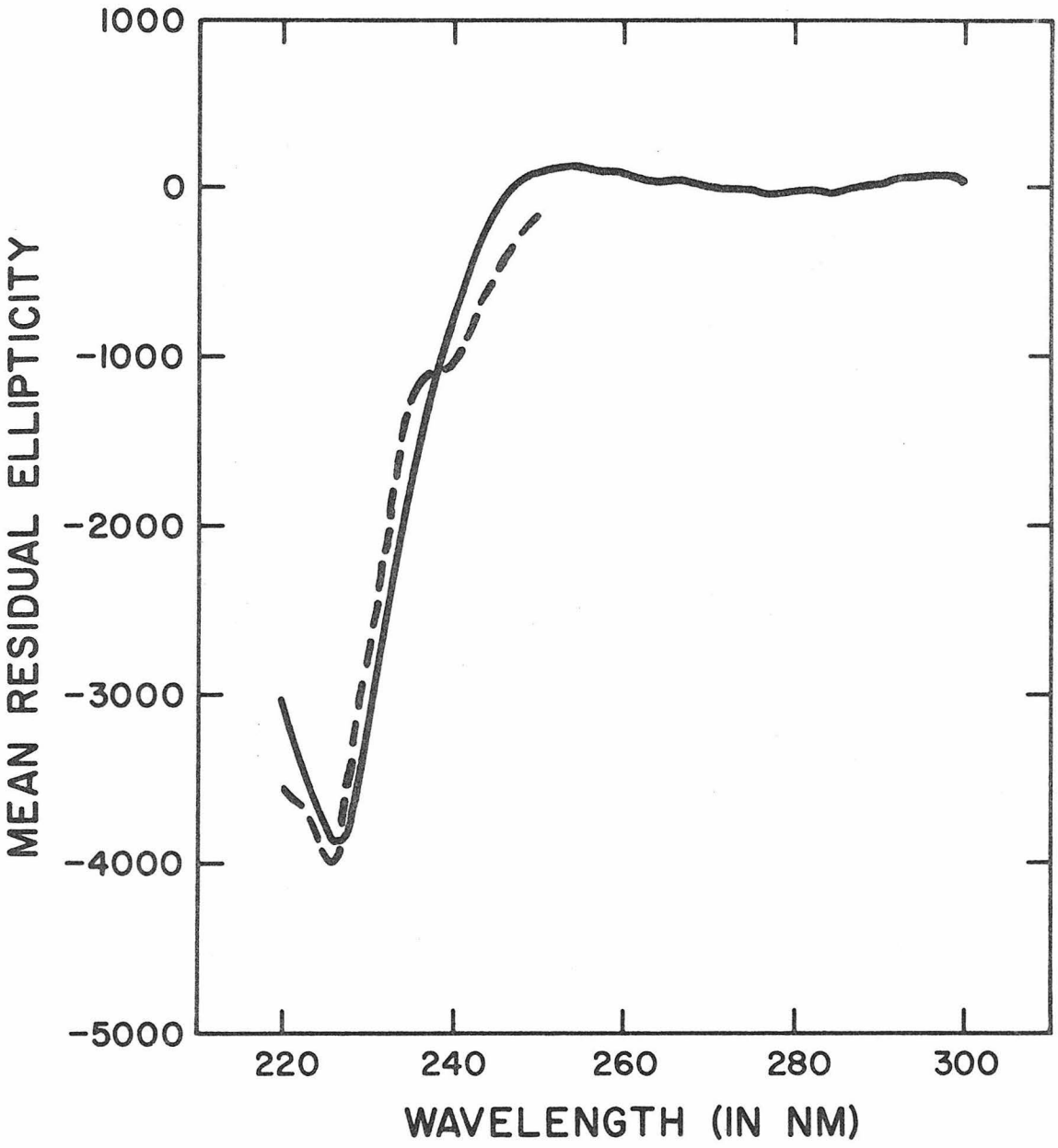
1000
0
-1000
-2000
-3000
-4000
-5000
MEAN RESIDUAL ELLIPTICITY
220
240
260
280
300
WAVELENGTH (IN NM)

Since no significant intensity remains at 370 cm^{-1} when copper is bound to plastocyanin, the entire helix structure in the protein must be perturbed. This suggests that the helix present is relatively short (no more than about three turns). Additional evidence in support of this suggestion was obtained from the ultraviolet CD spectrum of holoplastocyanin (Figure 4). The CD curve was decomposed into α-helix, β-sheet and random coil contributions by the constrained least squares method of Greenfield and Fasman[37]; the constraint being that all structures present that are not α-helix or β-sheet must be included in the random coil contribution. The standard α, β and random coil CD spectra generated by Chen, et al.[38] yielded a best fit of 3% helix, 5% sheet and 92% random coil. Chen, et al. pointed out that the intensity of the helical CD was chain length dependent, so that short sections of α-helix would be underestimated by their standard spectra. A correction factor of roughly 3/n, where n is the number of residues(~100 for plastocyanin), indicates the actual helical content of plastocyanin is closer to 6%.

A band at 250 cm^{-1} appears in all the spectra of Figure 3 except DD, the heat-denatured sample. It appears that protein conformation is also reflected by this absorption. There are two modes in this energy region

derived from backbone deformations, the torsional mode along the chains of the β-sheet[8], and the symmetric breathing deformation of the α-helix[18,39]. The mean value of reported frequencies in polypeptides in the sheet conformation is 249.6 cm^{-1} with a standard deviation of 10 cm^{-1} (see Table IV). The width at half maximum of this band has a mean of 38 cm^{-1} and a standard deviation of 13 cm^{-1}. The protein band at 250 cm^{-1} has a width of ~25-30 cm^{-1}, in accord with the results from polypeptide spectra. Further, the band does not shift when the metal ion is removed, contrary to what is observed for the symmetric helix deformation upon distortion of the α-helix. Thus, β-sheet is also present in bean plastocyanin.

The Amide III energy region is dominated by a band at 1240 cm^{-1}. The relative intensity of this peak remains constant in all spectra except that of the acidified sample. In view of its position (see Table I) and the observation that no shift occurs upon removal of metal, the band is assigned to the Amide III vibration of the composite sheet and random coil conformers present in plastocyanin. A shoulder at 1260 cm^{-1} gains intensity in apoplastocyanin (D, Figure 1) and is even more prominent in the acid-denatured sample (F, Figure 2). This pattern is similar to that observed for the 370 cm^{-1}

TABLE IV

Backbone Deformations Frequencies for Polypeptides

Polypeptide	Helix form	Helix energy	Sheet energy	Ref.
$(L\text{-Ala})_n$	α	371(32)[a]	247(37)	8,11
$(L\text{-norVal})_n$			261(25)	8
$(L\text{-Val})_n$	α	376(25)		8
$(L\text{-norLeu})_n$	α	390(20)		8
$(L\text{-Leu})_n$	α	396(25)		8
$(L\text{-α-aminobutyric acid})_n$	α	389(29)	240(67)	8
$(L\text{-Val-L-Ala-L-Ala})_n$	α	375(17)	235(35)	10
$(L\text{-Val-L-Ala})_n$	α	375(20)	235(28)	10
$(L\text{-Ala-Gly})_n$	α	375(27)	259(40)	10
$(L\text{-Leu-L-Leu-L-Ala})_n$	α	369(22)	252(46)	10
$(L\text{-Leu-L-Ala})_n$	α	371(19)	250(30)	10
$(L\text{-Phe-L-Ala})_n$	α	375(20)	240(22)	10
$(L\text{-Phe-L-Ala-L-Ala})_n$	α	375(19)	244(67)	10
$(L\text{-Ala-L-Ala-Gly})_n$			253(30)	9
$(L\text{-Ala-Gly-Gly})_n$	PG II[b]	352	260(57)	10,9
$(Gly)_n$	PG II	363	268(30)	19,9
$(L\text{-Ala-L-Pro-Gly})_n$	PLP II[c]	343		10
$(Gly\text{-L-Pro-Gly})_n$	PLP II	344		10

[a] width at half maximum in parentheses

[b] polyglycine trigonal helix

[c] polyproline trigonal helix

α-helix deformation. Further, the shoulder is located in the energy region associated with the Amide III mode of an α-helix[18]. Therefore, the 1260 cm^{-1} band is assigned to the α-helix conformation present in apoplastocyanin. The corresponding Amide III mode of the trigonal helix is observed at 1249 cm^{-1} in polyglycine II[19]. This feature, which is expected to be present in metal bound samples, is apparently masked by the strong 1240 cm^{-1} peak. A weaker shoulder at 1260 cm^{-1}, which occurs in all other samples, is attributable to a side chain vibration.

Evidence has recently been found for conformational changes upon lyophilizing of several proteins[30,40]. Intensity differences in certain side chain vibrations and in the Amide III mode have been interpreted as conformational transitions upon lyophilizing α-lactalbumin and lysozyme. Frushour and Koenig reported no structural differences between single crystals and freeze-dried powder occurred for β-lactoglobulin[32]. A film of plastocyanin was prepared to determine effects of sampling on the protein. The relative intensity of the 345 cm^{-1} band was somewhat larger in the film compared to the lyophilized mull, indicating some denaturation occurred upon freeze-drying. This may account for the low intensity of the 370 cm^{-1} band in

the sensitive apoplastocyanin, but otherwise should not affect the validity of the band assignments.

The infrared spectrum of cobalt(II) plastocyanin is identical to that of the holoprotein, except for an additional shoulder at 370 cm^{-1}. This energy corresponds to the previously-assigned helix mode of apoplastocyanin. The spectral data are consistent with the earlier observation that incorporation of Co(II) into plastocyanin is about seventy percent effective[35]. Furthermore, the results show that the incorporated Co(II) distorts the α-helix in the same manner as does copper. The combination of IR and XPS[1] experiments establishes conclusively that Co(II) and Cu(II) bind at the same site in bean plastocyanin. In addition, comparison of the reduced Cu(I) spectrum to that of the holoprotein indicates that the helix portion of the site remains structurally rigid upon reduction.

The presence of bands at 370 and 1260 cm^{-1} in spectrum D, Figure 1 has been attributed to a section of α-helix in the apoplastocyanin secondary structure. A shift from 370 to 345 cm^{-1} and a decrease in intensity of the 1260 cm^{-1} band are observed upon metal incorporation. These spectral changes may be interpreted in terms of a metal-induced distortion of the α-helix to a form similar to polyglycine II[7,10]. It is unlikely,

however, that a section of the polyglycine helix is present in the protein, as the stabilizing factor for this polypeptide structure is intercoil hydrogen bonding[41], which would certainly be difficult to reproduce in the protein. However, the trigonal coil of a 3_{10} helix, which does contain the necessary intracoil hydrogen bonding for a stable protein conformation, is expected to have a similar energy for the deformation mode. This mode is made up mainly of backbone angle deformations and the amide torsional motion. If the form of hydrogen bonding used to stabilize this structure were to affect the energy of this mode, then the deuterated polyglycine spectrum should show a considerable shift in the 363 cm^{-1} band. Suzuki, et al. have measured the isotope shift to be only 7 cm^{-1} [7], so the amide deformation of the trigonal 3_{10} helix should be comparable in energy to the corresponding mode in polyglycine II.

Resonance Raman spectral studies of several blue proteins, including spinach plastocyanin, have shown enhancement of amide modes at 750, 1240 and 1650 cm^{-1} [2], indicating an amide oxygen or nitrogen is coordinated to the copper. In model complexes containing primary amide ligands such as biuret, the carbonyl stretch occurs between 1680 and 1690 cm^{-1}, and does not shift upon

coordination to copper by either nitrogen or oxygen[42]. As both asparagine and glutamine also have side chain carbonyl absorptions around 1680 cm^{-1} [43], which are not expected to shift appreciably upon metal coordination, the amide side chains can be ruled out as possible ligands in plastocyanin. Further, the enhanced frequencies correspond quite well to A symmetry Amide V, III and I modes, respectively, in polyglycine II[19]. The 345 cm^{-1} band does not appear to be resonance enhanced, but this is a probable result of the fact that the mode has E symmetry in the helix. Since A symmetry modes are usually more intense in Raman spectra than those derived from E symmetry, the results are consistent with copper being bound to the backbone of a helix. It is of interest that the same bands are weakly enhanced in all blue copper proteins that have been studied, with no more than a 10 cm^{-1} variation in each of the frequencies[2]. Thus, each of the entire group of blue proteins would appear to have a copper(II) bound to the amide backbone of a short section of trigonal or distorted α-helix.

It should be emphasized that, at present, a metal-perturbed α-helix cannot be distinguished from a rearrangement to a 3_{10} type of structure. Examination of Dickerson and Geis' illustrations reveals the major

difference between the two helical structures to be the position of the amide hydrogen-carbonyl oxygen hydrogen bond[44]. This bond joins every four residues in the α-helix, whereas it connects every three in the 3_{10} structure, thereby forcing it into a tighter coil (4 Å versus 4.2 Å diameter) and a greater pitch (6 Å versus 5.4 Å). Coordination of copper to an amide nitrogen or oxygen on the helix could result in the destruction of a hydrogen bond and destabilization of the structure. By breaking the remaining hydrogen bonding scheme between every fourth residue of the α-helix and shifting to bonding between every third residue as in the 3_{10} helix, net loss of a hydrogen bond is circumvented. The structure is stabilized at the expense of a higher coil strain energy. Should two amide nitrogen or oxygen atoms be coordinated to copper, the transformation to a 3_{10} helix would be even more favored. A similar mechanism has been proposed by Heitz, et al. to explain the heat induced transformation of poly-γ-benzyl-DL-glutamate from an α-helix to the π (4.4_{16}) structure[15].

Although forming a picture of the metal site without an x-ray crystal structure is speculative, a compilation of the available physical data, a comparison of the primary amino acid sequences of several plasto-

cyanins, and a correlation of Chou and Fasman's statistics on the frequency amino acid residues appear in secondary conformations[45] with the bean plastocyanin sequence can lead to a reasonable and informative model. It has been shown that copper(II) is bound by at least one amide nitrogen or oxygen from a helix. According to Chou and Fasman, the most likely residues to be found at the beginning or end of a helix are proline, aspartate and histidine. A careful examination of the bean plastocyanin sequence[3] reveals that the highest number of helix-forming residues is found between proline-36—histidine-37 and proline-47. This string of residues from position 38 to 46 represents the most probable choice for finding a helix in the plastocyanin sequence. A comparison of the sequences of five plastocyanins in this region, in Table V, reveals a variation in only one residue, position 46 where structurally similar valine and isoleucine are interchanged. This strong correlation between species implies an important structural or functional role for this region of plastocyanin.

Recent XPS results have confirmed that cysteine sulfur is bound to copper(II) at the metal site[1]. As the lone cysteine residue is found at position 84 in every sequence, the model evolves to copper(II) being firmly bound by one or two amide groups of the helix plus

TABLE V

Selected Portions of the Sequences of Various Plastocyanins

```
   30          33          36          39          42          45          48
a  Phe-Lys-Asn-Asn-Ala-Gly-Phe-Pro-His-Asn-Val-Val-Phe-Asp-Glu-Asp-Glu-Ile-Pro-Ala-Gly
b      Lys-Asn-Asn-Ala-Gly-Phe-Pro-His-Asn-Val-Val-Phe-Asp-Glu-Asp-Glu-Ile-Pro-Ser-Gly
c      Lys-Asn-Asn-Ala-Gly-Phe-Pro-His-Asn-Val-Val-Phe-Asp-Glu-Asp-Glu-Ile-Pro-Ser-Gly
d      Lys-Asn-Asn-Ala-Gly-Phe-Pro-His-Asn-Val-Val-Phe-Asp-Glu-Asp-Glu-Val-Pro-Ser-Gly
e      Lys-Asn-Asn-Ala-Gly-Phe-Pro-His-Asn-Val-Val-Phe-Asp-Glu-Asp-Glu-Ile-Pro-Ser-Gly
f  Phe-Lys-Asn-Asn-Ala-Gly-Phe-Pro-His-Asn-Val-Val-Phe-Asp-Glu-Asp-Glu-Ile-Pro-Ala-Gly
g  Trp-Val-Asn-Asn-Ala-Gly-Phe-Pro-His-Asn-Ile-Val-Phe-Asp-Glu-Asp-Glu-Val-Pro-Ser-Gly

           80          83          86          89
a          Thr-Tyr-Ser-Phe-Tyr-Cys-Ser-Pro-His-Gln-Gly
b              Tyr-Lys-Phe-Tyr-Cys-Ser-Pro-His-Gln-Gly
c              Tyr-Lys-Phe-Tyr-Cys-Ser-Pro-His-Gln-Gly
d              Tyr-Lys-Phe-Tyr-Cys-Ser-Pro-His-Gln-Gly
e              Tyr-Ser-Phe-Tyr-Cys-Ser-Pro-His-Gln-Gly
f          Thr-Tyr-Thr-Phe-Tyr-Cys-Ala-Pro-His-Gln-Gly
g          Thr-Tyr-Gly-Tyr-Phe-Cys-Glu-Pro-His-Gln-Gly
```

a French bean(3) b Spinach(48) C Broad bean(46) d Elder(46)

e Vegetable marrow(47) f Potato(3) g Chlorella(3)

one or two other residues leaving a coordination position open for the cysteine sulfur. The protein backbone evidently bends back to present cysteine-84 at the appropriate location for coordination to copper. Markley, et al. have recently reported NMR evidence for histidine filling the remaining coordination positions[49]. The two histidine residues also have unique positions in the sequence at numbers 37 and 87. The former histidine appears at the beginning of the proposed helix location allowing coordination to both the imidazole side chain and an amide nitrogen or oxygen of the helix. The latter histidine lies three residues from the cysteine, an appropriate distance to allow both histidine nitrogen and cysteine sulfur to bind to the copper(II).

In summary, a helical secondary structure has been found to be associated with the metal site in bean plastocyanin. It is likely that such structure is also present in other blue copper proteins. This short section of helix is distorted by metal (copper or cobalt) incorporation, which is probably the result of coordination to an amide nitrogen or oxygen of the peptide backbone. The perturbed helical structure at the site remains conformationally rigid upon reduction of holoplastocyanin to the copper(I) derivative. Finally, a combination of known physical

data leads to a picture of the metal site where copper(II) is bound by histidine-37, an amide nitrogen or oxygen or one or more of the following residues which make up the helix, and by cysteine-84 and histidine-87 which provide the final coordinating positions.

BIBLIOGRAPHY

1. E. I. Solomon, P. J. Clendening, H. B. Gray and F. J. Grunthaner, J. Amer. Chem. Soc., 97, 3878 (1975).

2. O. Siiman, N. M. Young and P. R. Carey, J. Amer. Chem. Soc., 96, 5583(1974); J. Amer. Chem. Soc., in press.

3. P. R. Milne, J. R. E. Wells and R. P. Ambler, Biochem. J., 143, 691(1974).

4. T. Miyazawa, T. Shimanouchi and S.-I. Mizushima, J. Chem Phys., 29, 611 (1958).

5. A. Elliott and E. J. Ambrose, Nature, 165, 921 (1950).

6. T. Miyazawa in Polyamino Acids, Polypeptides, and Proteins , M. A. Stahmann, ed., University of Wisconsin Press, Madison, Wisconsin, 1962.

7. S. Suzuki, Y. Iwashita, T. Shimanouchi and M. Tsuboi, Biopolymers, 4, 337(1966).

8. K. Itoh, T. Shimanouchi and M. Oya, Biopolymers, 7, 649(1969).

9. K. Itoh and H. Katabuchi, Biopolymers, 11, 1593 (1972).

10. K. Itoh and H. Katabuchi, Biopolymers, 12, 921(1973).

11. K. Itoh, T. Nakahara, T. Shimanouchi, K. Uno and Y. Iwakura, Biopolymers, 6, 1759(1968).

12. B. Fanconi, Biopolymers, 12, 2759(1973).

13. Y. Masuda, K. Fukushima, T. Fujii and T. Miyazawa, Biopolymers, 8, 91(1969).

14. E. M. Bradbury, B. G. Carpenter and R. M. Stephens, Biopolymers, 6, 905(1968).

15. F. Heitz, B. Lotz and G. Spach, J. Mol. Biol., 92, 1(1975).

16. J. L. Koenig and P. L. Sutton, Biopolymers, 8, 167(1969).

17. M. C. Chen and R. C. Lord, J. Amer. Chem. Soc., 96, 4750(1974).

18. J. L. Koenig and P. L. Sutton, Biopolymers, 10, 89(1971).

19. E. W. Small, B. Fanconi and W. L. Peticolas, J. Chem. Phys., 52,4369(1970).

20. J. L. Koenig and B. G. Frushour, Biopolymers, 11, 1871(1972).

21. B. G. Frushour and J. L. Koenig, Biopolymers, 13, 455(1974).

22. B. G. Frushour and J. L. Koenig, Biopolymers, 14, 363(1975).

23. K. Itoh, T. Hinomoto and T. Shimanouchi, Biopolymers, 13, 307(1974).

24. E. J. Ambrose and A. Elliott, Proc. Roy. Soc.(London), A206, 206(1951).

25. W. B. Gratzer, E. Bailey and G. H. Beaven, Biochem.

Biophys. Res. Comm., 28, 919(1967).

26. B. B. Doyle, E. G. Bendit and E. R. Blout, Biopolymers, 14, 937(1975).

27. R. C. Lord and N.-T. Yu, J. Mol. Biol., 50, 509(1970).

28. R. C. Lord and N.-T. Yu, J. Mol. Biol., 51, 203(1970).

29. J. L. Koenig and B. G. Frushour, Biopolymers, 11, 2505(1972).

30. N.-T. Yu and B. H. Jo, Arch. Biochem. Biophys., 156, 469(1973).

31. B. G. Frushour and J. L. Koenig, Biopolymers, 14, 379(1975).

32. B. G. Frushour and J. L. Koenig, Biopolymers, 14, 649(1975).

33. B. Fanconi, E. W. Small and W. L. Peticolas, Biopolymers, 10, 1277(1971).

34. a. Yu. N. Chirgadze and A. M. Ovsepyan, Biopolymers, 12, 637(1973).

b. P. L. Gordon, C. Huang, R. C. Lord and I. V. Yannis, Macromolecules, 7, 955(1974).

35. D. R. McMillin, R. C. Rosenberg and H. B. Gray, Proc. Nat. Acad. Sci. (U. S. A.), 71, 4760(1974).

36. F. F. Bentley, L. D. Smithson and A. L. Rogak, Infrared Spectra and Characteristic Frequencies ~

700-300 cm^{-1}, Interscience, New York, New York, 1968.

37. N. Greenfield and G. D. Fasman, Biochemistry, 8, 4108(1969).

38. Y.-H. Chen, J. T. Yang and H. M. Martinez, Biochemistry, 11, 4120(1972).

39. K. Itoh and T. Shimanouchi, Biopolymers, 9, 383(1970).

40. N.-T. Yu, J. Amer. Chem. Soc., 96, 4664(1974).

41. F. H. C. Crick and A. Rich, Nature, 176, 780(1970).

42. A. W. McLellan and G. A. Melson, J. Chem. Soc. A., 137(1967).

43. L. Simons, G. Bergström, G. Blomfelt, S. Forss, H. Stenbäck and G. Wansen, Commentationes Physico-Mathematicae, Societas Scientiarum Fennica, Helsinki-Helsingfors, 42, 125(1972).

44. R. E. Dickerson and I Geis, The Structure and Action of Proteins, Harper and Row, Publishers, New York, New York, 1969.

45. P. Y. Chou and G. D. Fasman, J. Mol. Biol., 74, 263(1973).

46. J. A. M. Ramshaw, M. D. Scawen and D. Boulter, Biochem. J., 141, 835(1974).

47. M. D. Scawen and D. Boulter, Biochem. J., 143, 257(1974).

48. M. D. Scawen, J. A. M. Ramshaw and D. Boulter, Biochem. J., 147, 343(1975).

49. J. L. Markley, E. L. Ulrich, S. P. Berg and D. W. Krogmann, Biochemistry, in press.

50. D. F. H. Wallach, J. M. Graham and A. R. Oseroff, FEBS Letters, 7, 330(1970).

51. T. Isemura, H. Okabayashi and S. Sakakibara, Biopolymers, 6, 307(1968).

52. M. Goodman, Y. Masuda and A. S. Verdini, Biopolymers, 10, 1030(1971).

CHAPTER 2

ELECTRONIC STRUCTURE AND SPECTRA OF BLUE COPPER CENTERS IN PROTEINS

INTRODUCTION

The electronic structure of the cupric ion complexed to the blue copper proteins has been the subject of numerous physical and theoretical studies. The visible absorption spectrum of the blue copper center in each of these proteins is dominated by an intense (molar extinction coefficient ϵ of approximately 4000 l $mole^{-1}$ cm^{-1}) band in the region 600 to 630 nm which produces the characteristic blue color of the proteins. Weaker bands at 450 and 800 nm flank the major absorption[1-5]. The natural circular dichroism (CD) spectra of these proteins are also distinctive and similar. Negative rotations are observed at 450 and ~800 nm, corresponding to the weaker absorptions, whereas a smaller positive band with a shoulder towards high energy is present in the 600 nm region[6-8]. The origin of these transitions has been ascribed either to d-d excitations of four coordinate[1-3,9,10] or five coordinate geometry[11], intensified by mixing with allowed transitions via odd-order ligand field distortions, or to charge transfer from a strongly reducing ligand to the copper(II) ion[12]. Spectroscopic studies of the cobalt(II) derivatives of stellacyanin, plastocyanin and azurin have indicated that the charge transfer interpretation is preferred. Intense bands (ϵ>2000) that appear to be analogous to the 600 nm

manifold of the native proteins are observed between 300 and 350 nm in the cobalt(II) derivatives[13]. This shift in band position of about 16000 cm^{-1} to higher energy (Co(II) > Cu(II)) accords well with that anticipated for a ligand to metal charge transfer transition, cobalt(II) being less oxidizing than copper(II).

The electron paramagnetic resonance (EPR) spectra give valuable information concerning the ground state properties of the copper in these blue proteins. Plastocyanin[1] and azurin[2] have axial spectra, at least within band resolution, with $g_{||}$ at 2.226 and 2.261, respectively, and $g_{\perp}$ at 2.053 and 2.052. Stellacyanin, however, shows a slight rhombic distortion with $g_z = 2.287$, $g_y = 2.077$ and $g_x = 2.025$[4]. Ballhausen[14] has shown that a d^9 ion with axial symmetry is expected to show $g_{\perp} > g_{||}$ for a (z^2) ground state and $g_{||} > g_{\perp}$ for an (x^2-y^2) ground state.

The reasons that the reduction potentials of the blue copper proteins are substantially higher than the aqueous cupric-cuprous couple are not known, but suggest a utility in electron transport systems. Few studies have attempted to correlate, for example, blue copper protein reduction potentials to ligand field stabilization, varying degrees of complex formation and other physical data, largely due to insufficient evidence

concerning coordinating ligands and the lack of a solid assignment of the electronic spectrum. This chapter reports the low temperature near-infrared and visible absorption and room temperature near-infrared and visible CD and magnetic circular dichroism (MCD) spectra for stellacyanin, plastocyanin and azurin. These new spectral data have allowed, for the first time, assignments to be made of the d-d transitions in blue copper centers. Based on these assignments, ligand field parameters have been calculated and utilized in the examination of the reduction potentials of the proteins.

EXPERIMENTAL SECTION

The proteins used in this study are French bean (Phaseolus vulgaris) plastocyanin, azurin (Pseudomonas aeruginosa) and stellacyanin (Rhus vernicifera). Mr. Barry Dohner isolated the proteins, and I am indebted to him for all the leaf juicing, bacterial incubation, acetone-powder extraction and cold-room column purifications from which I was spared.

Near-infrared absorption spectra were obtained on protein films to minimize interference by water absorption and permit a wide variation of temperature. The protein solutions were first dialyzed against de-ionized distilled water and then concentrated from

roughly 10 to 0.5 ml by pressurized membrane ultrafiltration. The sample was then further concentrated by placing a drop of protein solution on a plexiglas disk in a metal dessicator over Drierite. After three or four drops had been successively concentrated (ten to fifteen for the thick films), the film was prepared by transferring the disk to a dessicator containing a saturated potassium acetate solution. This controlled humidity allowed the film to form slowly preventing most of the cracking caused by rapid removal of too much water. The drying process could be halted by transfer to a dessicator charged with a saturated sodium hydrogen phosphate solution. The humidity of this dessicator allowed slow dissolution of the sample. Films that had been over-dried could be redissolved by placing then in the sodium phosphate humidifier. While stellacyanin and azurin appeared unaffected by complete drying and redissolving, plastocyanin never completely redissolved. The undissolved plastocyanin was white, indicating partial denaturation upon complete removal of water. It is, therefore, advisable never to allow plastocyanin to dry past the elastic film form.

A lightly greased silicone rubber gasket was placed on the plastic disk and a second disk placed

over the gasket to prevent further drying upon evacuation in a cryocooler unit. The sample was masked with aluminum foil to prevent light leakage and to improve thermal contact with the cold station. The sample was then slowly cooled to minimum temperature. If cracks developed, the unit was warmed to near room temperature, slices of black masking tape applied to cover large cracks, and the unit then recooled. Plexiglas (½ inch in diameter by 1/32 inch thick) was chosen over quartz despite poorer optical quality (weak vibrational overtones at 1250 nm and lower wavelengths) because the thermal contraction more closely matched that of the protein film.

The near-infrared CD and MCD spectra were run in deuterated phosphate buffer in order to extend the spectral range to ~1850 nm. Although the infrared overtones of water do not give rise to a measurable CD spectrum, an absorbance of 1.0 or greater diminished the light level to the limit of detector response. The deuterated protein solutions were prepared by evaporating unbuffered, concentrated aqueous solutions in a Drierite dessicator as described above. The films were then transferred to a dessicator charged with D_2O. The films were allowed to equilibrate overnight, dried again to a film and placed a second night in the D_2O

humidifier. After the second equilibration with D_2O, the solutions were evaporated to a film and the film dissolved in deuterated phosphate buffer at pD 6. The deuterated buffer was prepared by dissolving vacuum-dried Na_3PO_4 in D_2O to form a 0.05 M solution. The pD was adjusted to 6 by adding small volumes of phosphoryl chloride ($POCl_3$), which reacted with D_2O to form D_3PO_4 and DCl. The final concentration of stellacyanin was 1.06 mM. Azurin concentrations were 0.69 and 1.50 mM for the MCD and CD spectra, respectively. The plastocyanin concentrations were 0.41 and 2.21 mM for the MCD and CD spectra, respectively. The proteins were reduced by adding a small amount of concentrated sodium dithionite dissolved in nitrogen-purged D_2O.

The deuterated protein solutions were pipetted into a small volume, 1 cm pathlength cell, specially designed for these experiments. A 1 cm length of 8 mm pyrex tubing was ground flat at both ends and a filling port fabricated on the side. Two $\frac{3}{4}$ inch quartz windows were cemented to the tubing with General Electric GTV silicone adhesive. A firm, pliable bond is preferred to the rigid bond formed by epoxy-type cements, in this case, to limit any strain in the quartz, which would certainly cause polarization problems in the infrared spectropolarimeter.

Solutions for the visible CD and MCD spectra were prepared by diluting the infrared solutions with deuterated phosphate buffer until an absorbance less than 1.0 in a 1 cm cell was recorded for the 600 nm band. The final concentrations were 0.206, 0.210 and 0.197 mM for stellacyanin, azurin and plastocyanin, respectively.

The absorption spectra were obtained on a Cary 17 I recording spectrometer, generously made available by Dr. George R. Rossman. The spectra were run at constant slit widths of 0.8 mm below 750 nm and 0.4 mm above 750 nm. Wavelength variations in lamp output, monochromator transmission and detector response, normally compensated by the slit feedback mechanism, were corrected by a feedback system on the source voltage supply, installed by Dr. Rossman. Higher resolution measurements (0.1 mm slit width in the near-infrared) revealed no fine structure at low temperatures. The samples were cooled by a Cryogenics Technology, Inc. Model 20 cryocooler equipped with quartz windows and a temperature controller, which allowed adjustment of the temperature to ±1 K over most of the range used.

The visible CD and MCD spectra were recorded on a Cary 61 spectropolarimeter in the laboratory of Professor P. J. Stephens of the University of Southern California.

The field of 40 kilogauss was supplied by a liquid helium-cooled Varian superconducting electromagnet. A slit width of 1 mm and a sensitivity of 0.1 degree full scale were standard settings used during the experiments. The near-infrared CD and MCD spectra were also recorded on an instrument in Professor Stephens' laboratory. The patient guidance of Dr. Jill Rawlings through the complexities of a "home-built" spectropolarimeter is gratefully acknowledged. Sensitivity varied between experiments, but was usually of the order of 1.3×10^{-3} ΔA full scale (ΔA is the difference between left and right circularly polarized light absorption). Instrument baselines were determined using deuterated phosphate buffer as a blank.

RESULTS

Absorption spectra of stellacyanin films from 28000 to 7000 cm^{-1} are shown in Figure 1. The solid line represents the spectrum at 270 K, whereas, the dashed line is a 35 K spectrum. The high temperature spectrum is consistent with the solution spectrum reported by Peisach, et al.[2] Extinction coefficients of the films are assumed to be the same as the solution values of Peisach, et al. A new band in the 8000-9000 cm^{-1} range is partially resolved when the thick film (spectrum 1B) is cooled. Figure 2 contains the Gaussian-

FIGURE 1

The near-infrared and visible absorption spectra of stellacyanin film. ϵ is the molar extinction coefficient. For the lower curves use the left-hand ϵ-scale and for the upper curves (thick film) use the right-hand ϵ-scale. The solid curves represent 270 K spectra, and the dashed curves represent 35 K spectra.

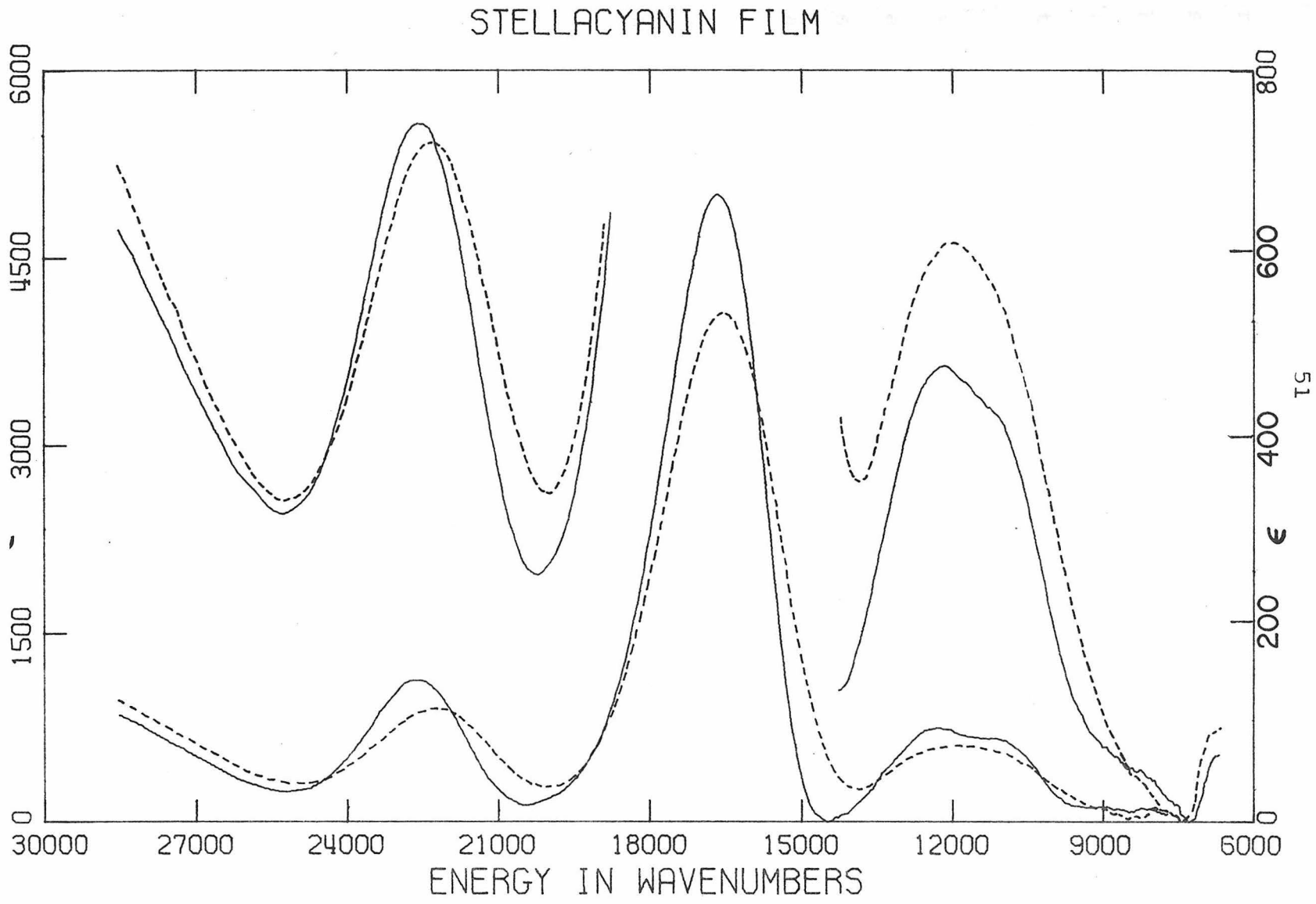
STELLACYANIN FILM
6000
4500
3000
1500
0
800
600
400
200
0
ε
30000
27000
24000
21000
18000
15000
12000
9000
6000
ENERGY IN WAVENUMBERS

resolved bands, their sum and the 35 K spectrum of stellacyanin (in symbols). The position, intensity (ϵ), half-width at half-maximum (HWHM) and oscillator strength (f) of the resolved Gaussian peaks as a function of temperature are given in Table I.

The visible CD curve is given in Figure 3. It agrees with the spectrum reported by Falk and Reinhammar[7] and is presented here for comparison. The MCD curve, shown in Figure 4, has not been reported and shows activity at 16500 and 13500 cm^{-1} plus a small negative band at 22000 cm^{-1}. The intense bands starting at 33000 cm^{-1} are probably due to tryptophan residues analogous to the reported ultraviolet MCD curves of azurin in this energy region[15]. The near-infrared CD spectrum of stellacyanin appears in Figure 5. The region 12500-9000 cm^{-1} was also reported by Falk and Reinhammar[7] in the only other blue protein CD study below 12500 cm^{-1}. New bands are prominent in the expanded spectrum (5B) at 8100 and approximately 5000 cm^{-1}. The latter band abruptly ends due to the onset of D_2O vibrational absorption. The MCD curve (Figure 6) in the near-infrared continues the 12500 cm^{-1} band and shows a weak positive peak at ~10800 cm^{-1} and a weak negative peak at 8800 cm^{-1}. An expanded curve (6B) more clearly defines the 8800 cm^{-1} activity and indicates the

FIGURE 2

Gaussian resolution of the 35 K near-infrared and visible absorption spectrum of a stellacyanin film. The individual Gaussian peaks and sum are solid curves. The symbols(+) represent the absorption spectrum.

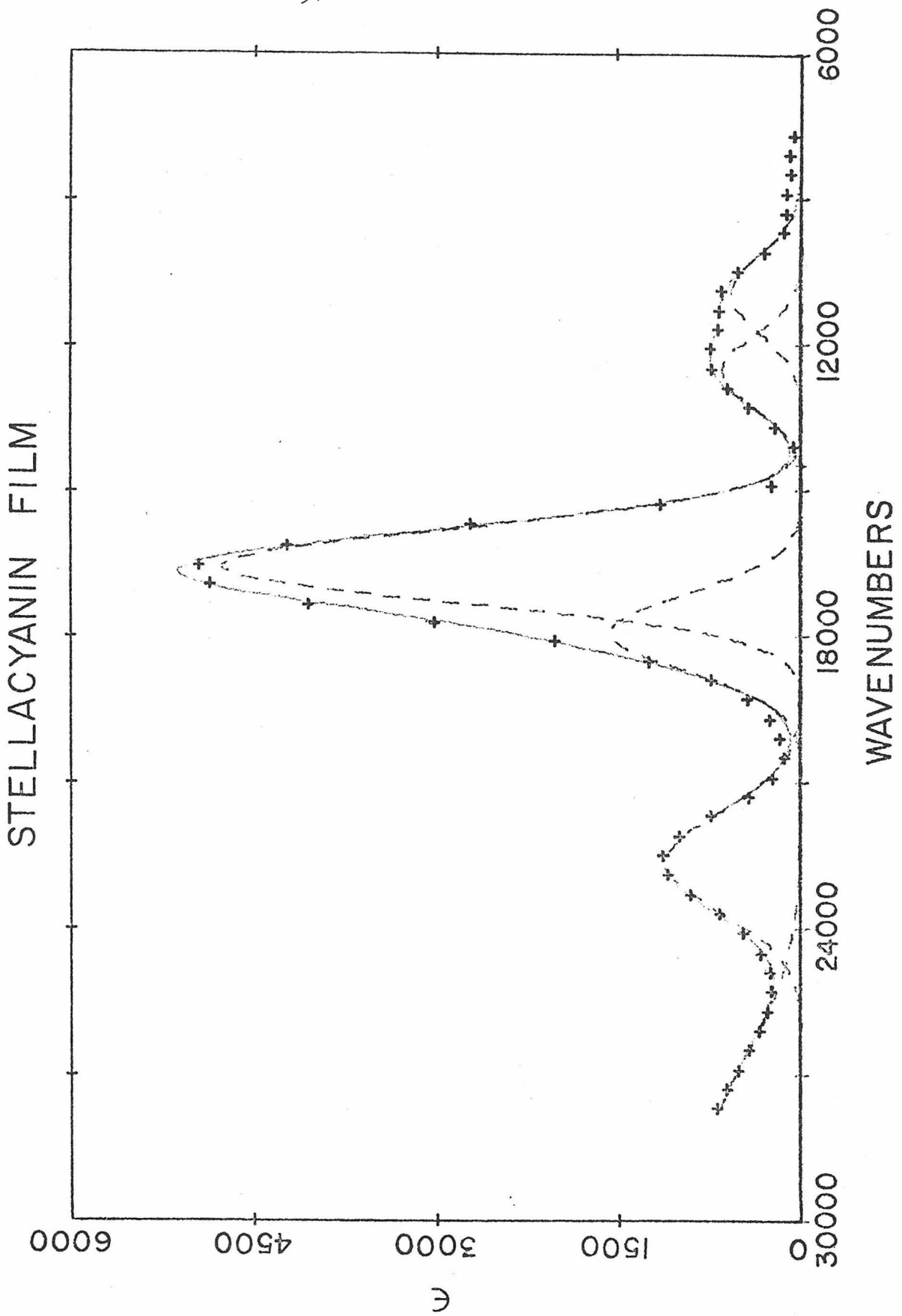
STELLACYANIN FILM
ε
0
1500
3000
4500
6000
30000
24000
18000
12000
6000
WAVENUMBERS

TABLE I

Gaussian Analysis of Stellacyanin Absorption Spectra

T = 35K	60K	120K	200K	270K
Band 1				
ν^1 = 22550	22570	22520	22380	22210
HWHM[2] = 1185	1196	1265	1457	1512
f[3] = 0.012	0.012	0.012	0.014	0.012
ϵ[4] = 1177	1174	1124	1110	942
Band 2				
ν = 17840	17750	17630	17620	17490
HWHM = 941.6	967	990	1134	1213
f = 0.013	0.015	0.017	0.016	0.016
ϵ = 1631	1769	1927	1658	1542
Band 3				
ν = 16460	16430	16350	16310	16220
HWHM = 883	876	889	1012	1090
f = 0.039	0.037	0.034	0.035	0.033
ϵ = 5064	4879	4371	3995	3549
Band 4				
ν = 12510	12590	12600	12680	12680
HWHM = 867	848	781	863	933
f = 0.0049	0.0039	0.0030	0.0031	0.0027
ϵ = 657	535	445	417	341
Band 5				
ν = 10910	11050	11060	11090	11110
HWHM = 999	1180	1219	1266	1375
f = 0.0053	0.0064	0.0065	0.0066	0.0067
ϵ = 610	627	615	600	565

[1]Frequency in wave numbers
[2]Half-width at half-maximum in wave numbers
[3]Oscillator strength
[4]Molar extinction coefficient

FIGURE 3

The visible CD spectrum of stellacyanin in pD 6 deuterated phosphate buffer. The left-hand scale is molar ellipticity in deg-cm^2/decimole (x 10^4) and the right-hand scale is $\Delta\epsilon$ in 1/mole-cm. The stellacyanin concentration was 0.206 m$\underline{M}$.

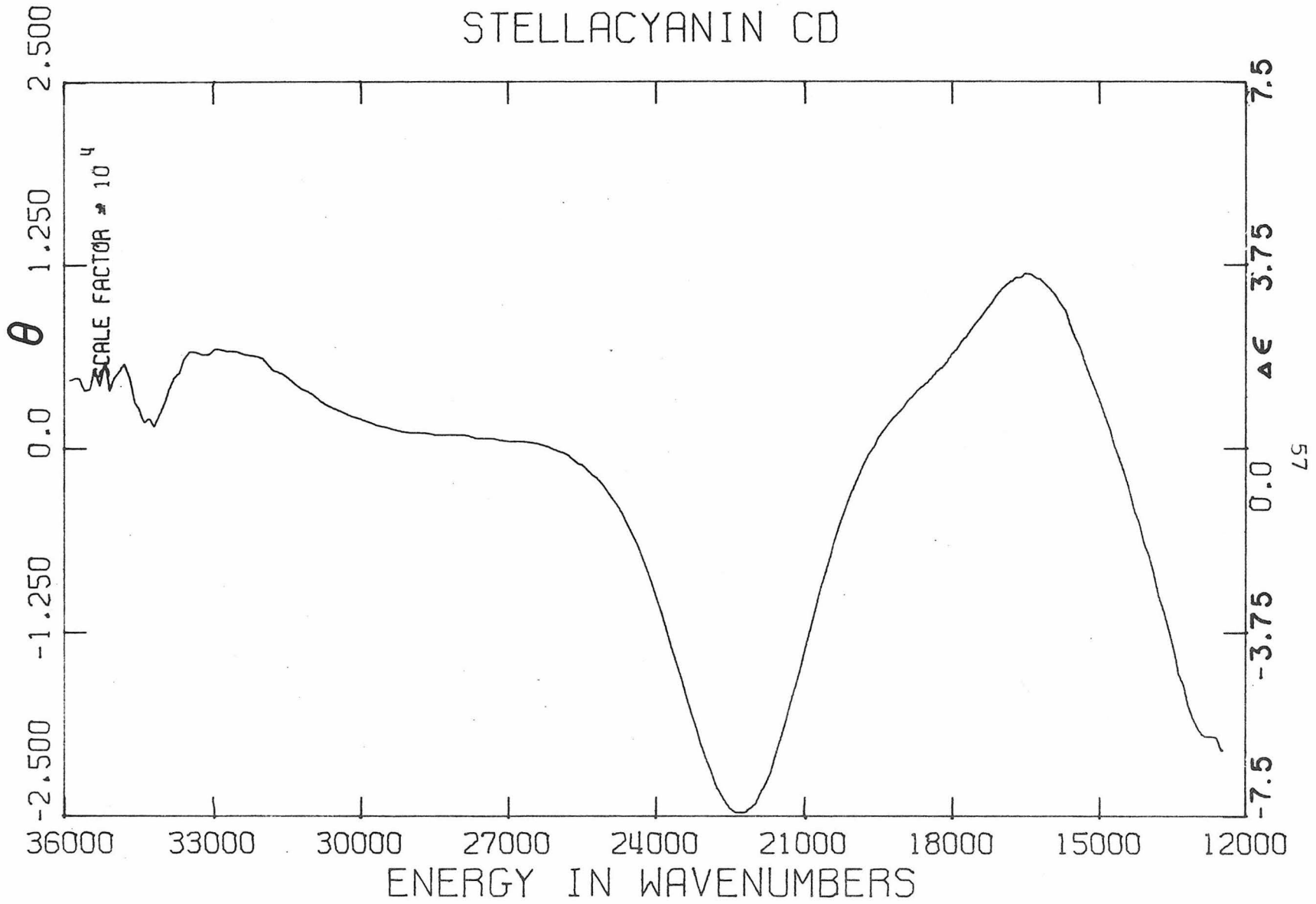
STELLACYANIN CD
θ
SCALE FACTOR = 10^4
2.500
1.250
0.0
-1.250
-2.500
Δε
7.5
3.75
0.0
-3.75
-7.5
36000
33000
30000
27000
24000
21000
18000
15000
12000
ENERGY IN WAVENUMBERS

FIGURE 4

The visible MCD spectrum of stellacyanin in pD 6 deuterated phosphate buffer. The left-hand scale is molar magnetic ellipticity in deg-cm^2/decimole-Gauss and the right-hand scale is $\Delta\epsilon$ per 10 kilogauss. The stellacyanin concentration was 0.206 m$\underline{M}$.

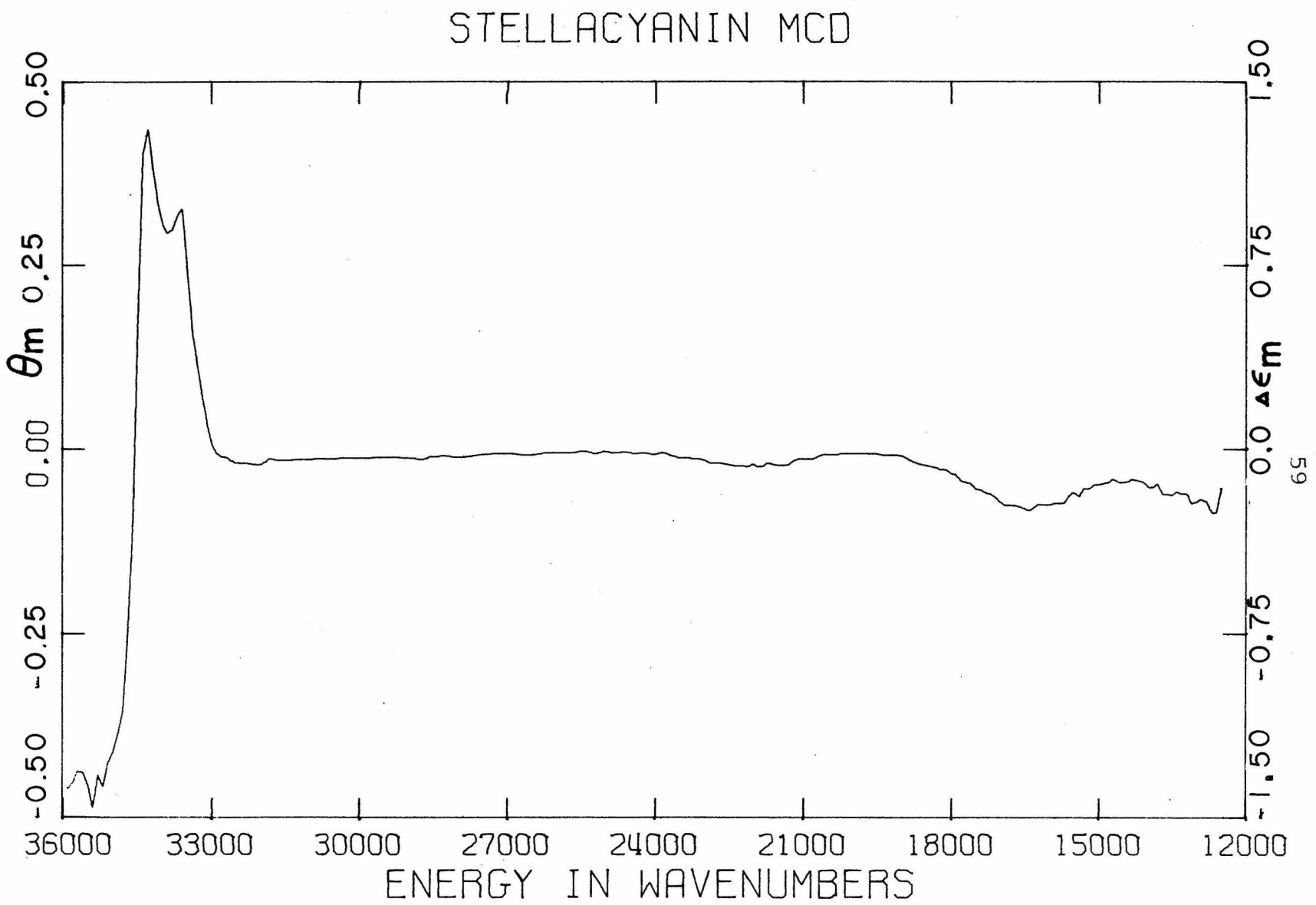
STELLACYANIN MCD
0.50
0.25
0.00
-0.25
-0.50
θm
1.50
0.75
0.0
-0.75
-1.50
Δεm
36000
33000
30000
27000
24000
21000
18000
15000
12000
ENERGY IN WAVENUMBERS

FIGURE 5

The near-infrared CD spectra of stellacyanin in a pD 6 deuterated phosphate buffer. Both scales are $\Delta\epsilon$ (1/mole-cm). For curve A use the left-hand scale and for curve B use the right-hand scale. The concentration of stellacyanin was 1.06 m<u>M</u>.

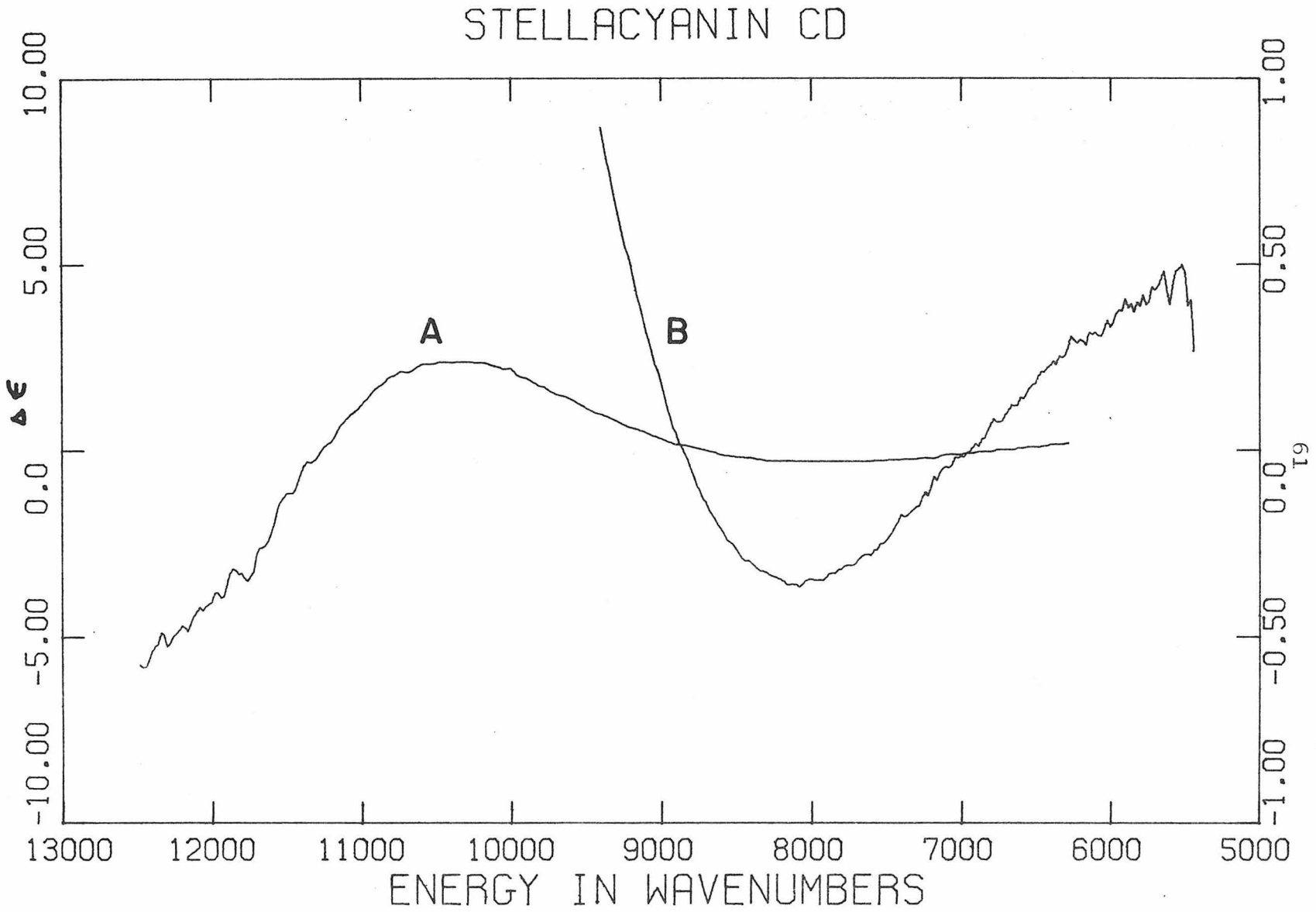
STELLACYANIN CD
10.00
5.00
0.0
-5.00
-10.00
Δε
1.00
0.50
0.0
-0.50
-1.00
A
B
13000
12000
11000
10000
9000
8000
7000
6000
5000
ENERGY IN WAVENUMBERS

FIGURE 6

The near-infrared MCD spectra of stellacyanin in pD 6 deuterated phosphate buffer. For curve A use the left-hand scale ($\Delta\epsilon$ per 10 kilogauss), and for curve B use the right-hand scale ($\Delta\epsilon$ per 10 kilogauss x 10^{-2}). The concentration of stellacyanin was 1.06 mM.

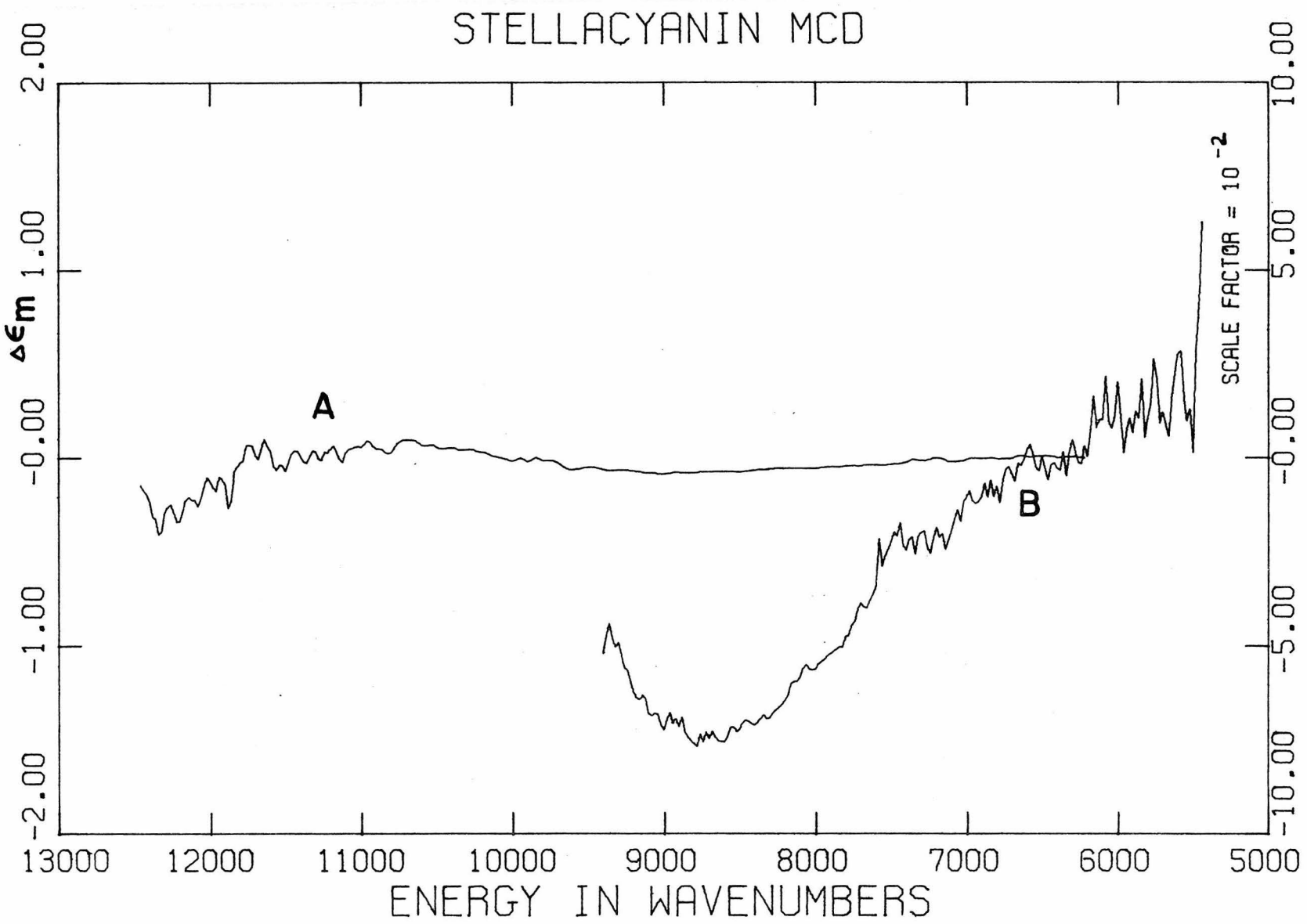
STELLACYANIN MCD
2.00
1.00
-0.00
-1.00
-2.00
Δεm
10.00
5.00
-0.00
-5.00
-10.00
SCALE FACTOR = 10 -2
A
B
13000
12000
11000
10000
9000
8000
7000
6000
5000
ENERGY IN WAVENUMBERS

presence of very weak magnetic activity in the lowest energy CD band.

The absorption spectra of French bean plastocyanin films are presented in Figure 7. The dashed curve represents the 35 K spectrum, and the solid curve is that obtained at 270 K. The latter spectrum is similar to that reported for Chenopodium album plastocyanin[1]. The major absorption band has a maximum at 16700 cm^{-1} and is assigned the solution molar extinction coefficient 4500 1 $mole^{-1}$ cm^{-1} [5]. Peaks are also observed at 12900 and 21800 cm^{-1}. The weak, high energy band shows considerable asymmetry in the thick film spectrum (7B), which resolves to a shoulder at ~24000 cm^{-1} at 35 K. As the film is cooled, all the bands narrow and increase in intensity. The decreasing breadth of the 12900 cm^{-1} peak reveals residual intensity at roughly 10000 cm^{-1}. A band at this low energy has not previously been observed. Figure 8 contains the Gaussian bands, their sum and the 35 K spectrum of plastocyanin (in symbols). The position, intensity, HWHM and oscillator strength of the Gaussian components of plastocyanin are presented as a function of temperature in Table II.

The visible CD and MCD curves of plastocyanin are shown in Figures 9 and 10, respectively. The plastocyanin CD spectrum has the same general shape as the stellacyanin CD curve. The negative band at 12800 cm^{-1} and

FIGURE 7

The near-infrared and visible absorption spectra of plastocyanin films. ϵ is the molar extinction coefficient. For the lower curves use the left-hand ϵ-scale and for the upper curves (thick film) use the right-hand ϵ-scale. The solid curves represent 270 K spectra, and the dashed curves represent 35 K spectra.

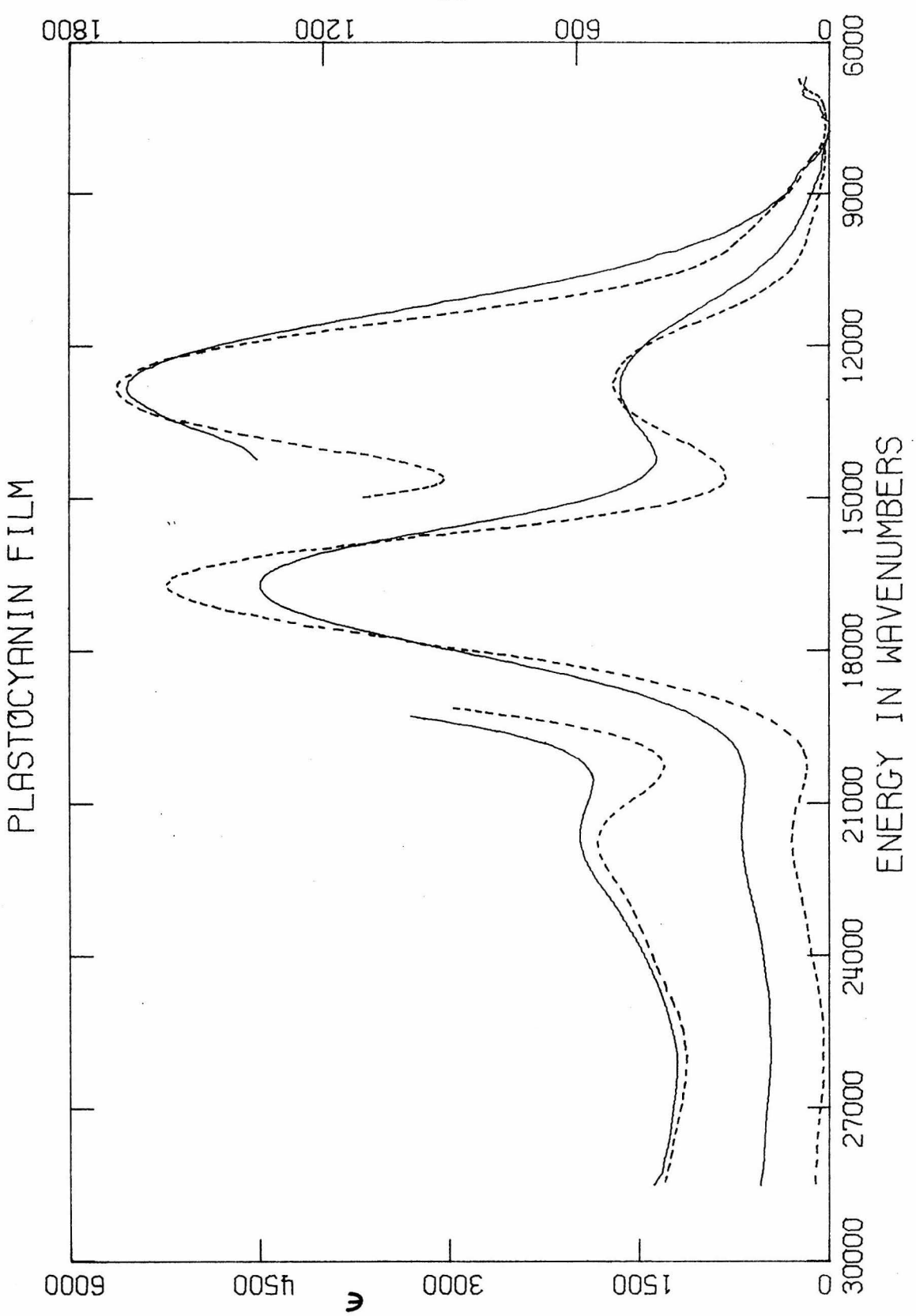
PLASTOCYANIN FILM
ε
0
1500
3000
4500
6000
1800
1200
600
0
30000
27000
24000
21000
18000
15000
12000
9000
6000
ENERGY IN WAVENUMBERS

FIGURE 8

Gaussian resolution of the 35 K near-infrared and visible absorption spectrum of a plastocyanin film. The individual peaks and sum are solid curves. The symbols(+) represent the absorption spectrum.

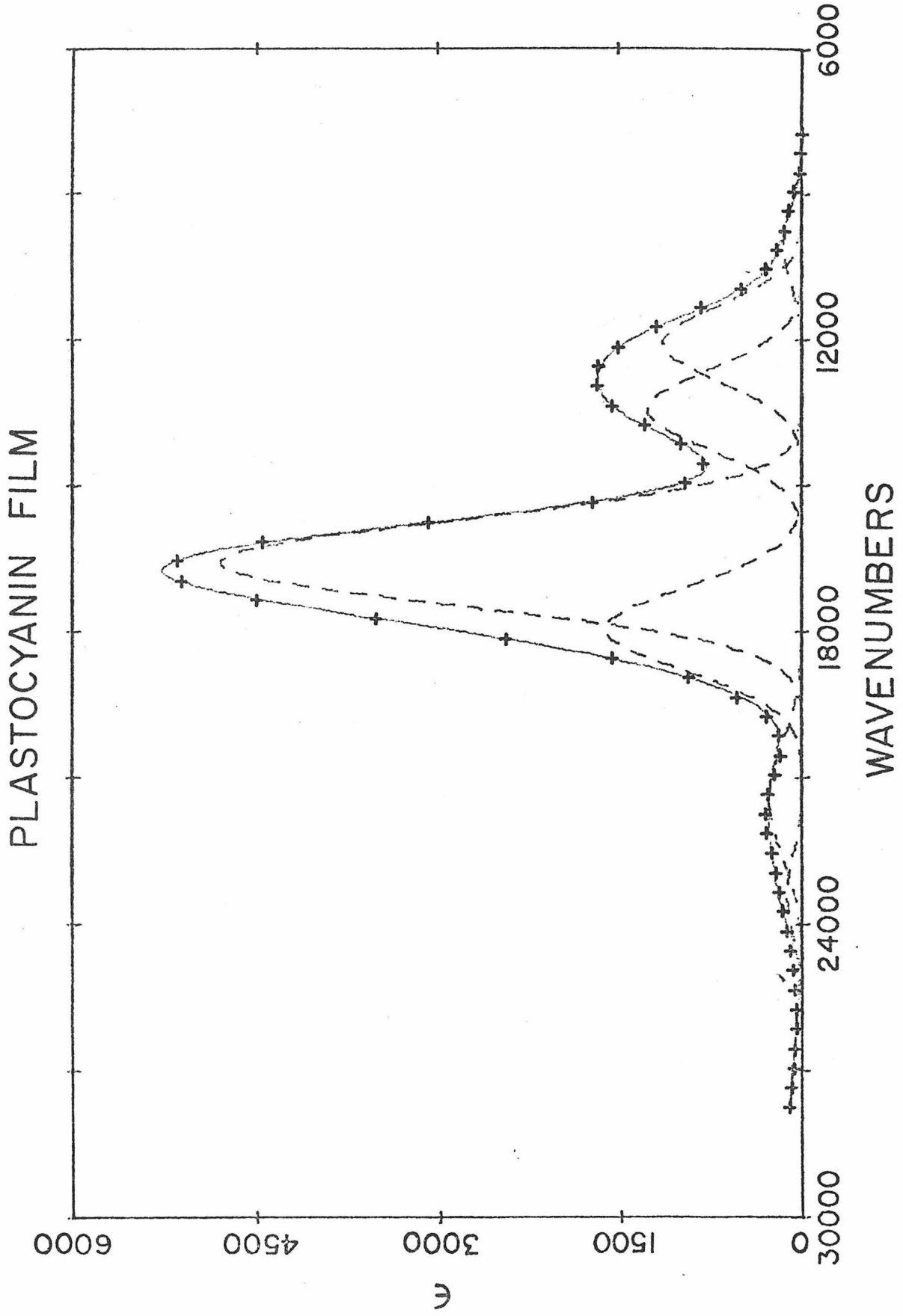
PLASTOCYANIN FILM
ε
0
1500
3000
4500
6000
30000
24000
18000
12000
6000
WAVENUMBERS

TABLE II

Gaussian Analysis of Plastocyanin Absorption Spectra

T = 35K	60K	120K	200K	270K
Band 1				
ν^1 = 23340				
f^3 = 0.0024				
Band 2				
ν = 21390	21310	22010	21910	22200
HWHM[2] = 1418	1874	2648	2757	2757
f = 0.0035	0.0060	0.011	0.012	0.019
ϵ^4 = 288	370	495	518	811
Band 3				
ν = 17870	18000	18020	17880	18100
HWHM = 985	921	926	1010	1162
f = 0.015	0.014	0.011	0.012	0.012
ϵ = 1719	1736	1314	1402	1163
Band 4				
ν = 16490	16620	16540	16440	16500
HWHM = 1003	980	1063	1148	1301
f = 0.044	0.046	0.049	0.043	0.049
ϵ = 5111	5407	5319	4354	4364
Band 5				
ν = 13350	13390	13300	13360	13330
HWHM = 959	962	966	1027	1108
f = 0.011	0.012	0.011	0.011	0.012
ϵ = 1354	1481	1371	1234	1289
Band 6				
ν = 11990	12080	11930	11870	11810
HWHM = 910	843	910	1043	1125
f = 0.0096	0.0084	0.0089	0.010	0.011
ϵ = 1222	1147	1136	1148	1162
Band 7				
ν = 9970	10150	10000	9820	9530
f = 0.0013	0.0013	0.0013	0.0014	0.0020

[1]Frequency in wave numbers
[2]Half-width at half-maximum in wave numbers
[3]Oscillator strength
[4]Molar extinction coefficient

FIGURE 9

The visible CD spectrum of plastocyanin in pD 6 deuterated phosphate buffer. The left-hand scale is molar ellipticity in deg-cm^2/decimole (x 10^4) and the right-hand scale is $\Delta\epsilon$ in 1/mole-cm. The plastocyanin concentration was 0.197 m$\underline{M}$.

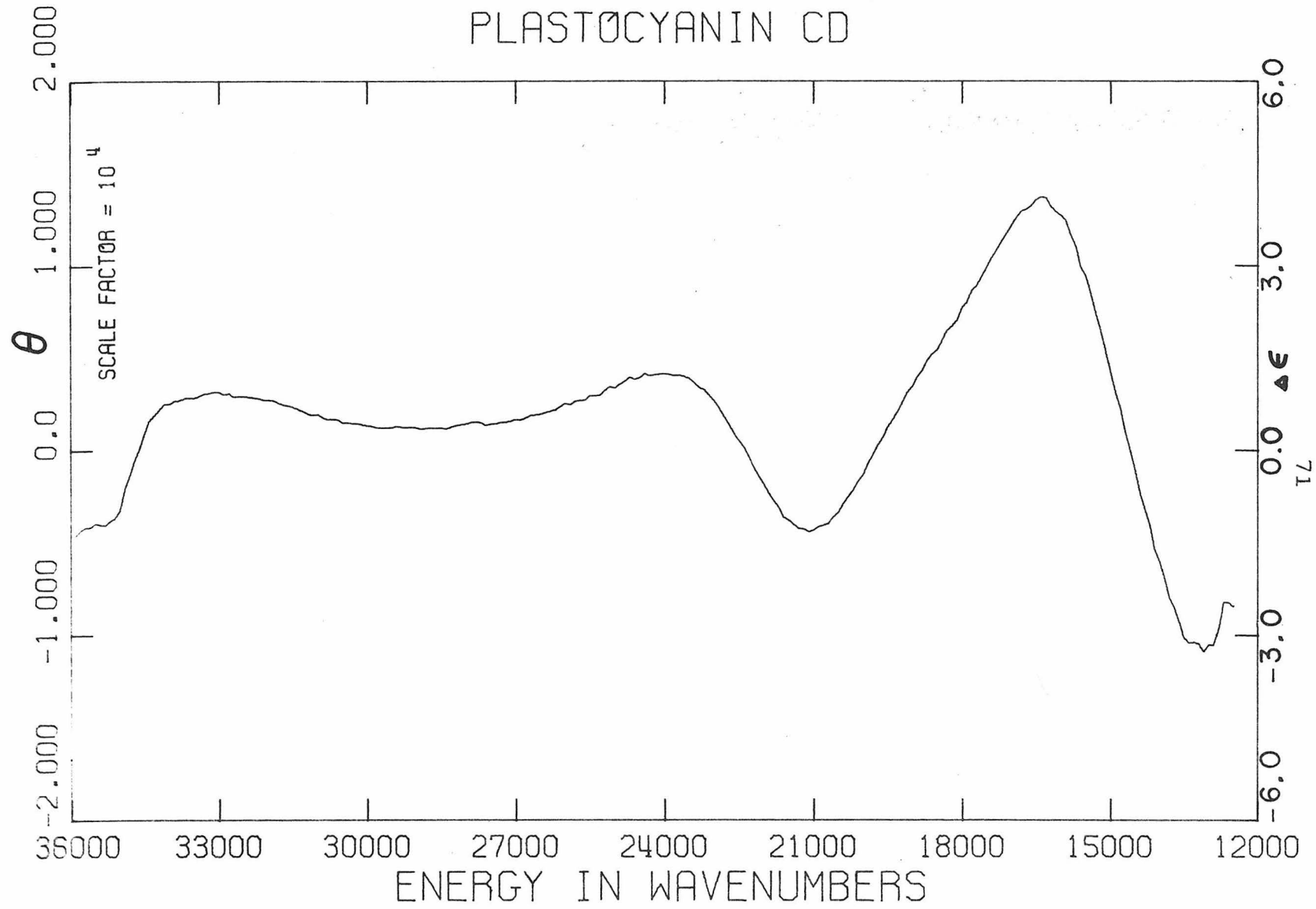
PLASTOCYANIN CD
SCALE FACTOR = 10^4
θ
Δε
2.000
1.000
0.0
-1.000
-2.000
6.0
3.0
0.0
-3.0
-6.0
36000
33000
30000
27000
24000
21000
18000
15000
12000
ENERGY IN WAVENUMBERS

FIGURE 10

The visible MCD spectrum of plastocyanin in pD 6 deuterated phosphate buffer. The left-hand scale is molar magnetic ellipticity in deg-cm^2/decimole-Gauss and the right-hand scale is $\Delta\epsilon$ per 10 kilogauss. The plastocyanin concentration was 0.197 m$\underline{M}$.

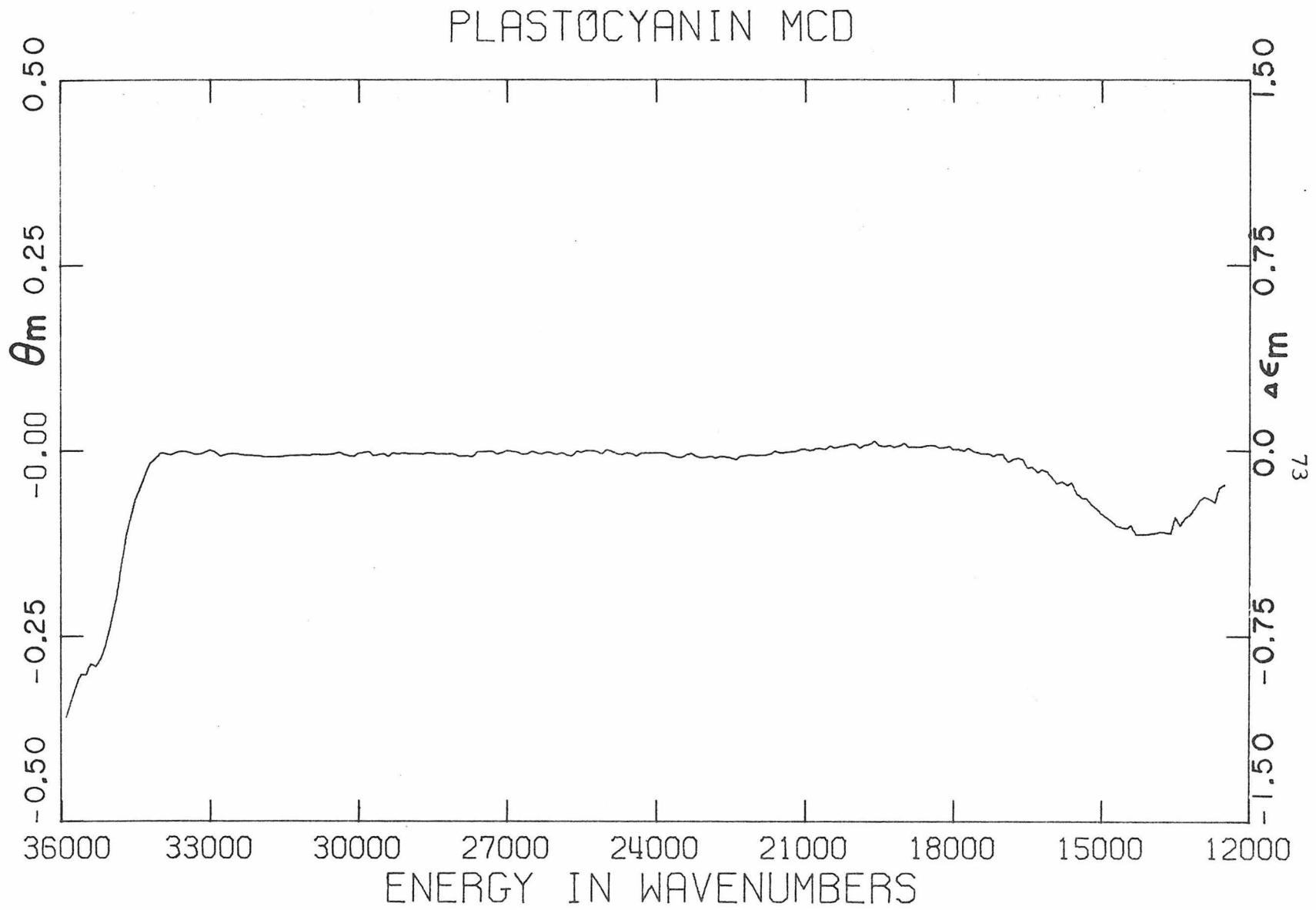
PLASTOCYANIN MCD
0.50
0.25
-0.00
-0.25
-0.50
θm
1.50
0.75
0.0
-0.75
-1.50
Δεm
36000
33000
30000
27000
24000
21000
18000
15000
12000
ENERGY IN WAVENUMBERS

the positive band at 16500 cm^{-1} are more intense in plastocyanin and the positive shoulder at ~19000 cm^{-1} is less prominent. The main difference between stellacyanin and plastocyanin occurs in the activity around 22500 cm^{-1}. In plastocyanin, two absorption peaks were observed at 21800 and 24000 cm^{-1}. The CD shows a negative band at 21200 cm^{-1} and a positive band at 24100 cm^{-1}. Stellacyanin exhibits only one absorption band and one CD band, both at 22500 cm^{-1}. The MCD spectrum shows a peak at 14100, very weak activity at ~22500 and stronger activity at 36000 cm^{-1}. No MCD activity due to tryptophan is observed in the 34000 cm^{-1} region, consistent with the amino acid analysis of Milne and Wells[5]. Figures 11 and 12 exhibit the near-infrared CD and MCD curves, respectively. These curves cut off around 10800 cm^{-1} because of the lower CD signal, more intense absorption in the 12800 cm^{-1} band and the rapid decay of detector response in this energy region. A negative band at 9200 cm^{-1} and positive activity at lower energy are observed in the expanded curve, analogous to stellacyanin. The less sensitive curve (11B) shows positive activity towards higher energy, as in stellacyanin, and presumably turns negative to match the minimum at 12500 cm^{-1} in the visible spectrum. The MCD has a minimum at ~11000 cm^{-1} and shows slight positive activity at lower energy. All CD activity

FIGURE 11

The near-infrared CD spectra of plastocyanin in pD 6 deuterated phosphate buffer. Both scales are $\Delta\epsilon$ (l/mole-cm). For curve A use the left-hand scale, and for curve B use the right-hand scale. The concentration of plastocyanin was 2.21 m<u>M</u>.

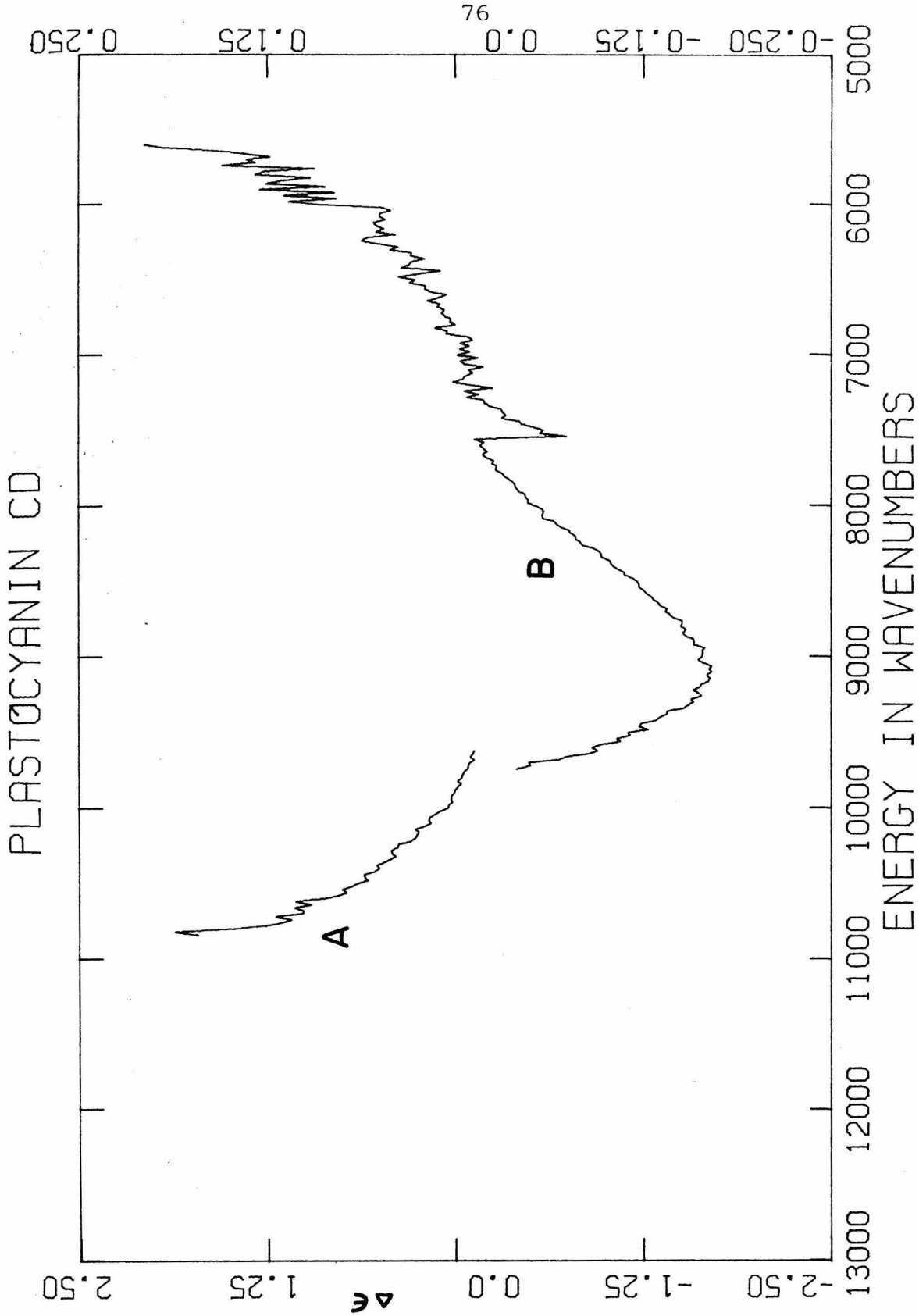
PLASTOCYANIN CD
Δε
2.50
1.25
0.0
-1.25
-2.50
0.250
0.125
0.0
-0.125
-0.250
A
B
13000
12000
11000
10000
9000
8000
7000
6000
5000
ENERGY IN WAVENUMBERS

FIGURE 12

The near-infrared MCD spectra of plastocyanin in pD 6 deuterated phosphate buffer. For curve A use the left-hand scale ($\Delta\epsilon$ per 10 kilogauss) and for curve B use the right-hand scale ($\Delta\epsilon$ per 10 kilogauss). The concentration of plastocyanin was 0.41 m$\underline{M}$.

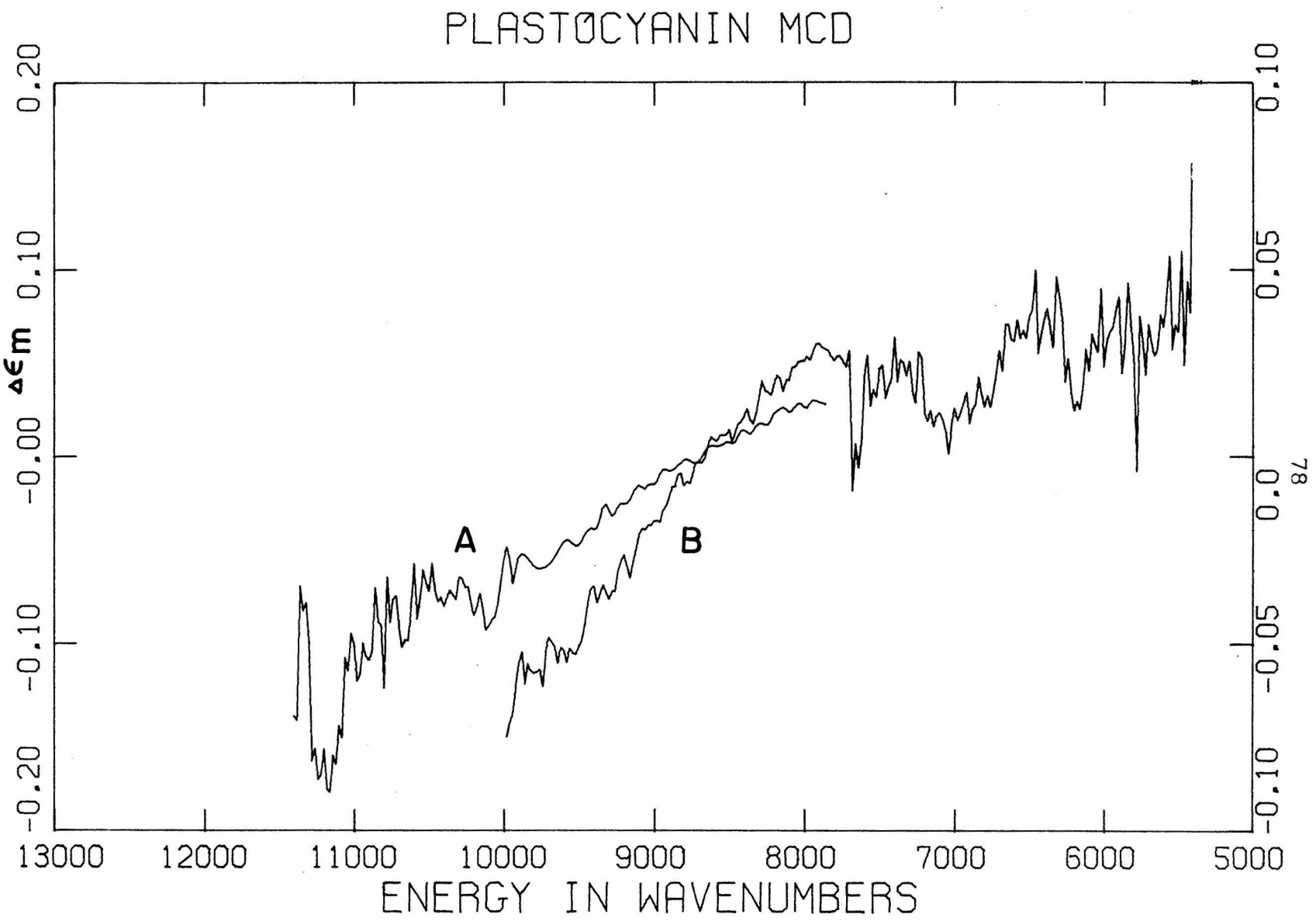
PLASTOCYANIN MCD
0.20
0.10
-0.00
-0.10
-0.20
Δεm
0.10
0.05
0.0
-0.05
-0.10
A
B
13000
12000
11000
10000
9000
8000
7000
6000
5000
ENERGY IN WAVENUMBERS

described above vanishes when the sample is reduced with dithionite.

Figure 13 contains the absorption spectra of azurin (Pseudomonas aeruginosa) films. Again, the dashed and solid lines represent spectra at 35 K and 270 K, respectively. The 270 K film spectrum matches the solution spectrum of Tang, et al.[6] Narrowing of the 12400 cm^{-1} band at 35 K reveals a weak absorption at ~10000 cm^{-1} in the thick film spectrum (13B). The resolved Gaussian bands, their sum and the 35 K spectrum (in symbols) of azurin are shown in Figure 14. The Gaussian positions, HWHM's, intensities and oscillator strengths are listed as a function of temperature in Table III.

The visible CD and MCD curves of azurin are shown in Figure 15 and 16, respectively. The CD spectrum is identical to that reported by Tang, et al.[6], except that the lowest energy band (~12500 cm^{-1}) is almost three times more intense in the present spectrum. (Tang, et al. used a Cary 60 spectropolarimeter, an earlier instrument than the Cary 61, which may have poorer response at the long wavelength limit of the instrument.) The visible MCD spectrum of azurin has a negative band at 14400 cm^{-1}, a weak derivative-like signal centered at 24300 cm^{-1} and a strong activity associated with tryptophan at ~34000 cm^{-1}. The infrared

FIGURE 13

The near-infrared and visible absorption spectra of azurin films. ϵ is the molar extinction coefficient. For the lower curves use the left-hand ϵ-scale and for the upper curves (thick film) use the right-hand ϵ-scale. The solid curves represent 270 K spectra, and the dashed curves represent 35 K spectra.

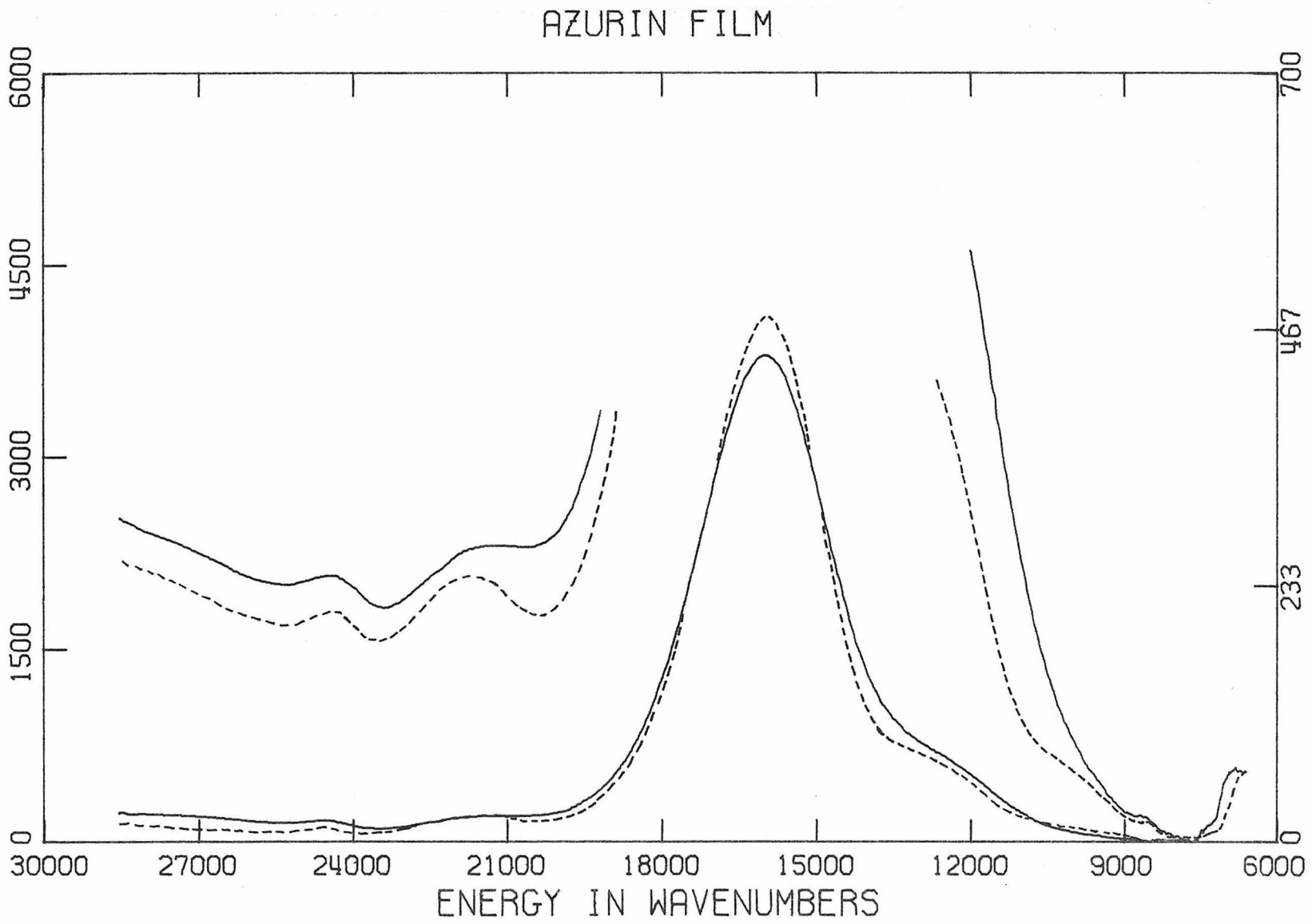
AZURIN FILM
6000
4500
3000
1500
0
700
467
233
0
30000
27000
24000
21000
18000
15000
12000
9000
6000
ENERGY IN WAVENUMBERS

FIGURE 14

Gaussian resolution of the 35 K near-infrared and visible absorption spectrum of a azurin film. The individual Gaussian peaks and sum are solid curves. The symbols(+) represent the absorption spectrum.

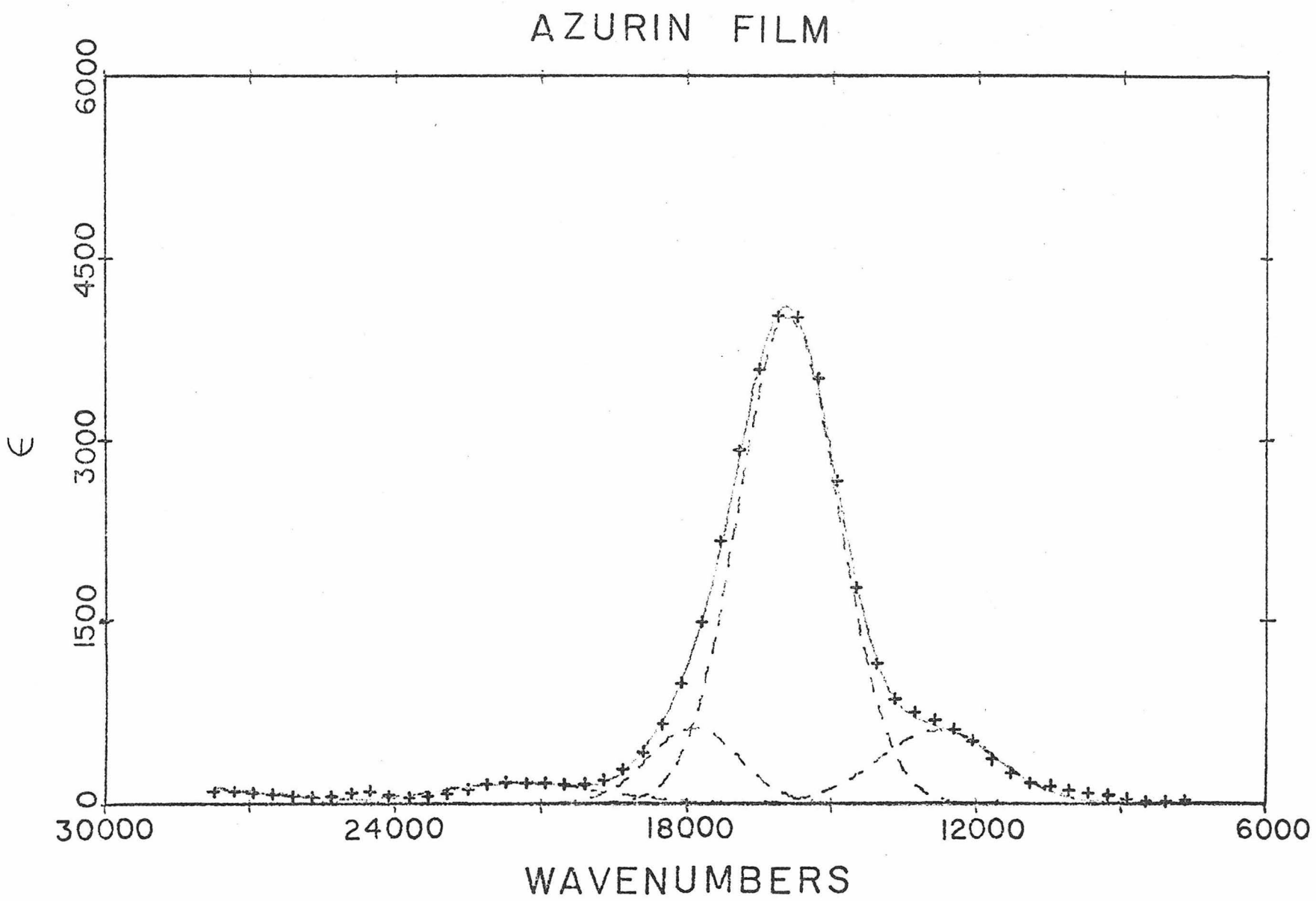
AZURIN FILM
6000
4500
3000
1500
0
ε
30000
24000
18000
12000
6000
WAVENUMBERS

TABLE III

Gaussian Analysis of Azurin Absorption Spectra

T = 35K	60K	120K	200K	270K
Band 1				
ν[1] = 21450	20060	20400	21410	20790
HWHM[2] = 2099	2090	2984	3670	4144
f[3] = 0.0034	0.0026	0.0026	0.0059	0.0071
ϵ[4] = 185	145	101	185	198
Band 2				
ν = 17820	17600	17540	17590	17650
HWHM = 1078	1038	1099	1156	1252
f = 0.006	0.007	0.0072	0.0064	0.0055
ϵ = 641	778	755	640	504
Band 3				
ν = 15870	15860	15820	15810	15850
HWHM = 1210	1174	1206	1261	1334
f = 0.045	0.042	0.042	0.042	0.044
ϵ = 4278	4167	4021	3826	3798
Band 4				
ν = 12770	12920	12800	12810	12830
HWHM = 1468	1592	1380	1500	1591
f = 0.008	0.0083	0.0067	0.0084	0.0094
ϵ = 632	605	566	647	686

[1]Frequency in wave numbers
[2]Half-width at half-maximum in wave numbers
[3]Oscillator strength
[4]Molar extinction coefficient

FIGURE 15

The visible CD spectrum of azurin in pD 6 deuterated phosphate buffer. The left-hand scale is molar ellipticity in deg-cm^2/decimole (x 10^4) and the right-hand scale is $\Delta\epsilon$ in 1/mole-cm. The azurin concentration was 0.21 m$\underline{M}$.

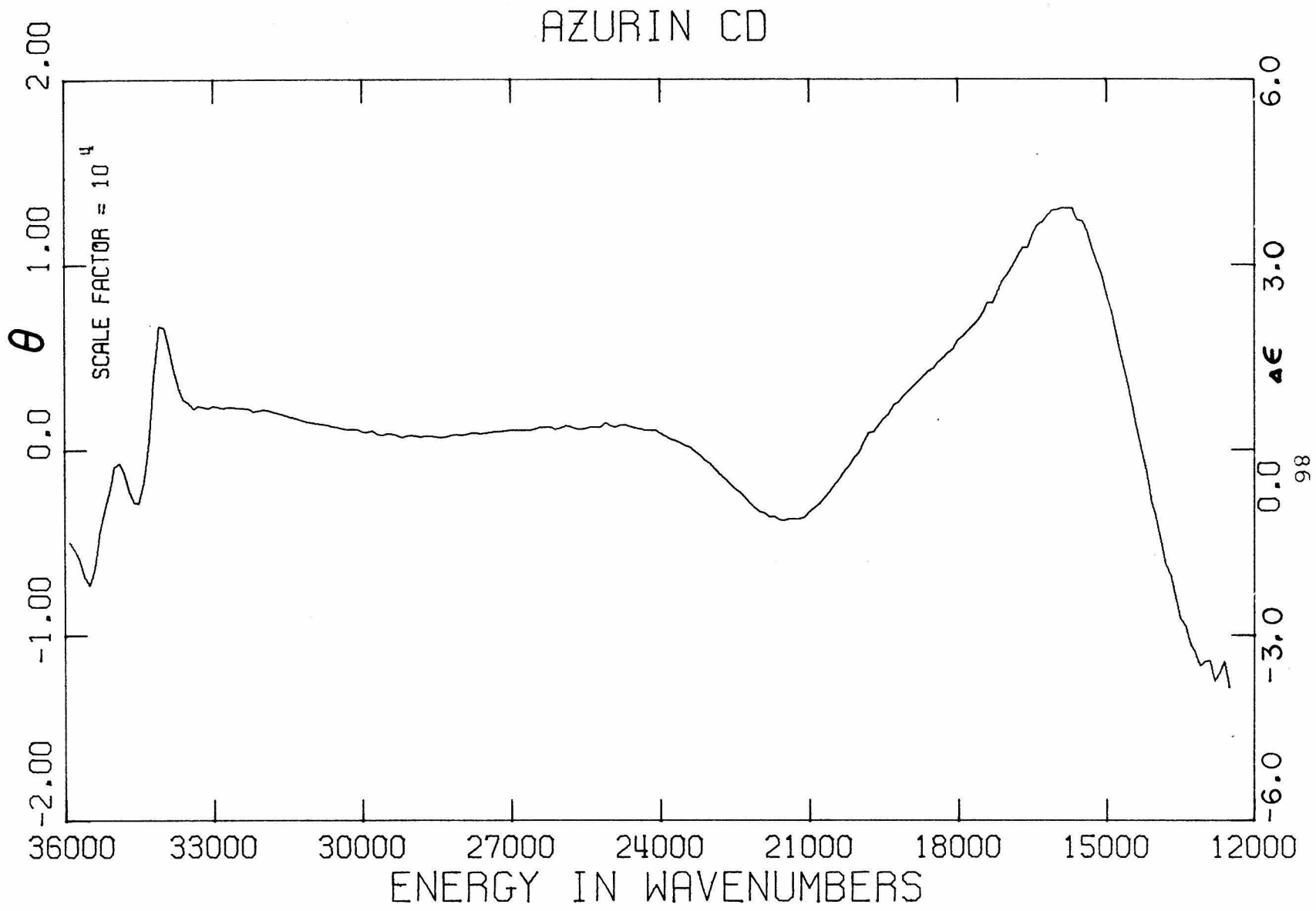
AZURIN CD
SCALE FACTOR = 10^4
θ
Δε
2.00
1.00
0.0
-1.00
-2.00
6.0
3.0
0.0
-3.0
-6.0
36000
33000
30000
27000
24000
21000
18000
15000
12000
ENERGY IN WAVENUMBERS

FIGURE 16

The visible MCD spectrum of azurin in pD 6 deuterated phosphate buffer. The left-hand scale is molar magnetic ellipticity in deg-cm^2/decimole-Gauss and the right-hand scale is $\Delta\epsilon$ per 10 kilogauss. The azurin concentration was 0.21 m$\underline{M}$.

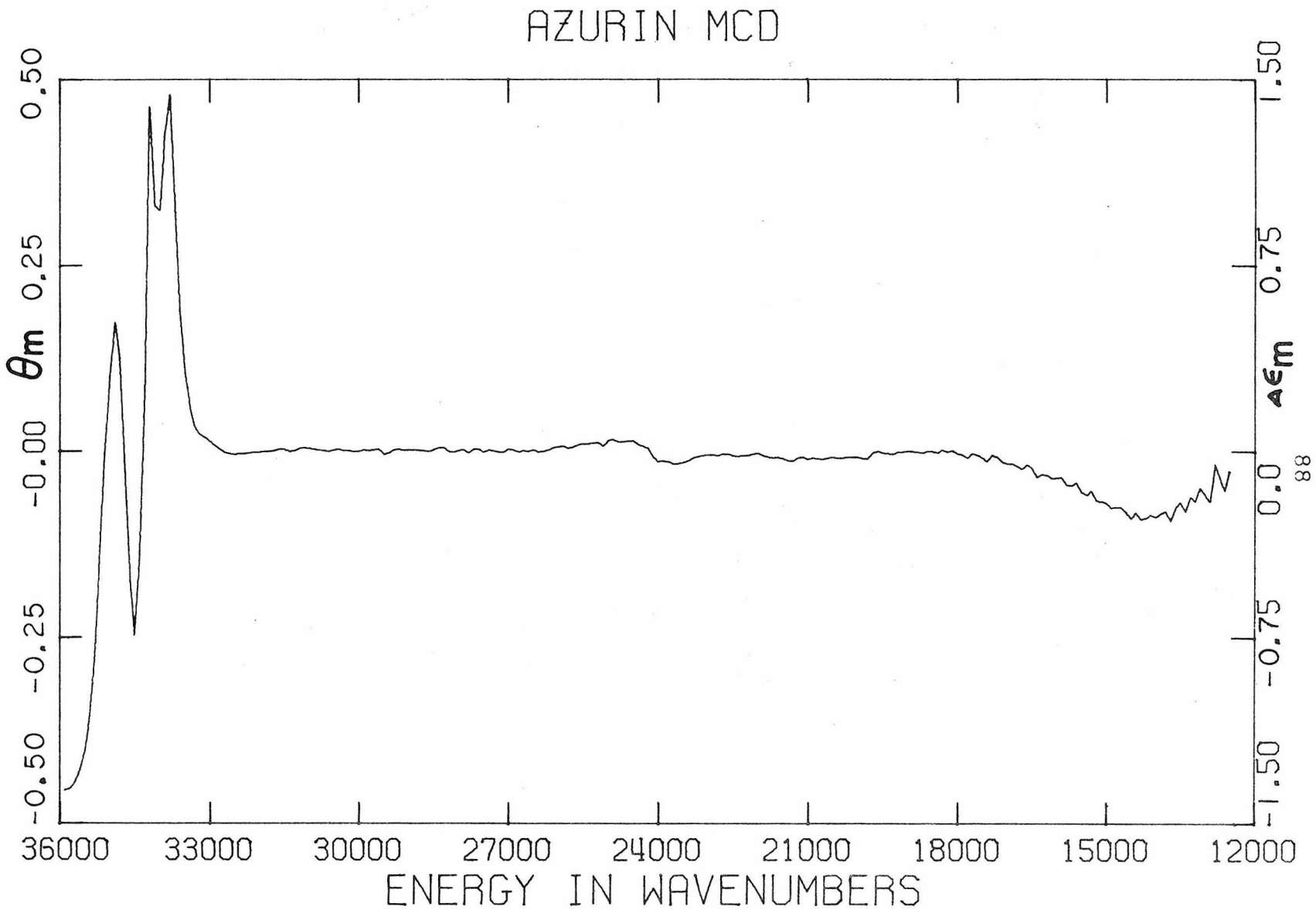
AZURIN MCD
0.50
0.25
-0.00
-0.25
-0.50
θm
1.50
0.75
0.0
-0.75
-1.50
Δεm
36000
33000
30000
27000
24000
21000
18000
15000
12000
ENERGY IN WAVENUMBERS

CD and MCD curves are given in Figures 17 and 18, respectively. Once again, there is a gap where the spectrum could not be recorded. The more sensitive spectrum (17B) shows a minimum at 9250 cm^{-1} and increasing positive activity towards lower energy to the instrument and solvent cutoff. Spectrum 17A shows no positive activity to the lower energy side of the 12500 cm^{-1} band, as observed in stellacyanin and indicated in plastocyanin. The MCD spectrum shows a negative band at ~10500 cm^{-1}. The infrared CD bands of azurin were not observed in a sample reduced with dithionite.

DISCUSSION

Before proceeding with the assignment of these spectra, a comment on actual symmetry compared to effective symmetry is worthwhile. The actual symmetry of the copper site in these blue metalloproteins is no doubt C_1. However, the resolution of a particular physical measurement may not be fine enough to detect the minor differences between certain ligands, which account for the actual symmetry. An effective symmetry, higher than the actual symmetry, can then be used to describe the system, resulting in a simplification of the parameters involved. For example, the plastocyanin[1] and azurin[2] EPR spectra have been described in terms of

FIGURE 17

The near-infrared CD spectra of azurin in pD 6 deuterated phosphate buffer. Both scales are $\Delta\epsilon$ (l/mole-cm). For curve A use the left-hand scale, and for curve B use the right-hand scale. The concentration of azurin was 0.21 m<u>M</u>.

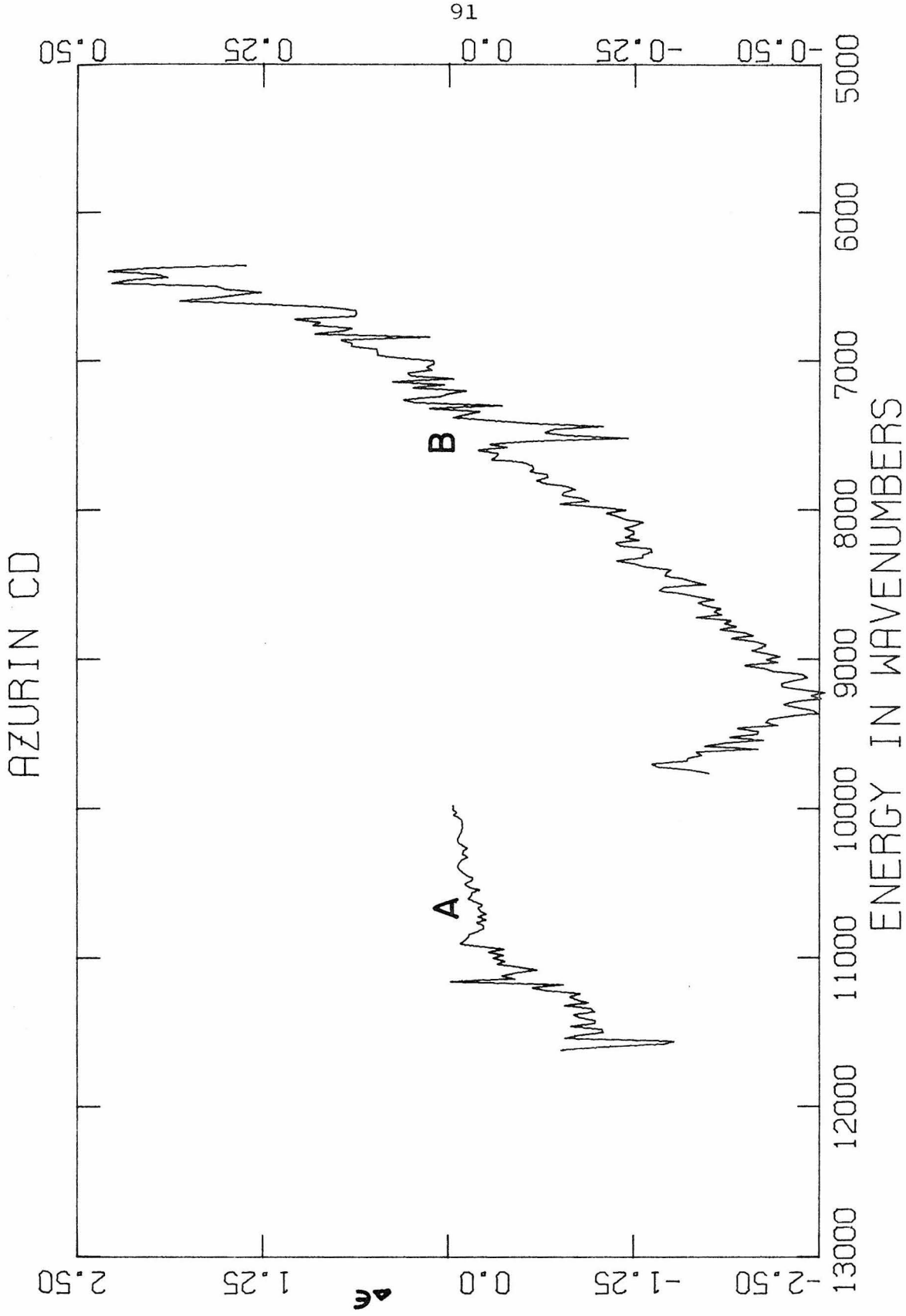
AZURIN CD
ENERGY IN WAVENUMBERS
Δε
A
B
-2.50
-1.25
0.0
1.25
2.50
13000
12000
11000
10000
9000
8000
7000
6000
5000
-0.50
-0.25
0.0
0.25
0.50

FIGURE 18

The near-infrared MCD spectrum of azurin in pD 6 deuterated phosphate buffer. The scale is $\Delta\epsilon$ per 10 kilogauss. The concentration of azurin was 0.69 m$\underline{M}$.

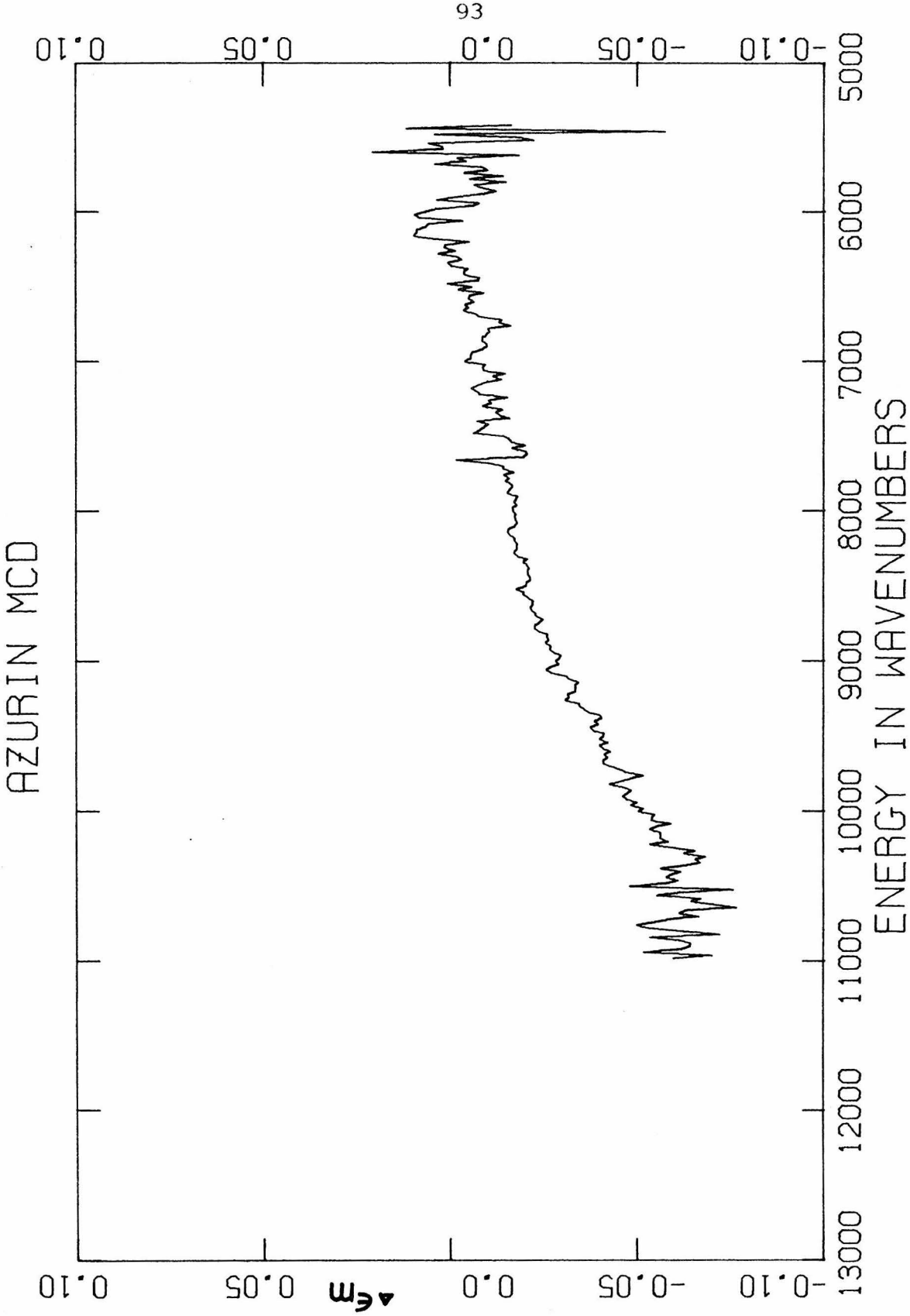
AZURIN MCD
ENERGY IN WAVENUMBERS
5000
6000
7000
8000
9000
10000
11000
12000
13000
0.10
0.05
0.0
-0.05
-0.10
Δε M

axial symmetry. The ligands perpendicular to a pseudo-major rotation axis are similar enough to observe no resolution of g_x and g_y. Stellacyanin is distorted enough to resolve g_x from g_y, so that the EPR spectrum must now contain a rhombic term[4]. The symmetries referred to below are effective in the sense that they are generally the highest ones that allow an adequate interpretation of the physical measurements.

New absorptions and CD spectral features have been observed in the near-infrared. The CD bands are dependent upon oxidation state of the copper and are, therefore, most likely electronic transitions within the blue site. The energy of the second transition ($\sim$10000 cm^{-1}) corresponds to that observed in the absorption spectrum. The energy and molar extinction coefficient (100-200 l $mole^{-1}$ cm^{-1}) of this transition are within the ranges normally found for a d-d transition of the cupric ion. The existence of d-d bands at $\sim$5000 and 10000 cm^{-1} rules out both six and five coordinate complexes. The lowest band of the $CuCl_5^{-3}$ ion is 8200 cm^{-1} [16]. As nitrogen coordination is most prevalent in amino acid copper complexes, a five coordinate site would be expected to have even higher energy bands. Transitions are observed at 15000 and 11400 cm^{-1} for square pyramidal $Cu(NH_3)_5^{+2}$ [17]. A trigonally distorted tetrahedron (C_{3v} symmetry) can be

discarded, as $g_{\perp}$ is expected to be larger than $g_{\parallel}$, contrary to the observed ordering. (Cupric ion doped into the trigonal site of ZnO has $g_{\parallel} = 0.74$ and and $g_{\perp} = 1.53$, as predicted[18].) Further, the excited states of C_{3v} Cu(II) are both ^2E in symmetry. Opposite signs for the 5000 and 10000 cm^{-1} CD bands establish that the two transitions are to excited states of different symmetries.

Square planar geometries are usually found in amino acid-copper complexes[19]. The g-values obtained from EPR spectra are generally quite close to those observed for the blue proteins[20,21]. However, the energies of the d-d transitions for square planar complexes of copper are unusually high for four coordinate geometries, being observed at 15400-17700 and 17500-20600 cm^{-1} for the amino acid complexes[20], at 15500, 18500, 19300 and 24000 cm^{-1} for a CuN_2S_2 complex[22] and at 10500-10900 and 12800-14300 cm^{-1} for $CuCl_4^{-2}$ [16,23]. The large d-orbital splittings of the square plane are greatly reduced by a D_{2d} distortion toward tetrahedral geometry. The $CuCl_4^{-2}$ ion is known to exist in both square planar and tetragonally distorted tetrahedral geometry, depending on the counter ion in the crystal lattice[24]. The ligand field bands of Cs_2CuCl_4 have been assigned by Ferguson[25], the ^2E state being split

by both spin-orbit coupling and low site symmetry to components at 4800 and 5550 cm^{-1}. The $^2B_1$ and $^2A_1$ transitions are found at 7900 and 9050 cm^{-1}, respectively. This strong dependence of the ligand field energy levels on the angle between the z-axis and the metal ligand bond (β) accounts for the large decrease observed in the energy levels of the blue proteins in comparison to the peptide-copper complexes. Flattened tetrahedral symmetry has been proposed for the blue copper site by several authors[9,26]. Their reasoning, however, was based on assigning the intense visible bands as d-d transitions and invoking the odd-order terms derived from D_{2d} distortion of the square plane to account for the unusually high intensities. (The molar extinction coefficient for Cs_2CuCl_4 is on the order of 500 l $mole^{-1}$ cm^{-1}, so that values in excess of 1000 l $mole^{-1}$ cm^{-1} would seem too high to be attributed to d-d transitions, even including odd-order intensification mechanisms.)

Recent x-ray photoelectron and resonance Raman spectral studies have identified cysteine sulfur[27] and deprotonated amide nitrogen (or oxygen)[28], respectively, as probable ligands at the blue site. The existence of highly reducing ligands at the site, the observed shift of the 600 nm system to higher energy upon Co(II)

substitution for Cu(II)[13] and the large molar extinction coefficients suggest that the manifold at 12500, 16000 and 21500 cm^{-1} is attributable to ligand to metal charge transfer transitions. Sulfur to copper charge transfer has been observed from 10400 to 28240 cm^{-1} in Cu(II) doped ZnS[29], at 26700 and 28000 cm^{-1} in a thiosemicarbazide complex[22], 25640 and 30000 cm^{-1} in a square planar penicillamine complex[30] and at 25300 and 30300 cm^{-1} in cysteine-copper complexes[31]. Recently, a peptide-copper complex containing cysteine has been prepared and reported to have a intense band at $\sim$ 25000 cm^{-1}, presumably due to sulfur to copper charge transfer[32]. A d-d band was identified at 17500 cm^{-1}. Bryce and Gurd have assigned ORD maxima at 28570, 31250 and 32260 cm^{-1} for copper complexes of acetyl-glycyl-glycyl-L-histidine, acetyl-glycyl-L-histidylglycine and glycyl-L-valine, respectively, as charge transfer transitions from coordinated amide nitrogen, or possibly histidine[33]. Wilson, et al. have assigned absorptions at 37000 and 42500 cm^{-1} to charge transfer transitions from the imidazole conjugated nitrogen to copper[34]. The transitions are moderate ($\epsilon \cong$ 800 and 2400 l $mole^{-1}$ cm^{-1}) and are masked by the more intense primary amine to copper charge transfer in histidine-copper complexes. As mentioned above, square planar CuN_2S_2 complexes,

where S represents a deprotonated sulfhydryl group, have a shoulder at ~25000 cm^{-1} and an intense peak ($\epsilon \cong 6000$ l $mole^{-1}$ cm^{-1}) at 30000 cm^{-1}, which have been assigned as sulfur to copper charge transfer transitions. The charge transfer energies assigned in this study are some 12-15000 cm^{-1} lower in energy. To account for this discrepancy, the charge transfer region of the tetrachlorocuprate(II) ion is considered. In square planar $CuCl_4^{-2}$, $\pi \rightarrow d_{x^2-y^2}$ charge transfer occurs at 33300 cm^{-1} and $\sigma \rightarrow d_{x^2-y^2}$ at 38500 and 49000 cm^{-1} [23]. The lowest π charge transfer transitions in tetragonal $CuCl_4^{-2}$ are observed at 24850 and 28400 cm^{-1}, while the lowest σ transitions occur at 33900 and 43000 cm^{-1} [25,35]. This shift of 6-8000 cm^{-1} as the square planar configuration is distorted towards a tetrahedron roughly corresponds to the energy decrease observed in the d-d transitions, and can be explained from the ligand field theory as a drop in energy of the $d_{x^2-y^2}$ orbital as the ligands are moved away from the xy plane. From the molecular orbital viewpoint, there is a decrease in overlap between the ligand LCAO's and the metal $d_{x^2-y^2}$ orbital as the ligands bend away from the xy plane. As the charge transfer is from the predominantly ligand bonding orbitals to the predominantly copper antibonding d-orbitals, a decrease in the overlap

will lower the energy difference between the two orbitals. This accounts for approximately half of the observed energy difference in the sulfur-copper system. The remainder may be due to different bond lengths between copper and sulfur available in the protein but not allowed in the simpler model complexes. Similar arguments can be made for lowering the energy of the amide nitrogen to copper charge transfer from ~31000 cm^{-1} to the visible region.

Pi to d_{xy} charge transfer has the symmetry E in D_{2d}, while σ to d_{xy} transitions are of B_2 symmetry.[60] Both are electric dipole allowed, but only the π transitions are magnetic dipole allowed. The rotational strength of a CD band (R) is related to the electric dipole moment ($\vec{\mu}_{el}$) and the magnetic dipole moment ($\vec{\mu}_{mag}$) by the equation:

$$R = \mathrm{Im}\left[\int \psi_i^* \, \vec{\mu}_{el} \, \psi_f \, d\tau \cdot \int \psi_i^* \, \vec{\mu}_{mag} \, \psi_f \, d\tau\right], \qquad (1)$$

where ψ_i and ψ_f are the initial and final states, respectively[36]. Gillard has also equated the rotational strength to the experimental quantity $\Delta\epsilon$ ($\epsilon_l - \epsilon_r$) by the equation:

$$R = 22.9 \times 10^{-40} \int (\Delta\epsilon/\nu) \, d\nu \qquad (2)$$

and the dipole strength (D) to the molar extinction

coefficient ϵ by

$$D = 91.8 \times 10^{-40} \int (\epsilon/\nu) d\nu. \qquad (3)$$

Finally, he has shown that $4R/D \approx \gamma$, the Kuhn anisotropy factor. Bands showing values of γ greater than 0.01 must be assigned as a magnetic dipole transition. Thus, evaluation of γ for the blue site transitions observed should be of value in identifying σ and π bands. Assuming a Gaussian band shape, Moscowitz has approximated the integral $\int (\epsilon/\nu) d\nu$ as $1n2\sqrt{\pi}\epsilon^{\circ}\delta^{\circ}/\nu^{\circ}$, where ϵ° is the maximum value of ϵ, δ° is the half-width at half maximum and ν° is the frequency of ϵ° [37]. If the value of δ° is assumed to be the same for corresponding absorption and CD bands, γ may be calculated from the equation:

$$\gamma = (\Delta\epsilon)/\epsilon. \qquad (4)$$

Values of γ, $\Delta\epsilon$ and ϵ for the electronic transitions of stellacyanin, plastocyanin and azurin are listed in Table IV. The bands at ~14000 and 22000 cm^{-1} are assigned to π charge transfer, as they have values of γ quite close to 0.01. The 16000 cm^{-1} bands have γ-values roughly five times smaller than the π charge transfer bands and, therefore, contain significantly less magnetic dipole character. These bands are attributed to σ

TABLE IV

Kuhn Anisotropy Factors for Blue Protein Electronic Transitions

	ν[1]	$\Delta\epsilon$[2]	ϵ[3]	γ[4]
Azurin	21600	-1.11	185	0.006
	18530	0.72	504	0.0014
	16700	3.96	3798	0.001
	13700	-3.6	686	0.005
	10300	-0.475	82	0.006
Stellacyanin	23000	-7.35	942	0.008
	18300	0.75	1542	0.0005
	17000	3.6	3549	0.001
	13500	-5.0	341	0.015
	11900	2.4	565	0.004
	8750	-0.35	~100	~0.0035
	5250	0.45	~100	~0.0045
Plastocyanin	24200	1.26	~100	~0.012
	22300	-1.32	300	0.0045
	18900	0.4	1163	0.0004
	17360	4.08	4364	0.0009
	14300	-3.78	1289	0.003
	12700	~1.5	1162	0.0013
	10300	-0.165	200	0.0008
	5500	0.125	~100	0.0013

[1]Frequency in wave numbers

[2]$\epsilon_l - \epsilon_r$

[3]Molar extinction coefficient

[4]Anisotropy factor

charge transfer transitions. Further, Ibarra, et al. have shown theoretically that π charge transfer transitions should be of opposite sign to σ charge transitions[38], as is observed experimentally.

It should be noted that the 24500 cm^{-1} band of azurin was not included in Table IV. This band has a unique MCD shape (see Figure 16) not observed for any other blue site transition. The MCD curve and energy position of the absorption band agree with the assignment of this band to the Soret transition of cytochrome impurities[39], which are often found in the Pseudomonas azurin isolation[40].

The MCD curves have the form of B- and C-terms[41]. The transitions observed are probably C-terms, although spectra at several temperatures are needed to prove their existence. Buckingham and Stephens also derived selection rules for the various MCD terms. A C-term must have a non-zero value for the integral $< a|\vec{m}|a >$, where a represents the ground state wavefunction, and $\vec{m}$ is the magnetic moment. For a transition metal ion the magnetic moment may be represented by the Zeeman operator, so that any ground state having Kramers degeneracy may exhibit a C-term in the MCD spectrum. The near-infrared bands assigned as d-d transitions have MCD activity in all three proteins. They also

have a negative peak at ~14000 cm^{-1}, near the first π charge transfer transition in the CD and absorption spectra. The MCD bands may also be derived from this transition, except that the energy ordering in the CD and absorption spectra is plastocyanin > azurin ≈ stellacyanin, whereas the MCD spectra have the order azurin ≈ plastocyanin > stellacyanin, the same as that observed for the second d-d transition. This band, therefore, may be associated with the third ligand field transition in the copper(II) center.

Low temperature absorption and CD spectral studies have produced new spectral information concerning the electronic structure of the blue site. Although the absorption spectra sharpened somewhat at low temperatures, the bands remained broad and featureless. Moment analysis is a method derived specially for extracting information from such bands. The n^{th} moment is defined as:

$$M^n = \int (\nu - \bar{\nu})^n I(\nu)d\nu / \int I(\nu)d\nu, \qquad (5)$$

where $\bar{\nu}$ is the mean frequency of the band and $I(\nu)$ is the intensity at ν. Lax has shown that the second moment can be related to the vibrational frequency of a single mode strongly coupled to the electronic wavefunction or the mean of many modes weakly coupled to the electronic wavefunction according to the equation[42]:

$$M^2 = C^2 \nu^2 \coth (\nu^2/2kT). \quad (6)$$

Numerical integration of the absorption band according to equation 5 is the most direct method of obtaining the desired moment, when the absorption band is due to one electronic transition. The absorption band at 17000 cm^{-1} has been shown (vide supra) to consist of two transitions, which must be resolved before the second moments can be calculated. This band has been resolved into Gaussian components and the results presented in Tables I, II and III for stellacyanin, plastocyanin and azurin, respectively. The second moment of a Gaussian band is easily found to be $(HWHM)^2/ 2 \ln 2$, so that the half-width at half-maximum may be related to temperature according to the equation:

$$(HWHM)^2 = 2 C'^2 \nu^2 \coth (\nu^2/2kT). \quad (7)$$

The values of C'^2 and ν are presented in Table V. The mean vibrational energy coupled with the σ charge transfer transition varies from 242 ± 60 cm^{-1} for plastocyanin to 387 ± 145 cm^{-1} for azurin. In accord with these calculations, major resonance Raman transitions are observed at ~420 and 350 cm^{-1} in azurin and at ~260 cm^{-1} in plastocyanin[28].

Ligand field calculations

Location of d-d bands in the spectra of blue

TABLE V

Temperature Dependence of the Bandwidth of the 600 nm Absorption in Blue Proteins

Stellacyanin

	Band 2			Band 3	
T	HWHM(calc)[a]	HWHM(obs)	T	HWHM(calc)[b]	HWHM(obs)
200	1171	1134	200	994	1012
120	1036	990	120	905	889
60	984	967	60	877	876
35	981	942	35	876	883

[a] $h\nu = 282 \pm 80\ cm^{-1}$ $\quad C'^2 = 5.88$

[b] $h\nu = 288 \pm 80\ cm^{-1}$ $\quad C'^2 = 4.63$

Plastocyanin

	Band 3			Band 4	
T	HWHM(calc)[c]	HWHM(obs)	T	HWHM(calc)[d]	HWHM(obs)
200	1056	1010	200	1171	1148
120	954	926	120	1036	1063
60	922	921	60	984	980
35	921	985	35	981	1003

[c] $h\nu = 277 \pm 70\ cm^{-1}$ $\quad C'^2 = 5.52$

[d] $h\nu = 242 \pm 60\ cm^{-1}$ $\quad C'^2 = 8.21$

Azurin

	Band 2			Band 3	
T	HWHM(calc)[e]	HWHM(obs)	T	HWHM(calc)[f]	HWHM(obs)
200	1151	1156	200	1249	1261
120	1062	1099	120	1185	1206
60	1039	1038	60	1174	1174
35	1038	1078	35	1174	1210

[e] $h\nu = 316 \pm 97\ cm^{-1}$ $\quad C'^2 = 5.40$

[f] $h\nu = 387 \pm 145\ cm^{-1}$ $\quad C'^2 = 4.60$

copper proteins allows a recalculation of the ligand field parameters. Previous calculations have been based on the assignment of the intense visible bands to ligand field transitions[9,26]. As noted earlier, the energies of these absorptions require a nearly planar arrangement of four nitrogen-like ligands (fifth and sixth axial ligands may be present, but situated at much longer distances from the copper). The unusual intensity of these bands was accounted for by small out-of-plane distortion allowing the mixing of charge transfer character into the d-wavefunctions. The observation of low energy electronic excitations imply a considerable distortion from square planar geometry towards a tetrahedron, thus the electronic structures of the blue proteins are more correctly described as tetragonally distorted tetrahedra.

The coordinate system used for the calculations is illustrated in Figure 19. A rotation of 45° about the z-axis will transform this system into the standard tetrahedral system. The present system corresponds to the square planar coordinates commonly used and was chosen for consistency with the molecular orbital calculations, where computations were somewhat simplified by this coordinate scheme. For T_d symmetry, the e set now consists of d_{z^2} and d_{xy} and the t_2 set

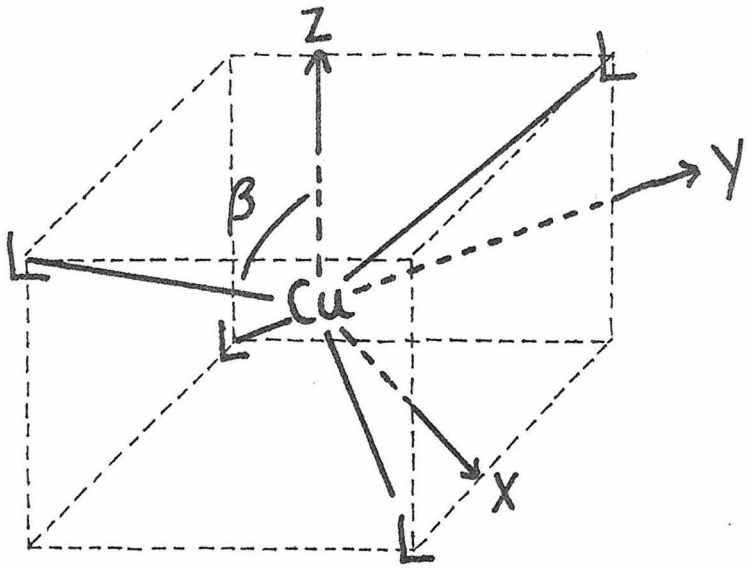

FIGURE 19

Coordinate system for ligand field and molecular orbital calculations.

d_{xz}, d_{yz} and $d_{x^2-y^2}$.

The major distortion from tetrahedral to square planar geometry is the change of the angle (β) between the z-axis and the metal-ligand bonds. The crystal field potential should, therefore, retain this angle as a variable, along with the usual radial integrals. The D_{2d} potential has the following form:

$$V = \gamma_2^0 \left[3z^2-r^2\right] + \gamma_4^0 \left[35z^4-30z^2r^2+3r^4\right] + \gamma_4^4 \left[x^4-6x^2y^2+y^4\right] \quad (8)$$

where $\gamma_n^m = \left[4\pi ze/(2n+1)a^{n+1}\right] \sum_i Y_n^m (r_i,\theta_i,\varphi_i)$ and $Y_n^m(r_i,\theta_i,\varphi_i)$ is a spherical harmonic. Evaluation of the spherical harmonics for ligands at $(a,\beta,0)$, (a,β,π), $(a,180-\beta,\pi/2)$ and $(a, 180-\beta,3\pi/2)$ yeilds:

$$V = ze(3\cos^2\beta-1)\left[3z^2-r^2\right]/a^3 + ze(35\cos^4\beta-30\cos^2\beta+3) \left[35z^4-30z^2r^2+3r^4\right]/16a^5 + ze(35\sin^4\beta)\left[x^4-6x^2y^2+y^4\right]/16a^5. \quad (9)$$

the values of the one electron energies may be evaluated by direct integration using this form of the potential. However, conversion to Stevens' operator equivalent form saves a great deal of computation. The operator equivalent for D_{2d} symmetry is:

$$\hat{V} = ze\alpha_2(\cos^2\beta-1)\left[3\hat{I}_z^2-\hat{I}^2\right]\langle r^2\rangle/a^3 + ze\alpha_4(35\cos^4\beta-30\cos^2\beta+3) \left[35\hat{I}_z^4-30\hat{I}^2\hat{I}_z^2+25\hat{I}_z^2-6\hat{I}^2+3(\hat{I}^2)^2\right]\langle r^4\rangle/16a^5 + 35ze\alpha_4\sin^4\beta \left[\hat{I}_+^4 + \hat{I}_-^4\right]\langle r^4\rangle/32a^5 \quad (10)$$

where $\alpha_2 = 2/21$, $\alpha_4 = -2/63$ and $\langle r^n\rangle$ is the radial integral

$\int r^{n+2} R^2_{(n,1)} dr$. The tetrahedral parameter Dq may be factored out of this expression, but is valid for only a small range of β-values near the tetrahedral angle 54.74°. Thus, the potential is used as shown, so that comparisons to tetrahedral or square planar geometries can be made directly by extrapolating to appropriate values of the angle β. The one electron energies are calculated to be (these are actually one-electron hole energies for d^9):

$$
\begin{aligned}
&^2A_1 \ (d_{z^2}) = -12(\cos^2\beta - 1)Ds - 3\delta Dt \\
&^2B_1 \ (d_{xy}) = 12(3\cos^2\beta - 1)Ds + \tfrac{1}{2}(35\sin^4\beta - \delta)Dt \\
&^2E \ \ (d_{xz} = d_{yz}) = -6(3\cos^2\beta - 1)Ds + 2\delta Dt \\
&^2B_2 \ (d_{x^2-y^2}) = 12(3\cos^2\beta - 1)Ds - \tfrac{1}{2}(35\sin^4\beta + \delta)Dt
\end{aligned}
\qquad (11)
$$

where $\delta = 35\cos^4\beta - 30\cos^2\beta + 3$, $Ds = ze\langle r^2\rangle/21a^3$ and $Dt = ze\langle r^4\rangle/21a^5$. The angular dependence of these energies is shown in Figure 20 for several values of Ds and Dt. It is obvious that square planar geometries have a much larger splitting and, therefore, higher energy d-d transitions than tetrahedra with similar values for the radial integrals. Further, small distortions from square planar arrangement have little effect on the energies, whereas small distortions from the tetrahedron have pronounced effects on the splittings.

Using the values 8750 and 5250 cm^{-1} for the energies of d_{xy} and $d_{xz,yz}$, respectively, and a value of 60° for β,

FIGURE 20

The angular dependence of the d-orbitals as a tetrahedral d^9 case is flattened by D_{2d} distortion to a square plane. Curve A was evaluated for Ds = 1000 cm^{-1} and Dt = 500 cm^{-1}, curve B was evaluated for Ds = 800 cm^{-1} and Dt = 400 cm^{-1}, and curve C was evaluated for Ds = 600 cm^{-1} and Dt = 300 cm^{-1}.

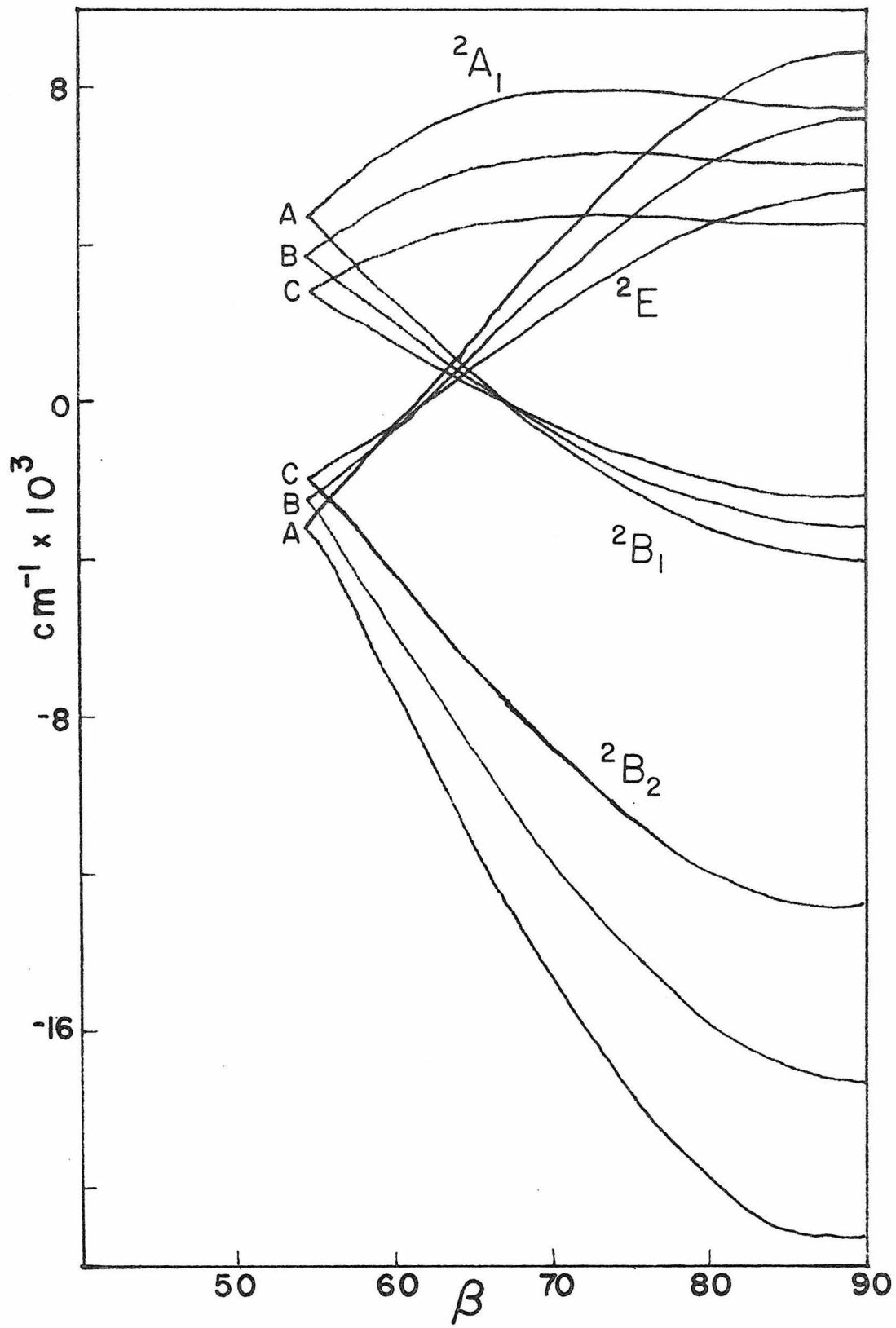
$^2A_1$
^2E
$^2B_1$
$^2B_2$
A
B
C
C
B
A
8
0
-8
-16
$cm^{-1} \times 10^3$
50
60
70
80
90
β

the radial integrals for stellacyanin are calculated to be 825 and 445 cm^{-1} for Ds and Dt, respectively. The energy of the d_{z^2} orbital is predicted to be 11900 cm^{-1} above $d_{x^2-y^2}$ using these parameters. Since only two of the energy levels are assigned, one cannot independently calculate Ds, Dt and β. Reasonable values of β must be determined by examination of the calculated radial parameters for a fixed β-value. For 57°, Ds and Dt are 2240 and 505 cm^{-1}, respectively. Values of 77 and 320 cm^{-1} are calculated for Ds and Dt, respectively, when β is 70°. Computation of the energy difference between $d_{x^2-y^2}$ and d_{z^2} for tetrahedral and square planar symmetries, using the calculated radial parameters, can be accomplished by the following formulas:

$$\Delta E_{T_d} = 15.55\ Dt = 10Dq$$
$$\Delta E_{D_{4h}} = 24\ Ds + 10\ Dt. \qquad (12)$$

The values calculated for the 57° distortion are 7850 cm^{-1} for tetrahedral and 58800 cm^{-1} for square planar symmetry. Such an energy difference for D_{4h} is certainly unreasonable. At 70° values of 4975 cm^{-1} for 10 Dq and 5050 cm^{-1} for $\Delta E_{D_{4h}}$ are calculated. Here, the square planar energy difference is much too small. Energies of 24260 and 6900 cm^{-1} are calculated for D_{4h} and T_d energy splittings, respectively, for an angle of 60°.

A value of 24000 cm^{-1} for the $d_{x^2-y^2} \rightarrow d_{z^2}$ transition agrees favorably with the visible absorption maxima observed in copper-peptide complexes[20].

Plastocyanin and azurin have quite similar excited d-level energies. Values of 5500 and 10300 cm^{-1} for the $d_{xz,yz}$ and d_{z^2} orbitals, respectively, are used for both proteins. If β is again 60°, Ds and Dt are calculated to be 750 and 525 cm^{-1}. In this case the $d_{x^2-y^2} \rightarrow d_{z^2}$ splitting is predicted to be at 12675 cm^{-1}.

Activity near 14000 cm^{-1} in the MCD curves was suggested above to be the result of transitions from the ground state to the d_{z^2} orbital. If β is 57°, the d_{z^2} orbital for stellacyanin is predicted to be at 13850 cm^{-1}, consistent with this assignment. However, these values of Ds and Dt yield an unreasonable energy splitting when extrapolated to the square planar limiting case. Unless the copper site is quite unique electronically, these MCD transitions more likely result from excitation to the π charge transfer states.

The preferred ligand field parameters ($\beta = 60°$, $Ds = 825$ cm^{-1} and $Dt = 445$ cm^{-1}) predict the d_{z^2} orbital to be 11900 cm^{-1} above the $d_{x^2-y^2}$ ground state for stellacyanin. An absorption band and CD maximum are observed near this energy. The resolved absorption band has a molar extinction coefficient of 565, approximately five times more intense than the band at 8750 cm^{-1}.

However, the $d_{x^2-y^2} \rightarrow d_{z^2}$ excitation is electric dipole allowed, whereas the $d_{x^2-y^2} \rightarrow d_{xy}$ transition is magnetic dipole allowed and, therefore, expected to be less intense. Both transitions appear to be magnetic dipole allowed according to the respective anisotropy factors (Table IV). Plastocyanin has a similar transition at 12700 cm^{-1}, as predicted from the ligand field parameters. The CD activity is somewhat lower in plastocyanin, but the ratios between the various transitions in this energy region are similar. In azurin, the charge transfer band is shifted to lower energy (13700 cm^{-1}) and probably overlaps extensively with the predicted d_{z^2} transition at 12700 cm^{-1}. This absorption band did not require more than one Gaussian to yield a reasonable fit, although two closely spaced Gaussians would yield a similar fit. Further, the azurin CD curve does not show the positive band at ~13000 cm^{-1}. Here the overlap of this intense CD minimum may completely mask the weaker positive band.

The identification of d-orbital splittings also allows a more detailed analysis of the EPR spectra of the blue copper proteins. Stellacyanin's EPR spectrum has been fit by a rhombic spin Hamiltonian with values of $g_z = 2.287$, $g_y = 2.077$ and $g_x = 2.025$[4]. Using the mean of g_x and g_y as $g_\perp$, the orbital reduction factors $k_\parallel$ and $k_\perp$ can be calculated from the ligand field

formulas:

$$g_{\parallel} = 2(1-4k_{\parallel}\lambda^{\circ}/\Delta_2)$$
$$g_{\perp} = 2(1- k_{\perp}\lambda^{\circ}/\Delta_1) \qquad (13)$$

where $\lambda^{\circ} = -828\ cm^{-1}$, $\Delta_2 = d_{x^2-y^2} \rightarrow d_{xy}$ and $\Delta_1 = d_{x^2-y^2} \rightarrow d_{xz,yz}$. For stellacyanin $k_{\parallel}$ and $k_{\perp}$ are computed to be 0.38 and 0.16, respectively. These values are much lower than those calculated for copper-peptide complexes, where $k_{\parallel}$ is found in the range of 0.64 and 0.55 and $k_{\perp}$ between 0.71 and 0.45[20]. The orbital reduction factors for the square planar N_2S_2 complex Cu(thiosemicarbazide)$_2$ are 0.36 and 0.30 for parallel and perpendicular directions, respectively, to the magnetic field[22]. Here, the covalency along the z-axis is quite similar to that of stellacyanin, but perpendicular to z the metal-ligand bonds in the protein are much more covalent than in the square planar complex. Using the orbital reduction factors calculated for stellacyanin and the energy splittings observed for plastocyanin and azurin, $g_{\parallel}$ is calculated to be 2.244 and $g_{\perp}$ is 2.048. The values experimentally observed are 2.260 and 2.052 for azurin[3] and 2.226 and 2.053 for plastocyanin[1]. The agreement is strikingly good, indicating that these sites are indeed quite similar with regards to covalent bonding.

A model for the blue site

A more detailed physical model for the blue copper

centers can be formulated from recent physical studies on plastocyanin. Solomon, et al. have reported x-ray photoelectron spectral results which confirm cysteine sulfur is bound to copper[27]. More recent spectra show that sulfur is also bound to copper in azurin[43]. Resonance Raman studies on several of the blue proteins have shown that amide nitrogen or oxygen is present in the copper coordination sphere in all cases[28]. Infrared studies have shown this amide group to be part of the protein backbone. Nuclear magnetic resonance data on plastocyanin indicate histidine is strongly influenced by the copper ion and quite likely bound to it[44]. Low energy absorptions, previously undetected, have been interpreted as ligand field transitions, and a model based on a tetragonally distorted tetrahedral arrangement has been proposed (vide supra). The visible absorption bands have been assigned as charge transfer transitions, consistent with the identification of highly reducing ligands in the copper coordination sphere. The two lowest bands at 12500 and 17500 cm^{-1} are probably sulfur π and σ sulfur charge transfer transitions, respectively. The third band at 23000 cm^{-1} is assigned to an amide nitrogen to copper π charge transfer transition. This assignment is in accord with the ordering observed in square planar complexes[30,31,33].

A self-consistent charge and configuration (s.c.c.c.) molecular orbital calculation was performed on this model (illustrated in Figure 21). As no calculations were available for the deprotonated amide moiety, a third imidazole ring was substituted for the amide group in the calculation. Although similar extended Hückel calculations have been performed on imidazole[45,46], no eigenfunctions were reported. The two highest energy π-bonding orbitals of pyridine were assumed to be similar to those describing the conjugated region of imidazole. The Slater basic eigenfunctions of pyridine reported by Rein, et al.[47] were, therefore, chosen to describe the two highest energy π levels of the conjugated nitrogen of imidazole. The σ bonding lone pair of the pyridine-like nitrogen was assumed to be non-bonding within the imidazole molecule, thus the Clementi and Raimondi version of the Slater orbital of the nitrogen atom was used to describe the lone pair of pσ electrons[48]. Values of the valence state ionization potentials (VSIP's) were taken from the orbital energies calculated for imidazole by Berthier, et al.[49] The cysteine sulfur was represented by the atomic sulfur wavefunctions of Clementi and Raimondi. The sulfur 2s VSIP was calculated from the equations reported by Basch, et al.[50] assuming a charge midway between the values of -0.04 for sulfhydryl sulfur and -0.60 for sulfide ion assigned by

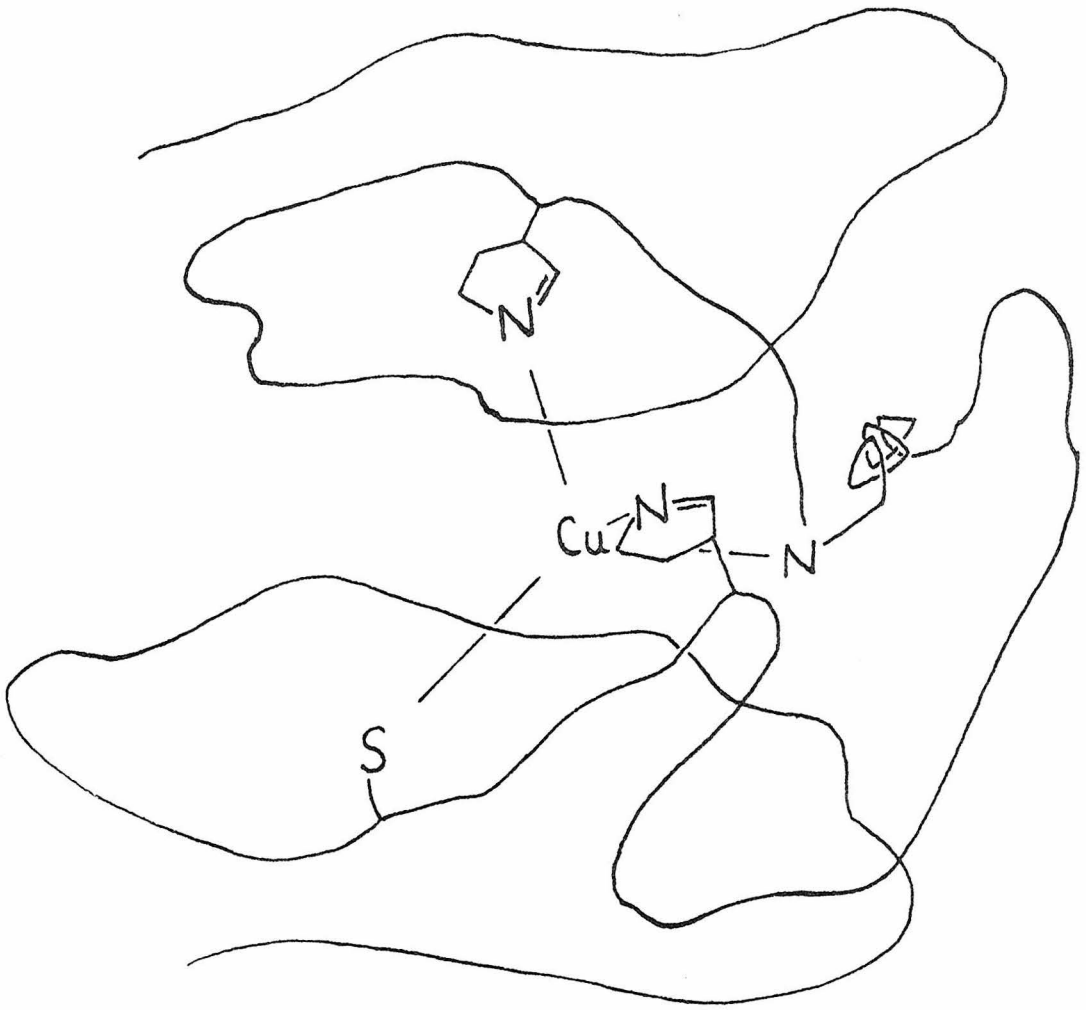

FIGURE 21

A model of the blue site in plastocyanin.

Siegbahn, et al.[51] The radial wavefunctions of copper calculated by Richardson, et al.[52] were assigned the VSIP's reported by Basch[53]. The linear charge dependence calculated by Basch for copper VSIP's was reduced, as recommended by Lohr and Lipscomb[54]. Two center electron-nuclear coulombic terms were added to the ligand and metal VSIP's, following Basch's calculation on CuO[53].

The total electronic energy calculated for copper-sulfur bond lengths of 2.5, 2.3, 2.1, and 1.9 Å are -8644, -8799, -9177, and -9023 kilowavenumbers, respectively. These results indicate a minimum electronic energy exists for the copper-sulfur bond length in the vicinity of 2 Å. This distance is probably shorter than the actual equilibrium bond length, as nuclear-nuclear repulsion terms were not included in the calculation. There is an indication, however, that the copper-sulfur equilibrium distance may be significantly shorter in the distorted tetrahedral geometry than the 2.3 Å observed for the square planar system[55]. Assuming the copper-sulfur bond dominates the secondary interactions in the protein, the observed charge transfer energies would be expected to red shift from the values reported for square planar model complexes, as the result of both stabilization of the σ anti-bonding $d_{x^2-y^2}$ orbital and

a decrease in the copper-sulfur bond distance.

Spectral correlation to reduction potential

An attempt is now made to establish the relationship between electronic structural properties of blue copper centers and the protein reduction potentials. The form of the reduction potential of a metal ion in the presence of ligating molecules or ions is given by Laitinen[56]:

$$\xi = \xi^{\circ'}_{aq} + RT/nF \ln \beta^{II}/\beta^{I} + RT/nF \ln C_T^{II}/C_T^{I} \qquad (14)$$

where $\xi^{\circ'}_{aq} = \xi^{\circ}_{aq} + RT/nF \ln f^{II}/f^{I}$, f^i being the activity coefficient of the ion i, $\beta^i = [\sum_n K^i_n [L]^n]^{-1}$, K^i_n being the nth successive formation constant for ion i in the presence of ligand L and C_T^i is the total concentration of ion i, for the reduction reaction $M^{II}L_n + e^- \rightleftarrows M^{I}L_n$. The blue proteins of this study bind a single copper ion so that the equilibrium Cu^i + protein $\rightleftarrows$ Cu^i(protein) may be represented by the binding constant K_b^i. The electrode potential may now be written:

$$\begin{aligned}\xi &= \xi^{\circ'}_{aq} + RT/nF \ln C_T^{II}/C_T^{I} + RT/nF(\ln K_b^{I} - \ln K_b^{II}) \\ &= \xi' + 1/nF(\Delta G_b^{II} - \Delta G_b^{I}) \\ &= \xi' + 1/nF(\Delta H_b^{II} - \Delta H_b^{I} - T\Delta S_b^{II} + T\Delta S_b^{I}). \qquad (15)\end{aligned}$$

Using a Born-Haber cycle,

$$\begin{array}{ccc} Cu^{II}{}_L + e^- & \rightleftarrows & Cu^{I}{}_L \\ \downarrow -\Delta G_L{}^{II} & & \uparrow \Delta G_L{}^{I} \\ Cu^{II}{}_{(g)} + L + e^- & \rightleftarrows & Cu^{I}{}_{(g)} + L \end{array}$$

$$-IP_2$$

the reduction potential may also be written:

$$\begin{aligned} nF\xi &= -(\Delta G^\circ - \Delta G_L{}^{II} + \Delta G_L{}^{I} - IP_2) \\ &= nF\xi^\circ + \Delta H_L{}^{II} - \Delta H_L{}^{I} - T\Delta S_L{}^{II} + T\Delta S_L{}^{I} + IP_2 \\ &= nF\xi^\circ + \eta^{II} - \eta^{I} + LFSE^{II} - LFSE^{I} - T\Delta S_b{}^{II} + T\Delta S_b{}^{I} - \\ &\quad T\Delta S_H{}^{II} + T\Delta S_H{}^{I} + IP_2 \end{aligned} \qquad (16)$$

where η^i is $H_i - LFSE^i$ ($LFSE^i$ is the ligand field stabilization energy of ion i) and can be described as a coulombic term consisting of ligand electron-metal ion attraction and ligand-metal nuclear repulsion, and $\Delta S_H{}^i$ is the entropy associated with the reaction $M^i{}_{(g)} + nH_2O \rightarrow M^i(H_2O)_n$ [57]. Thus, the reduction potential may also be written ($LFSE^I = 0$):

$$\xi = \xi' + 1/nF(\eta^{II} - \eta^{I} + LFSE^{II} + IP_2 - T(\Delta S_H{}^{II} - \Delta S_H{}^{I}) - T(\Delta S_b{}^{II} - \Delta S_b{}^{I})). \qquad (17)$$

The entropy of hydration for Cu(II) and Cu(I) are equivalent, if minor differences in the gaseous ions and the partial molal entropy of the aquo complexes are disregarded. Wagman reports a value of 9.4 e.u. for $Cu(I)_{(aq)}$ [58] and George and McClure give a value of

-23 e.u. for $Cu(II)_{(aq)}$ [57]. Thus the term $-T(\Delta S_H^{II} - \Delta S_H^{I})$ accounts for 9 kcal/mole in the reduction potential formula. The second ionization potential of gaseous copper is 469 kcal/mole so that the reduction potential may now be written:

$$\xi = \xi' + 1/nF(\eta^{II} - \eta^{I} + LFSE^{II} + 478 \text{ kcal/mole} - T(\Delta S_b^{II} - \Delta S_b^{I})). \quad (18)$$

For complexes in solution $\eta^{II} - \eta^{I}$ is usually in the range -450 to -500 kcal/mole, $LFSE^{II}$ -25 to -50 kcal/mole and $-T(\Delta S_b^{II} - \Delta S_b^{I})$ 5 to 10 kcal/mole.

The reduction potentials of stellacyanin, azurin and plastocyanin have been reported to be +184, +300 and +370 mv, respectively, in a recent review by Fee[59]. The potentials are expected to be more positive than the aquo ion potentials as the LFSE's of the proteins are considerably lower. The ligand field stabilization for stellacyanin is -6340 cm^{-1}, where -2760 cm^{-1} is due to the tetrahedral field and -3580 cm^{-1} is due to the tetragonal distortion. For plastocyanin and azurin, LFSE is -6790 cm^{-1}, where -3250 cm^{-1} is due to the tetrahedral field and -3540 cm^{-1} is the result of the tetragonal distortion. The LFSE difference between plastocyanin and aqueous copper(II) is 5.6 kcal/mole or 240 mv. Thus, a value of 390 mv is predicted for

plastocyanin and azurin. Stellacyanin is destabilized by 6.9 kcal/mole or +300 mv with respect to the aquated ion. Thus stellacyanin is predicted to be at +450 mv. These predictions are based on the assumption that $\eta^{II} - \eta^{I}$ and $T(\Delta S_b^{I} - \Delta S_b^{II})$ have the same value for the proteins and the aqueous copper system. This approximation is not expected to be valid, but was invoked to compare ligand field effects on the potential. If the LFSE were not present in plastocyanin, the potential would be approximately +1060 mv, which corresponds to a value of -454 kcal/mole for $\eta^{II} - \eta^{I} - T(\Delta S_b^{II} - \Delta S_b^{I})$. If the protein sites were exactly the same, then the reduction potentials would follow the ordering plastocyanin $\approx$ azurin < stellacyanin. However, small changes in the site will cause differences in the binding constants. A change in these large numbers, which are roughly one order of magnitude larger than the LFSE, can easily overwhelm any ligand field effects. This must be the case for stellacyanin, as the potential is 200 mv lower than plastocyanin, rather than 70 mv higher as predicted. This difference of 270 mv corresponds to a destabilization of the copper(II) (or a stabilization of Cu(I)) binding energy of 6.2 kcal/mole. This value is small enough to be accounted for by either the enthalpy term $\eta^{II} - \eta^{I}$ or the entropy

term. The difference between azurin and plastocyanin is 70 mv which corresponds to 1.6 kcal/mole. Thus, the ligand field stabilization is important but far from dominant in determining blue protein potentials. Binding constants will have to be determined for these proteins before any differences in enthalpy and entropy contributions can be assigned.

Summary

New low energy electronic transitions at ~10000 and 5000 cm^{-1} have been identified as ligand field bands of the blue site of the single copper proteins stellacyanin, plastocyanin and azurin from low temperature absorption as well as CD and MCD studies in the near-infrared. The well known visible series of absorption bands are assigned as charge transfer transitions of π and σ character from sulfur to copper and of π character from deprotonated amide nitrogen to copper, based on comparison of visible absorption and CD intensities. Ligand field calculations have shown that the observed d-d excitation energies are consistent with a tetrahedral model distorted approximately 4 to 8° towards a square plane. A model of the blue site, which incorporates recent physical evidence for specific ligands, is presented. The reduction potentials have been shown to be influenced, but not dominated, by ligand field effects.

BIBLIOGRAPHY

1. W. E. Blumberg and J. Peisach, Biochim. Biophys. Acta, 126, 269(1966).

2. J. Peisach, W. G. Levine and W. E. Blumberg, J. Biol. Chem., 242, 2847(1967).

3. A. S. Brill, G. F. Bryce and H. J. Maria, Biochim. Biophys. Acta, 154, 342(1968).

4. B. G. Malmström, B. Reinhammar and T. Vänngård, Biochim. Biophys. Acta, 205, 48(1970).

5. P. R. Milne and J. R. E. Wells, J. Biol. Chem., 245, 1566(1970).

6. S.-P. W. Tang, J. E. Coleman and Y. P. Myer, J. Biol. Chem., 243, 4286(1968).

7. K.-E. Falk and B. Reinhammar, Biochim. Biophys. Acta, 285, 84(1972).

8. T. Stigbrand and I. Sjöholm, Biochim. Biophys. Acta, 263, 244(1972).

9. A. S. Brill and G. F. Bryce, J. Chem. Phys., 48, 4398(1968).

10. B. L. Vallee and R. J. P. Williams, Proc. Nat. Acad. Sci.(U. S. A.),59, 498(1968).

11. H. B. Gray, "Bioinorganic Chemistry" in Advances in Chemistry,Series 100, R. F. Gould, ed., American Chemical Society, Washington, D. C., 1971.

12. A. S. Brill, R. B. Martin and R. J. P. Williams,

"Copper in Biological Systems" in Electronic Aspects of Biochemistry, B. Pullman, ed., Academic Press, New York, New York, 1964.

13. D. R. McMillin, R. C. Rosenberg and H. B. Gray, Proc. Nat. Acad. Sci.(U. S. A.), 71, 4760(1974).

14. C. J. Ballhausen, Introduction to Ligand Field Theory , McGraw-Hill Book Company, New York, New York, 1962.

15. T. M. McFarland and J. E. Coleman, Eur. J. Biochem., 29, 591(1972).

16. W. E. Hatfield and T. S. Piper, Inorg. Chem., 3, 841(1964).

17. B. J. Hathaway and A. A. G. Tomlinson, Coord. Chem. Rev., 5, 1(1970).

18. R. H. Dietz, H. Kamimura, M. D. Sturge and A. Yariv, Phys. Rev., 132, 1559(1963).

19. H. C. Freeman, "Crystal Structure Studies of Cupric-Peptide Complexes" in The Biochemistry of Copper, J. Peisach, P. Aisen and W. E. Blumberg, eds., Academic Press, New York, New York, 1966.

20. G. F. Bryce, J. Phys. Chem., 70, 3549(1966).

21. B. Jezowska-Trzebiatowska, A. Antonow and H. Kozlowski, Bull. Acad. Pol Sci., Ser. sci. chim. 22, 399(1974).

22. E. Buluggiu, A. Vera and A. A. G. Tomlinson, J. Chem. Phys., 56, 5602(1972).

23. R. D. Willett, O. L. Liles, Jr. and C. Michelson, Inorg. Chem., 6, 1885(1967).

24. R. D. Willett, J. Chem. Phys., 41, 2243(1964).

25. J. Ferguson, J. Chem. Phys., 40, 3406(1964).

26. W. E. Blumberg, "Some Aspects of Models of Copper Complexes" in The Biochemistry of Copper, J. Peisach, P. Aisen and W. E. Blumberg, eds., Academic Press, New York, New York, 1966.

27. E. I. Solomon, P. J. Clendening, H. B. Gray and F. J. Grunthaner, J. Amer. Chem. Soc., 97, 3878(1975).

28. O. Siiman, N. M. Young and P. R. Carey, J. Amer. Chem. Soc., 96, 5583(1974); J. Amer. Chem. Soc., in press.

29. I. Broser, K.-H. Franke and H.-J. Schulz, "Correlation Between the Absorption and Excitation Spectra Due to Cu^{2+} Impurities and the Valence Band Structure of ZnS" in International Conference on II-VI Semiconducting Compounds(1967), D. G. Thomas, ed., W. A. Benjamin, Inc., New York, New York, 1967.

30. E. W. Wilson, Jr. and R. B. Martin, Arch. Biochem. Biophys., 142, 445(1971).

31. G. Rotilio, C. De Marco and S. Dupre, in Magnetic Resonances in Biological Research , C. Franconi, ed., Gordon and Breach Science Publishers, New York, New York, 1971, paper 13.

32. Y. Sugiura, Y. Hirayama, H. Tanaka and K. Ishizu, J. Amer. Chem. Soc., 97, 5577(1975).

33. G. F. Bryce and F. R. N. Gurd, J. Biol. Chem., 241, 122(1966).

34. E. W. Wilson, Jr., M. H. Kasperian and R. B. Martin, J. Amer. Chem. Soc., 92, 5365(1970).

35. M. Sharnoff and C. W. Reimann, J. Chem. Phys., 46, 2634(1967).

36. R. D. Gillard, "Optical Rotatory Dispersion and Circular Dichroism" in Physical Methods in Advanced Inorganic Chemistry, H. A. O. Hill and R. Day, eds., Interscience Publishers, London, 1968.

37. A. Moscowitz, "Theory and Analysis of Rotatory Dispersion Curves" in Optical Rotatory Dispersion, C. Djerassi, ed., McGraw-Hill, New York, New York, 1960.

38. C. Ibarra, R. Soto, L. Adan, A. Decinti and S. Bunel, Inorg. Chim. Acta, 6, 601(1972).

39. T. A. Kaden, in Metal Ions in Biological Systems, H. Sigel, ed., Marcel Dekker, Inc., New York, New York, 1974, Vol. 3, Chap. 1.

40. R. P. Ambler, Biochem. J., 89, 341(1963).

41. A. D. Buckingham and P. J. Stephens, Ann. Rev. Phys. Chem., 17, 399(1966).

42. M. Lax, J. Chem. Phys., 20, 1752(1952).

43. E. I. Solomon, personal communication.

44. J. L. Markley, E. L. Ulrich, S. P. Berg and D. W. Krogmann, Biochemistry, in press.

45. I. Fischer-Hjalmers and J. Nag-Chaudhuri, Acta Chem. Scand., 23, 2963(1969).

46. M. Sundbom, Acta Chem. Scand., 25, 487(1971).

47. R. Rein, G. A. Clarke and F. E. Harris in Quantum Aspects of Heterocyclic Compounds in Chemistry and Biochemistry, E. D. Bergmann and B. Pullman, eds., Israel Academy of Sciences and Humanities, Jerusalem, 1970, p.68.

48. E. Clementi and D. L. Raimondi, J. Chem. Phys., 38, 2686(1963).

49. G. Berthier, L. Praud and J. Serre in Quantum Aspects of Heterocyclic Compounds in Chemistry and Bio-Chemistry, E. D. Bergmann and B. Pullman, eds., Israel Academy of Sciences and Humanities, Jerusalem, 1970, p.40.

50. H. Basch, A Viste and H. B. Gray, Theoret. Chim. Acta, 3, 458(1965).

51. K. Siegbahn, C. Nordling, A. Fahlman, R. Nordberg, K. Hamrin, J. Hedman, G. Johansson, T. Bergmark, S.-E. Karlsson, I. Lindgren and B. Lindberg, "ESCA; Atomic, Molecular and Solid State Structure by Means of Electron Spectroscopy" in Nova Acta Reg. Soc. Sci. Ups., Ser IV, Vol. 20 (1967).

52. J. W. Richardson, R. R. Powell and W. C. Nieuwpoort, J. Chem. Phys., 38, 796(1963).

53. H. Basch, Thesis, Columbia University(1966).

54. L. L. Lohr, Jr. and W. N. Lipscomb, Inorg. Chem., 2, 911(1963).

55. H. J. Shugar, personal communication.

56. H. A. Laitinen, Chemical Analysis, McGraw-Hill Book Company, Inc., New York, New York, 1960, Chap. 15.

57. P. George and D. S. McClure, Prog. in Inorg. Chem., 1, 381(1959).

58. D. D. Wagman, J. Amer. Chem. Soc., 73, 5463(1951).

59. J. A. Fee, Structure and Bonding, 23, 1(1975).

60. These selection rules refer to the tetrahedral coordinate system of the D_{2d} point group. All future calculations are performed in the square planar coordinate system, where $d_{x^2-y^2}$ and d_{xy} exchange symmetry designations.

II. ELECTRONIC STRUCTURE AND SPECTRA OF IRON GROUP OLIVINES

INTRODUCTION

The olivine structure, named for the mineral with the composition $[Mg, Fe]_2SiO_4$, is one of two major structures that exhibits the stoichiometry A_2BO_4. The spinel form consists of a cubic close-packed array of oxide ions with A cations filling octahedral sites and B cations filling tetrahedral sites. For B cations smaller than 0.53 Å (ionic radius), the hexagonal close-packed olivine structure is preferred[1]. The borate sinhalite, $Al[Mg,Fe]BO_4$[2], berylate chrysoberyl, Al_2BeO_4[3], silicate olivine[4] and phosphate triphylite, $Li[Fe,Mn]PO_4$[5] all have the olivine structure.

The olivine structure, space group Pnma, contains two distinct octahedral sites, designated M_1 and M_2, which occupy C_i and C_s crystallographic sites, respectively. The M_1 position shares opposite edges with nearest neighbor M_1 sites, forming an infinite ribbon along the b-axis. The arrangement of M_1 positions in one unit cell ($z = 4$) is illustrated in Figure 1[6]. M_2 octahedra share edges with adjacent M_1 positions, giving the infinite ribbon a sawtooth appearance. The M_2 sites also share corners with adjacent M_2 positions, linking the M_1 ribbons in the plane perpendicular to b. The chicken-wire sheet of M_2 octahedra is shown in

FIGURE 1

An ORTEP perspective view of the M_1 chains in triphylite viewed down the c crystallographic axis. The chains run parallel to b.

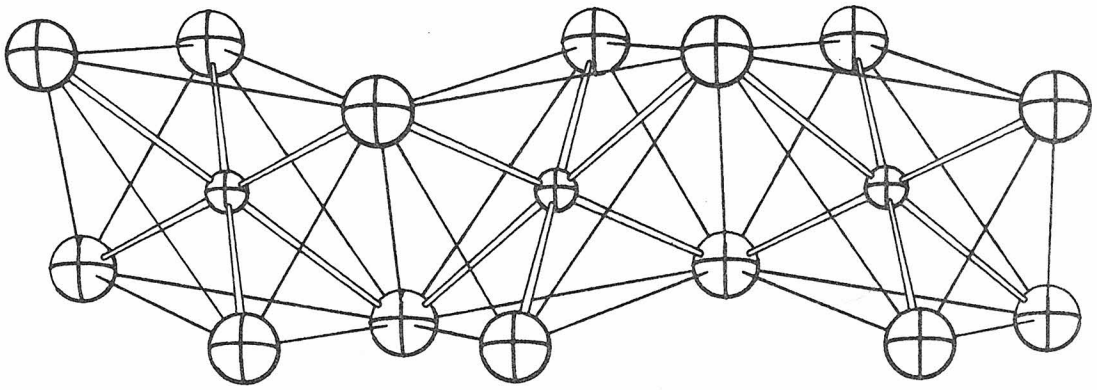

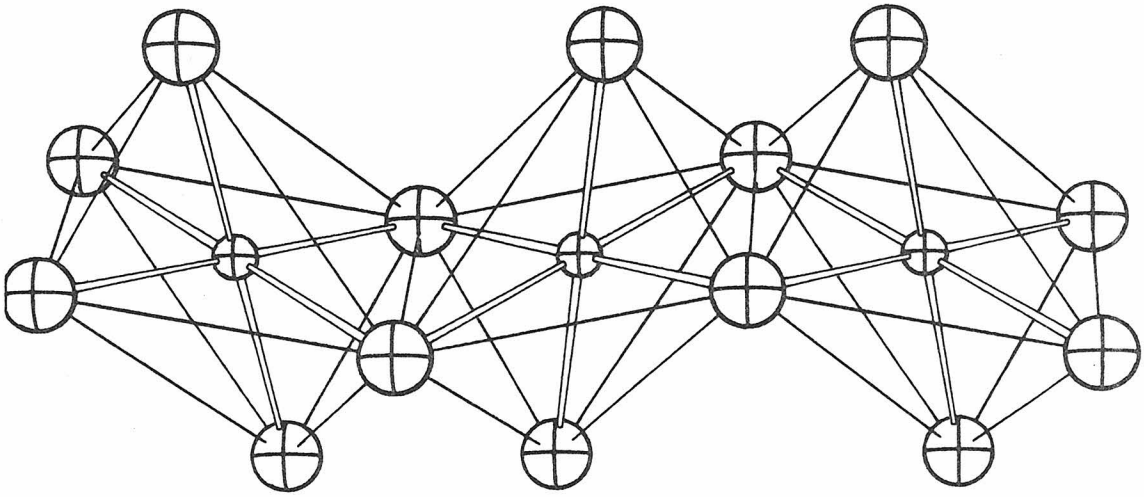

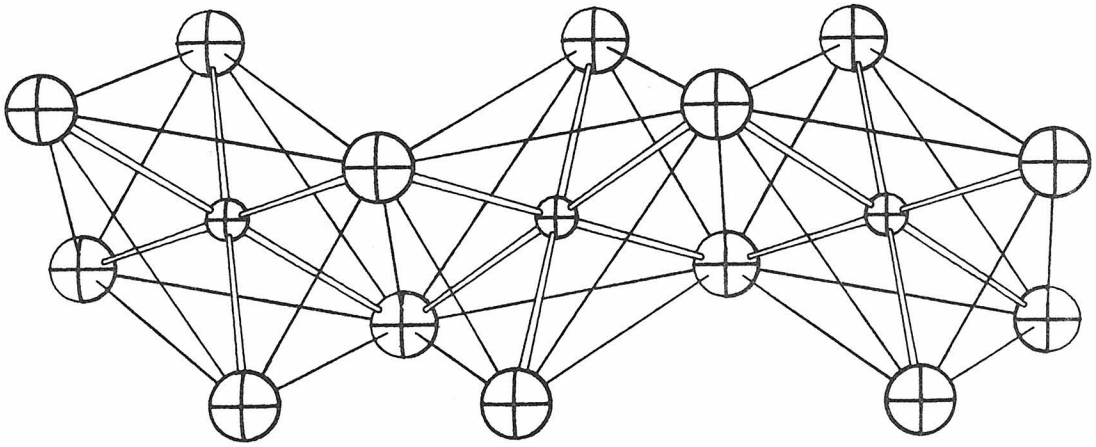

Figure 2. The silicon atoms are located in the tetrahedral position formed by the M_1-M_1-M_2 cluster.

The distribution of first row transition metals in these two sites is of considerable geochemical interest. Olivines crystallize out of basaltic magmas at an early stage, and are considered to be an important constituent of the upper mantle. The driving forces behind the partitioning of metal ions between the octahedral sites has been the subject of a ligand field analysis[7] and several structural analyses[8,9]. However, the assignment of the electronic absorption bands is still under debate, so that Burns' ligand field analysis may need refinement in light of further spectral evidence. The object of this study is the assignment of the absorption spectra of several olivines according to metal site, by examination of corresponding triphylite spectra (the triphylite M_1 site is filled by lithium, so that complete partitioning of the pertinent transition metal into the M_2 site is observed), the assignment of effective electronic symmetries from polarized absorption spectra, and an analysis of ligand field effects on the observed distribution.

EXPERIMENTAL SECTION

The metal substituted triphylites $LiCoPO_4$ and

FIGURE 2

An ORTEP perspective view of the M_2 sheet in triphylite viewed down the a crystallographic axis.

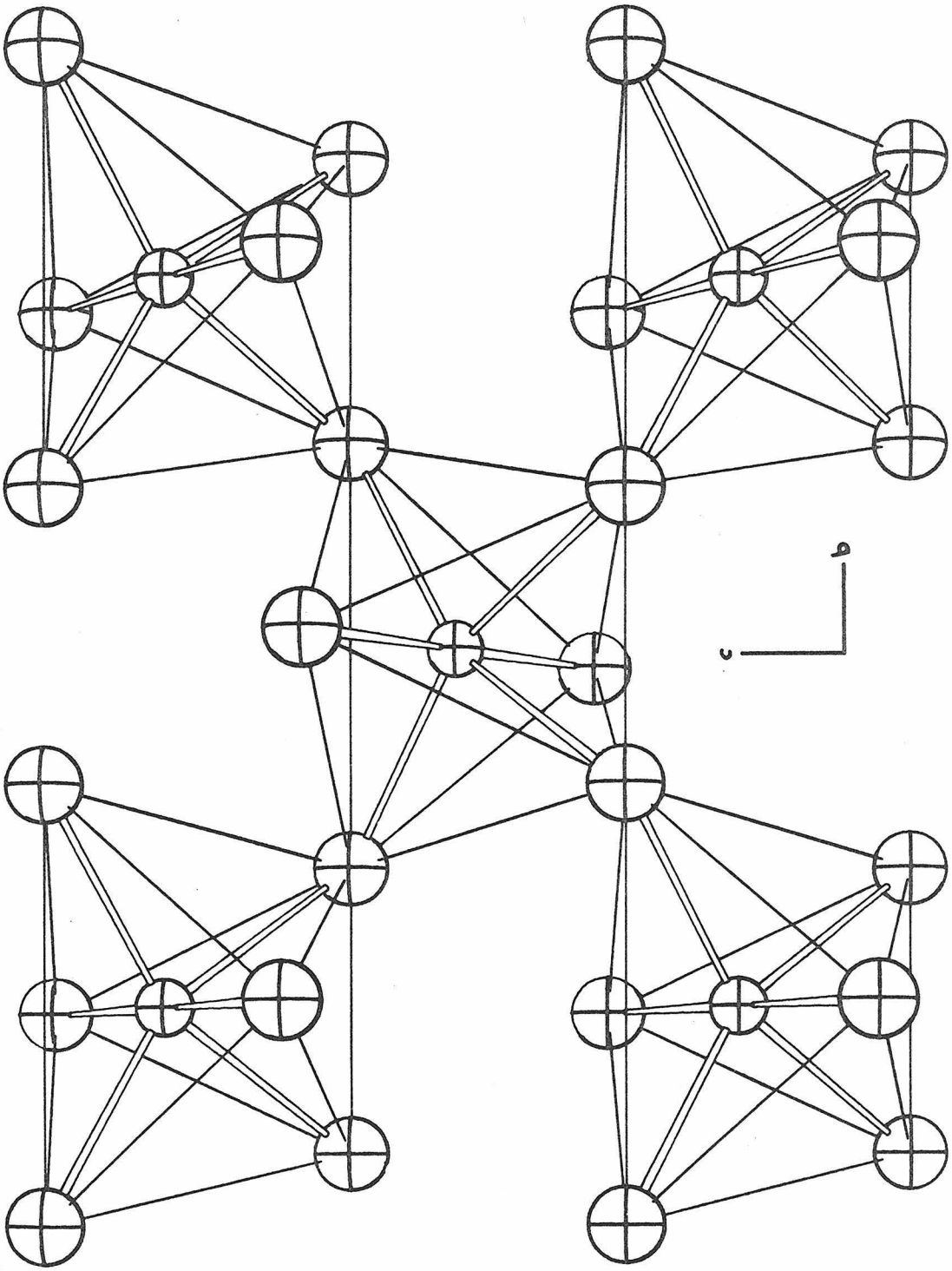
ص
ب

$LiNiPO_4$ were synthesized by firing equimolar mixtures of Li_2CO_3, $(NH_4)_3PO_4$ and $Co_3(PO_4)_2 \cdot 8H_2O$ or $Ni_3(PO_4)_2$ at 800° for two days in a porcelain crucible according to Santoro, et al.[10] Firing equimolar mixtures of $NH_4MPO_4 \cdot 2H_2O$ (M = Ni or Co) and Li_2CO_3 for two days at 800°[11] or equimolar mixtures of $M_3(PO_4)_2$ and Li_3PO_4 for two days at 800°[12] were equally successful methods of preparing cobalt and nickel triphylites. The microcrystalline products were identified to be the correct phases by comparison with known x-ray powder diffraction data and the infrared spectrum of a natural triphylite. Attempts to grow larger crystals of these compounds were unsuccessful.

Finely ground samples of Ni_2SiO_4 and Co_2SiO_4 were prepared by Dr. H. Fujisawa[13] and donated by Professor Arden Albee of Caltech. Single crystals of cobalt and nickel olivines were grown from a tungstate flux by Dr. Jun Ito of the University of Chicago. The crystals were analyzed by Dr. Ito to have the stoichiometries $Mg_{1.5}Ni_{0.5}SiO_4$ and $Mg_{1.62}Co_{0.38}SiO_4$.

The natural triphylite samples were collected from Center Strafford, New Hampshire. Tentative molar extinction coefficients are based on the analysis of a triphylite from this locality reported by Switzer[14].

The crystals used for absorption studies were

oriented with the aid of external morphology and a petrographic microscope. As olivine is an orthorhombic crystal, the principal dielectric axes are also crystal axes. The correlation between optical directions and crystal axes was achieved by the precession x-ray diffraction method. The crystals were ground to appropriate thickness, determined by the observation of absorption < 2 over the desired spectral range, by mounting them in the desired orientation with apiezon wax on a brass block and grinding with 600 grit tungsten carbide. The ground surfaces were then polished with 0.3 μ alumina. The crystals were mounted on ½ inch diameter copper disks, which had holes precut to match the crystal size, and held in place with a thin film of Vaseline.

The absorption spectra of microcrystalline samples were obtained from TlCl pellets. This medium was preferred to KBr because its higher index of refraction more closely matched that of the samples, allowing better discrimination of the absorption spectrum from the ever-present scattering curve. The TlCl pellets were prepared by pressing ~200 mg of TlCl and ~5 mg sample in a standard KBr die. Several cycles of grinding and repressing usually improved the quality of the pellets. Better spectral discrimination was achieved by

placing ground quartz plates (such as broken quartz solution cells) behind the sample and reference pellets. The samples were also ground in a boron nitride mortar to minimize scattering.

The low temperature pellet spectra were obtained by placing the pellet in a Cryogenics Technology, Inc. Model 21 Cryocooler, equipped with a variable temperature controller. The crystals were cooled to 77 K or 10 K in a Cary Model liquid helium dewar modified to hold ½ inch disks. The samples were cooled by contact with either liquid nitrogen or liquid helium. Temperatures were monitored with a calibrated carbon resistor attached to the sample block. Near-infrared and visible absorption spectra were obtained on a Cary 17 I recording spectrophotometer in the laboratory of Professor George Rossman. Infrared spectra were obtained on a Perkin-Elmer 180 infrared spectrometer, also made available by Professor Rossman. The C. I. T. powder camera (Co radiation) and precession camera (Mo radiation) were used in the x-ray diffraction studies.

RESULTS

The infrared spectra of KBr pellets of synthetic $LiNiPO_4$ and $LiCoPO_4$ and natural triphylite ($Li[Mn,Fe]PO_4$) are presented in Figure 3. Low temperature (35 K) near-

FIGURE 3

The infrared spectra of potassium bromide pellets containing natural triphylite (a), $LiCoPO_4$ (b) and $LiNiPO_4$ (c).

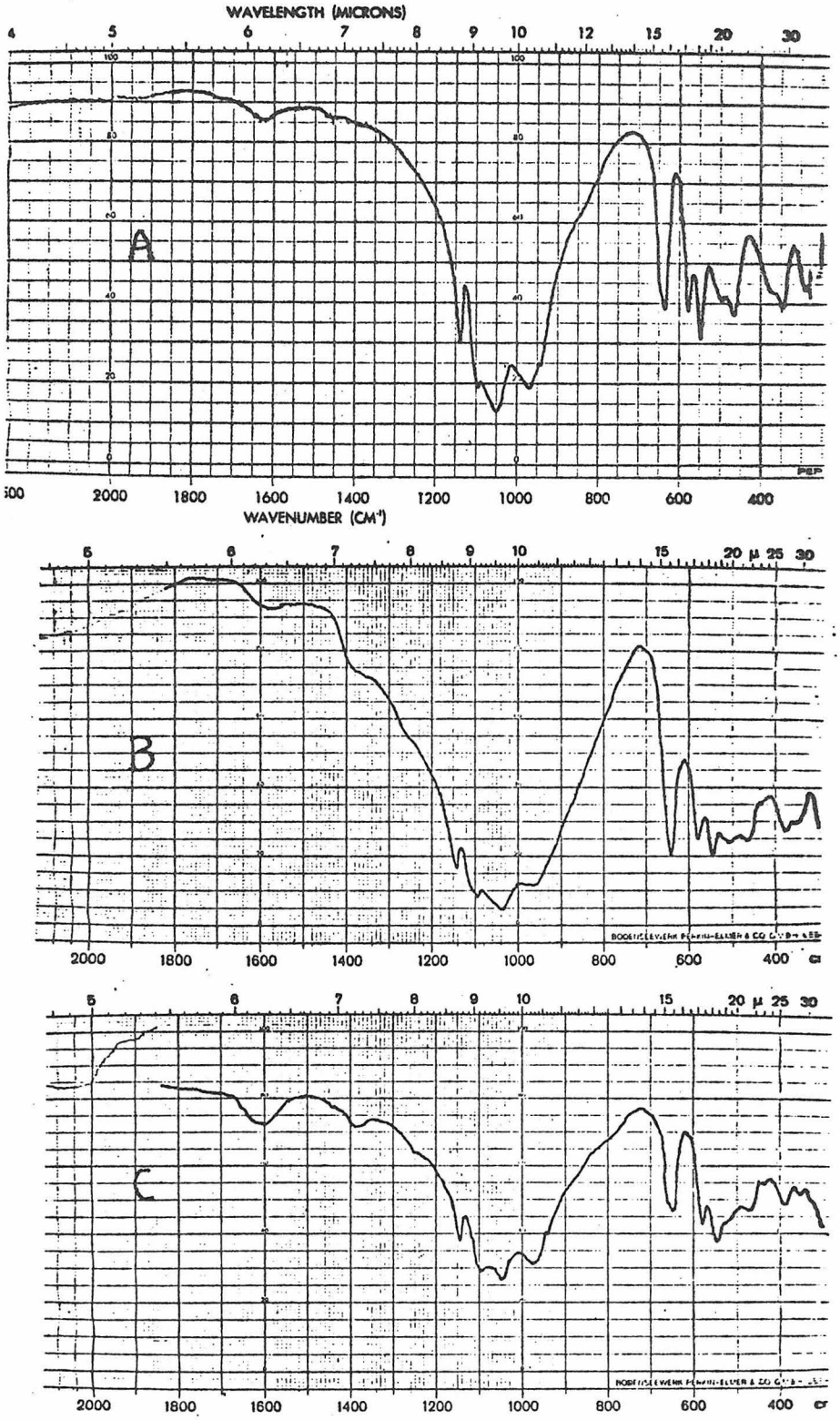
WAVELENGTH (MICRONS)
4 5 6 7 8 9 10 12 15 20 30
A
2000 1800 1600 1400 1200 1000 800 600 400
WAVENUMBER (CM⁻¹)
5 6 7 8 9 10 15 20 μ 25 30
B
2000 1800 1600 1400 1200 1000 800 600 400
5 6 7 8 9 10 15 20 μ 25 30
C
2000 1800 1600 1400 1200 1000 800 600 400

infrared and visible absorption spectra of $LiCoPO_4$, Co_2SiO_4, $LiNiPO_4$ and Ni_2SiO_4 thallous chloride pellets are shown in Figures 4, 5, 6, and 7, respectively.

Figure 8 contains the polarized, room temperature absorption spectra of a Center Strafford, New Hampshire triphylite. The 77 K polarized spectra appear in Figure 9. The thickness required to observe the intense band in α-polarization necessitated the use of two separate crystals to obtain all three polarization. Correlation of unit cell lengths with principal electric vibration directions was obtained by x-ray diffraction using a precession camera. The correlations are α = c, β = b and γ = a.

Figures 10a and b contain the room temperature, visible and near-infrared polarized absorption spectra of cobalt olivine single crystals. As thin sections were required to record the spectra, two crystals ground down different cell axes were used to obtain the three polarizations. The corresponding 77 K spectrum is shown in Figures 11a and b. The selected cobalt-magnesium olivine crystal was large enough to saw a section perpendicular to the longest external direction. Thus, the polarized spectra of $Mg_{1.62}Co_{0.38}SiO_4$ (room temperature spectra are in Figures 12a and b and 77 K spectra in Figures 13a and b) were obtained from the

FIGURE 4

The 35 K near-infrared and visible absorption spectrum of $LiCoPO_4$ in TlCl. The 200 mg pellet contained 5.4 mg of cobalt triphylite.

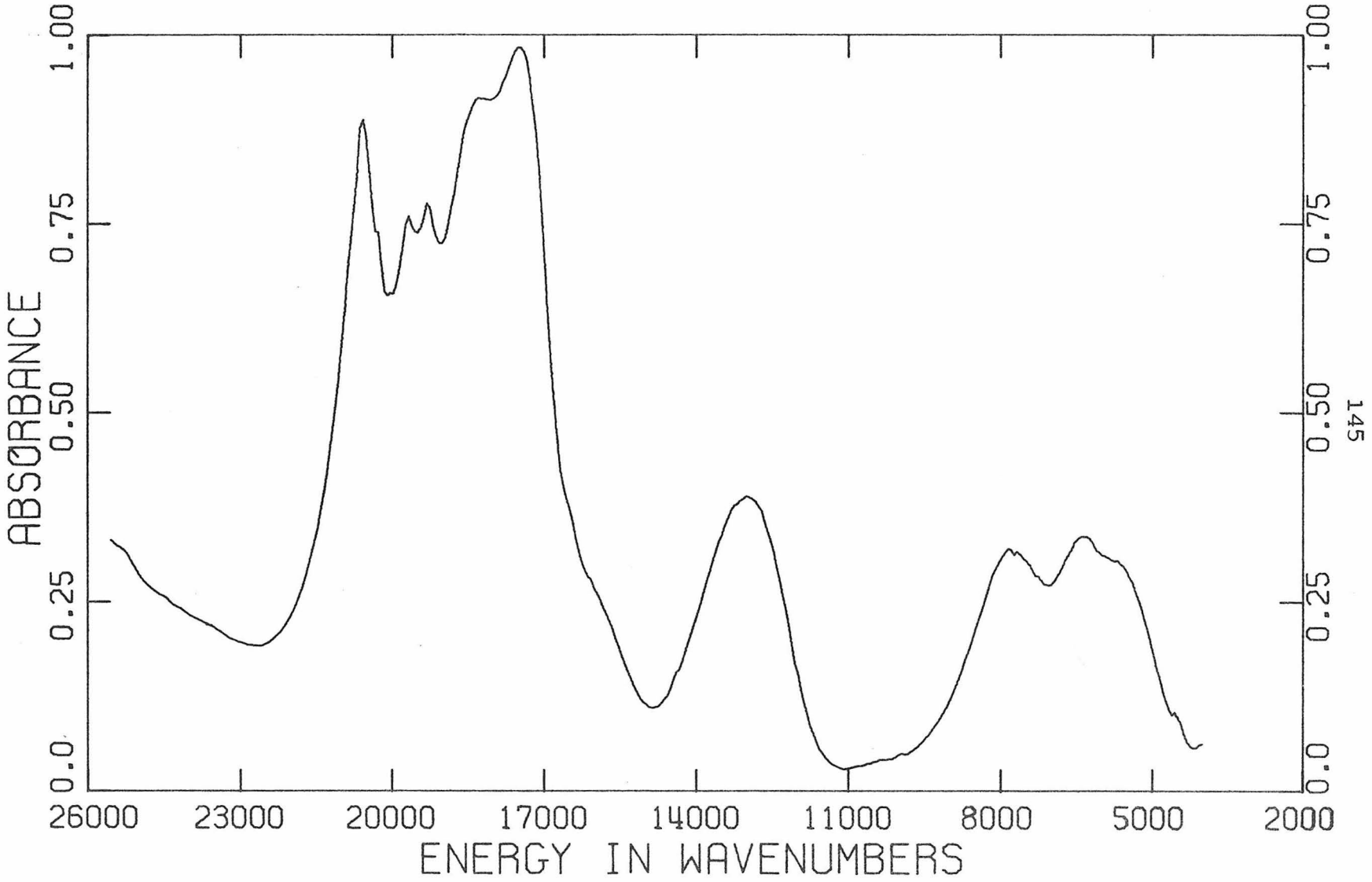
ABSORBANCE
1.00
0.75
0.50
0.25
0.0
26000
23000
20000
17000
14000
11000
8000
5000
2000
ENERGY IN WAVENUMBERS

FIGURE 5

The 35 K near-infrared and visible absorption spectrum of Co_2SiO_4 in TlCl. The 200 mg pellet contained 4.7 mg of cobalt olivine.

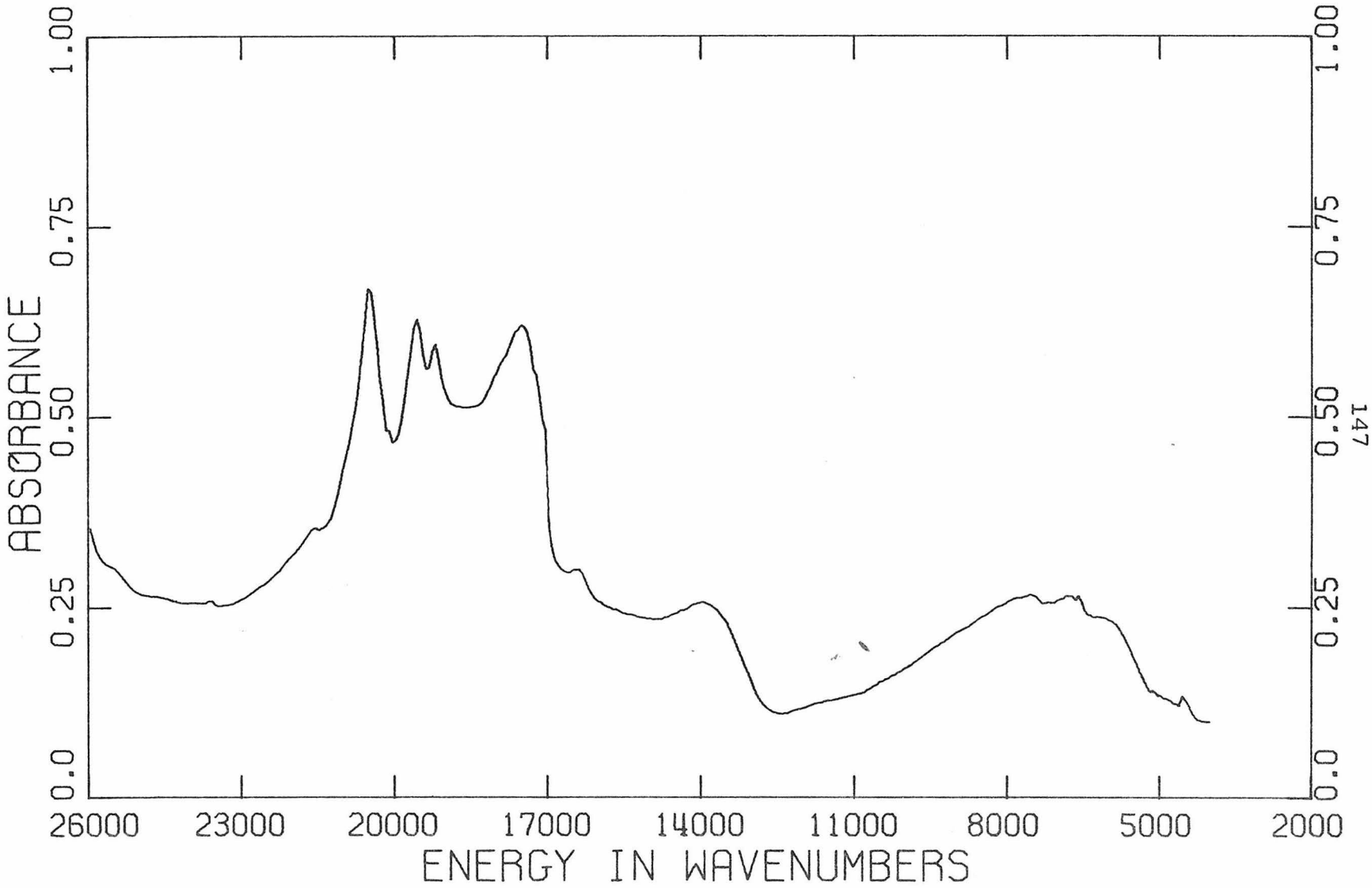
ABSORBANCE
1.00
0.75
0.50
0.25
0.0
26000
23000
20000
17000
14000
11000
8000
5000
2000
ENERGY IN WAVENUMBERS

FIGURE 6

The 35 K near-infrared and visible absorption spectrum of $LiNiPO_4$ in TlCl. The 200 mg pellet contained 4 mg of nickel triphylite.

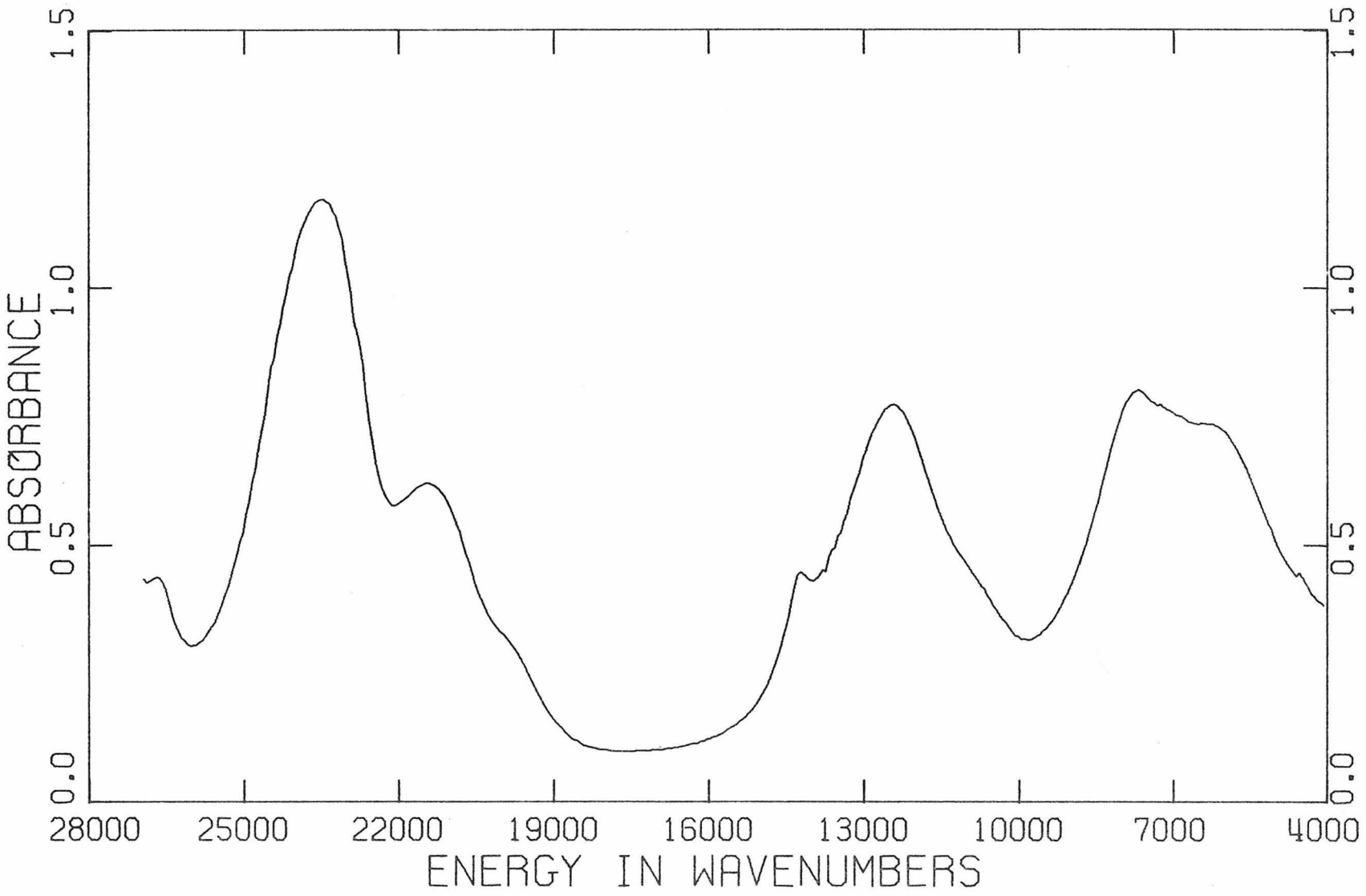
ABSORBANCE
0.0
0.5
1.0
1.5
28000
25000
22000
19000
16000
13000
10000
7000
4000
ENERGY IN WAVENUMBERS

FIGURE 7

The 35 K near-infrared and visible absorption spectrum of Ni_2SiO_4 in TlCl. The 200 mg pellet contained 4.1 mg of nickel olivine.

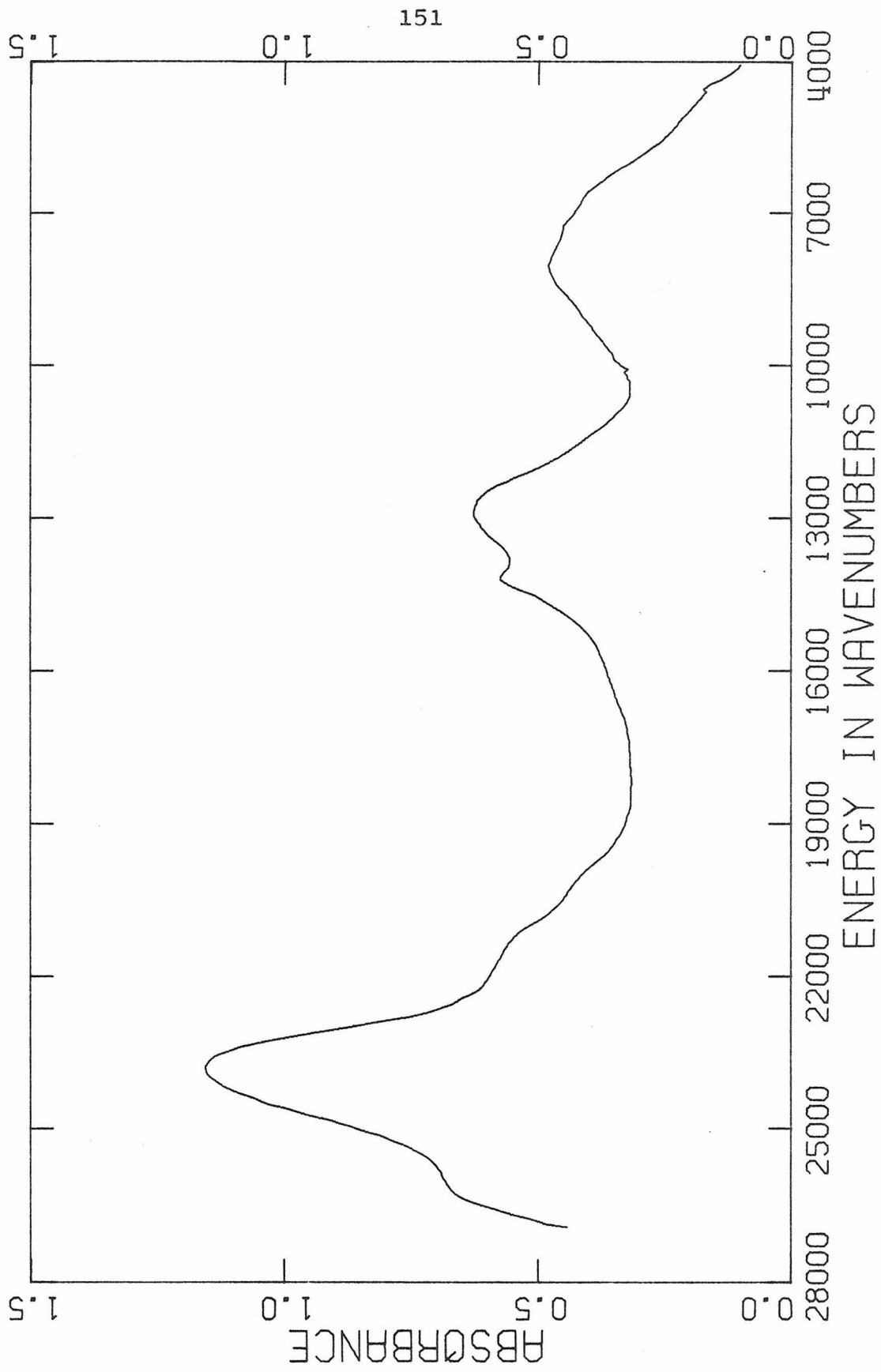
ABSORBANCE
0.0
0.5
1.0
1.5
28000
25000
22000
19000
16000
13000
10000
7000
4000
ENERGY IN WAVENUMBERS

FIGURE 8

The room temperature polarized absorption spectra of $LiFe_{0.64}Mn_{0.36}PO_4$. The β and γ spectra are plotted according to the left-hand scale, and the α spectrum is plotted according to the right-hand scale. α = c, β = b, γ = a.

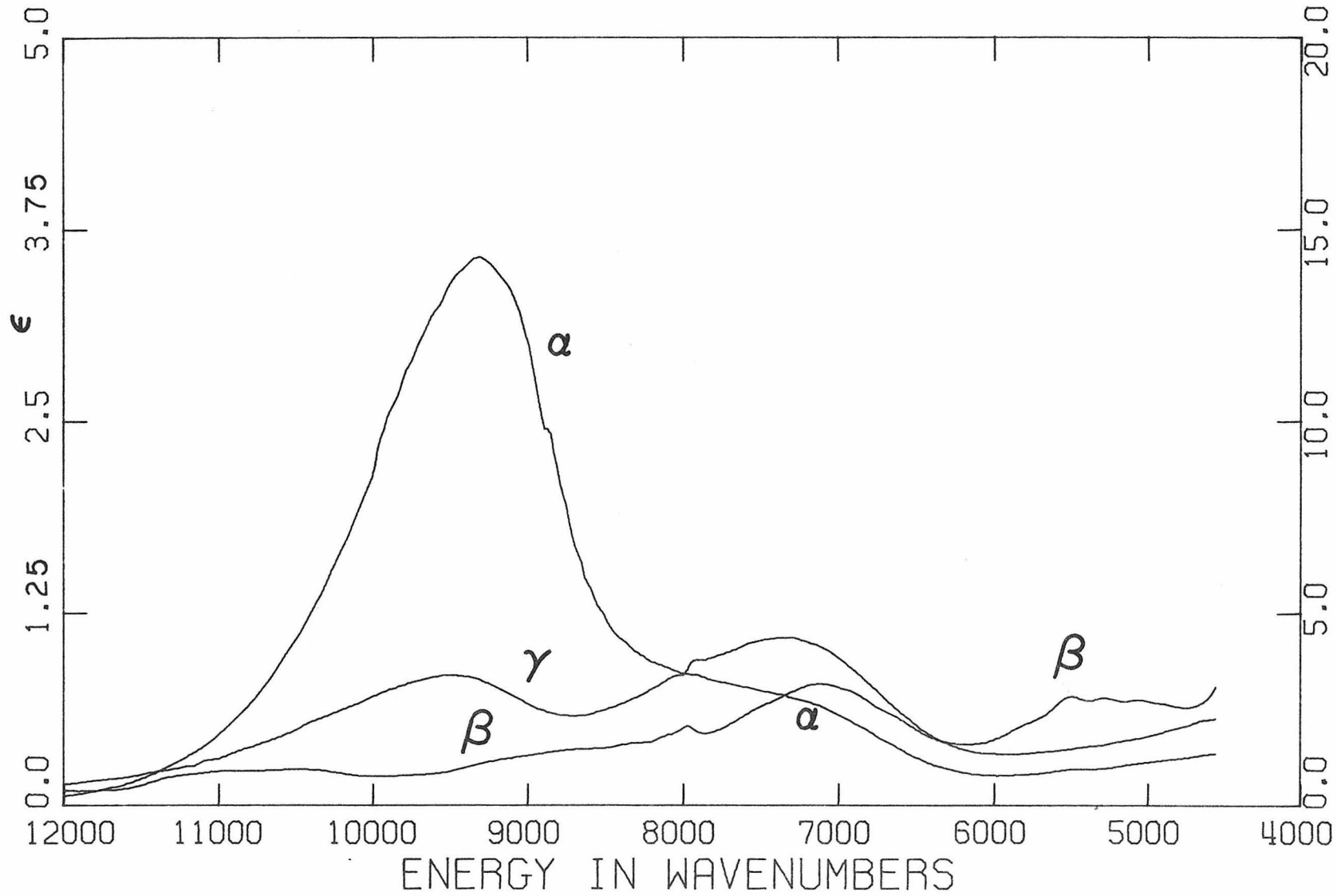
5.0
3.75
2.5
1.25
0.0
ε
20.0
15.0
10.0
5.0
0.0
α
γ
β
β
α
12000
11000
10000
9000
8000
7000
6000
5000
4000
ENERGY IN WAVENUMBERS

FIGURE 9

The 77 K polarized, near-infrared absorption spectra of $LiFe_{0.64}Mn_{0.36}PO_4$. The β and γ spectra are plotted according to the left-hand scale, and the α spectrum is plotted according to the right-hand scale. α = c, β = b, γ = a.

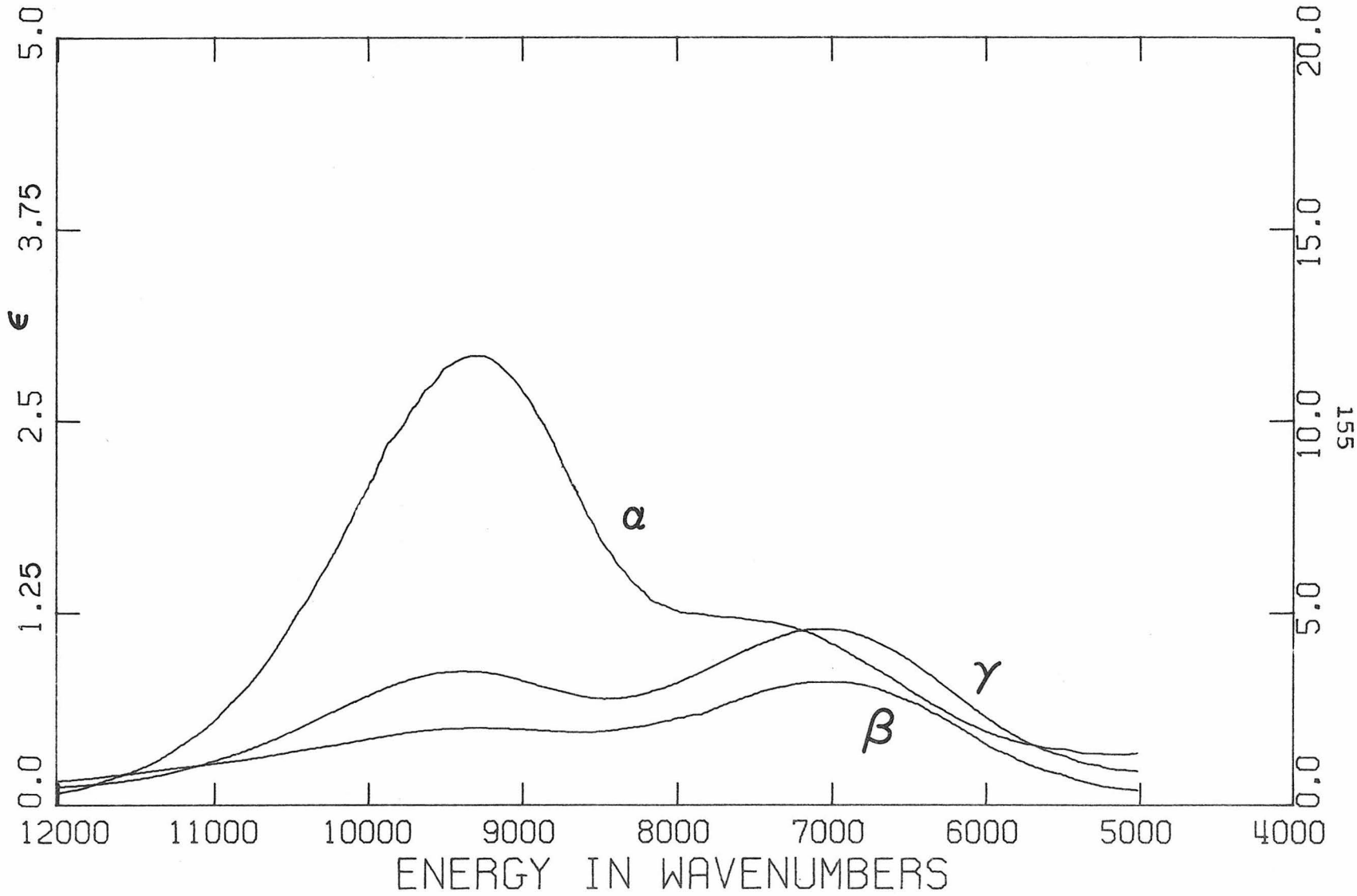
5.0
3.75
2.5
1.25
0.0
ε
20.0
15.0
10.0
5.0
0.0
α
β
γ
12000
11000
10000
9000
8000
7000
6000
5000
4000
ENERGY IN WAVENUMBERS

FIGURE 10

The room temperature polarized, visible (a) and near-infrared (b) absorption spectra of Co_2SiO_4. α = a, β = b, γ = c.

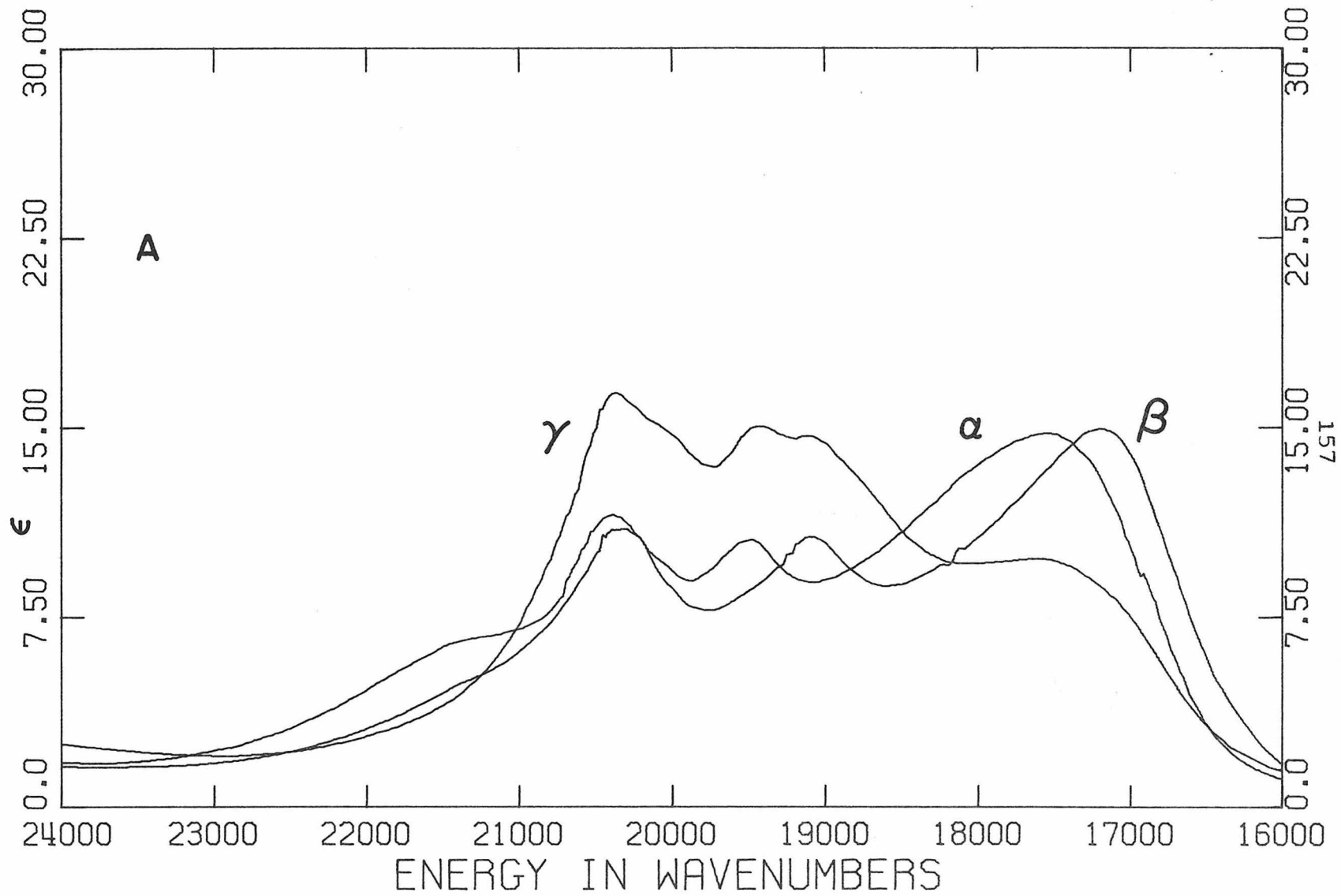
A
γ
α
β
ε
30.00
22.50
15.00
7.50
0.0
24000
23000
22000
21000
20000
19000
18000
17000
16000
ENERGY IN WAVENUMBERS

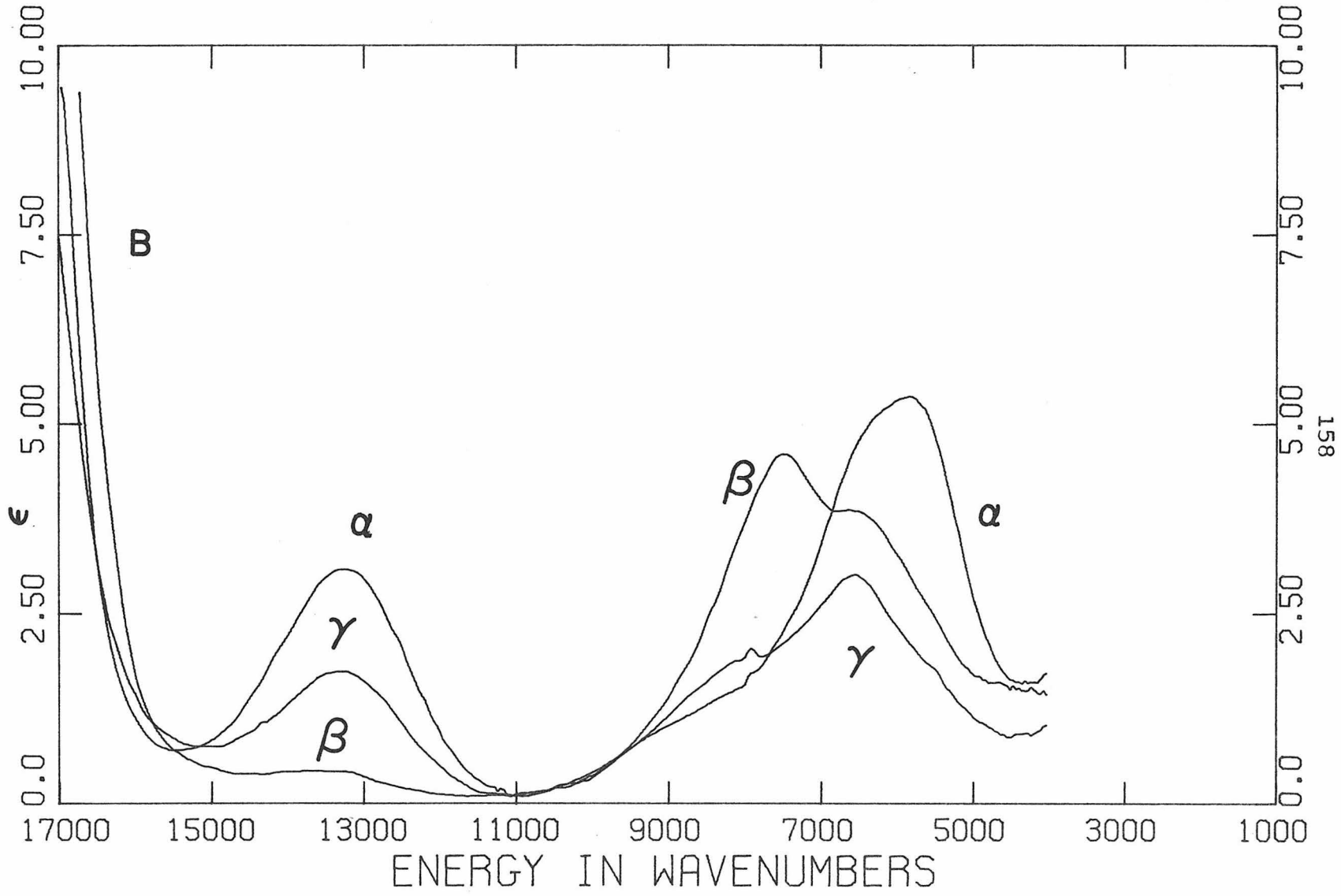
B
α
γ
β
β
α
γ
ε
10.00
7.50
5.00
2.50
0.0
17000
15000
13000
11000
9000
7000
5000
3000
1000
ENERGY IN WAVENUMBERS

FIGURE 11

The 77 K polarized visible (a) and near-infrared (b) absorption spectra of Co_2SiO_4. A crystal thickness of ~20μ is required to keep the visible bands below an absorbance of 2. α = a, β = b, γ = c.

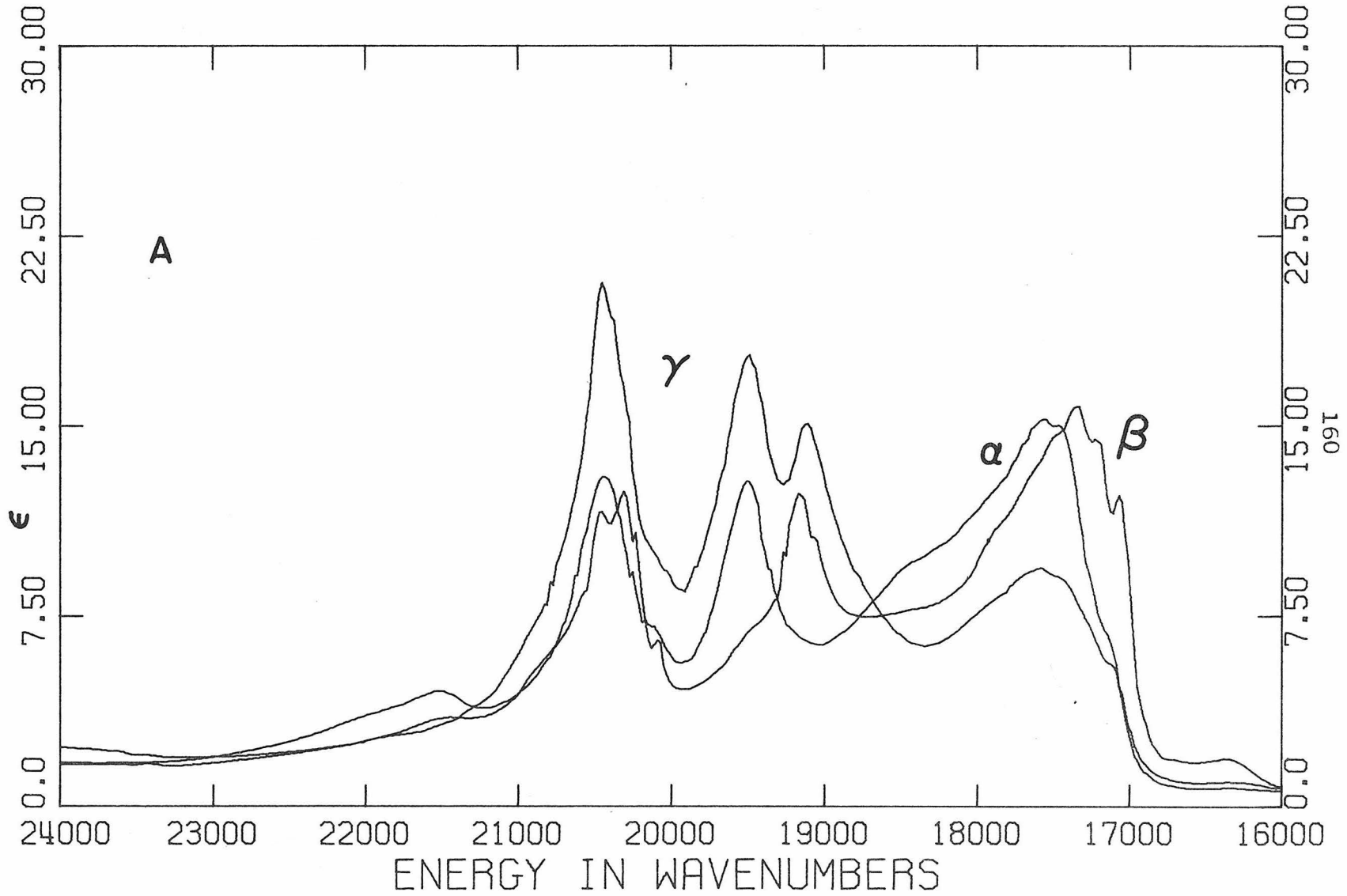
A
γ
α
β
ε
30.00
22.50
15.00
7.50
0.0
24000
23000
22000
21000
20000
19000
18000
17000
16000
ENERGY IN WAVENUMBERS
160

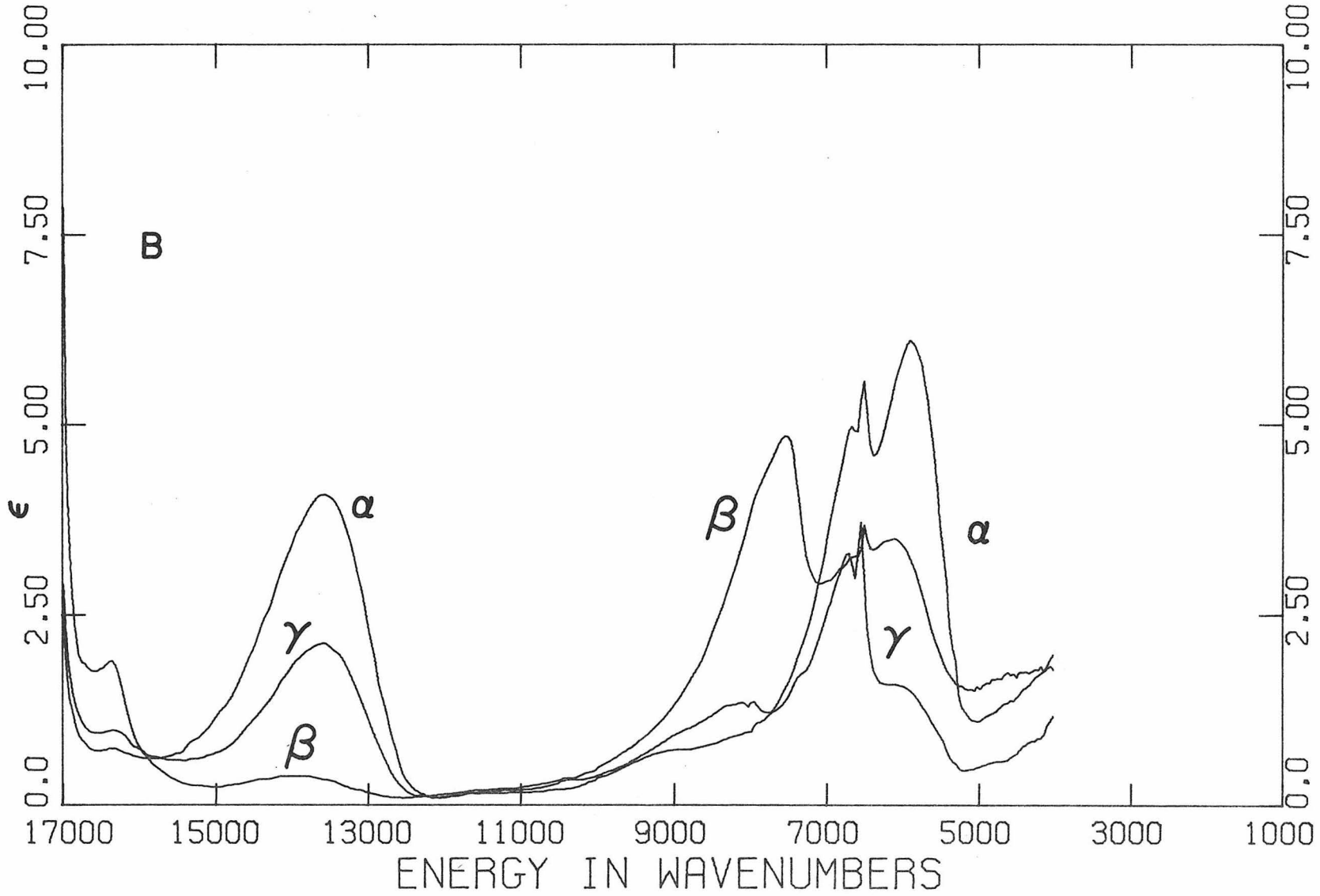
B
α
β
γ
β
α
γ
ε
10.00
7.50
5.00
2.50
0.0
17000
15000
13000
11000
9000
7000
5000
3000
1000
ENERGY IN WAVENUMBERS

FIGURE 12

The room temperature, polarized visible (a) and near-infrared (b) absorption spectra of $Mg_{1.62}Co_{0.38}SiO_4$. α = a, β = b, γ = c. ϵ-values are extinction coefficients per cobalt atom.

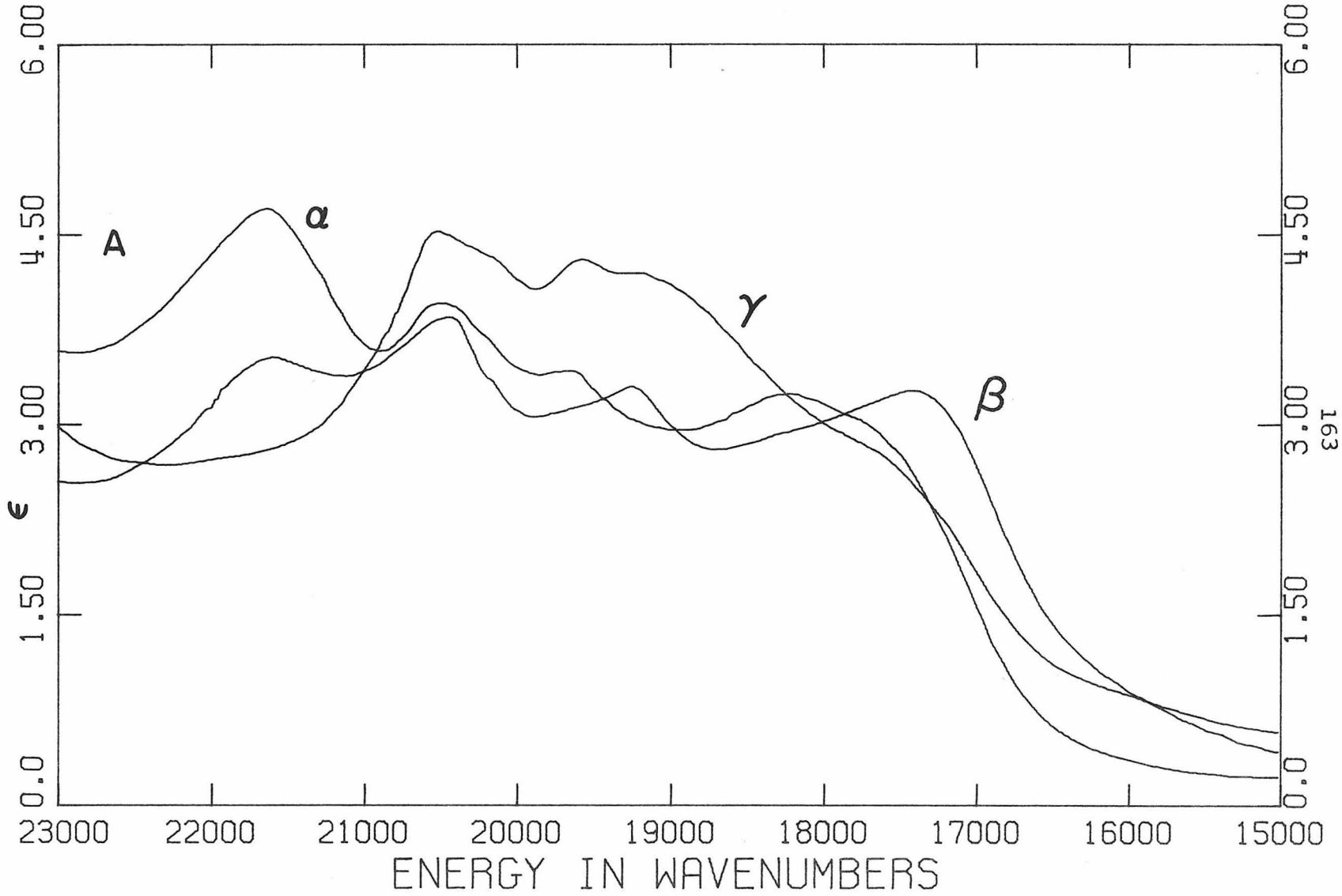
6.00
4.50
3.00
1.50
0.0
ε
A
α
γ
β
23000
22000
21000
20000
19000
18000
17000
16000
15000
ENERGY IN WAVENUMBERS

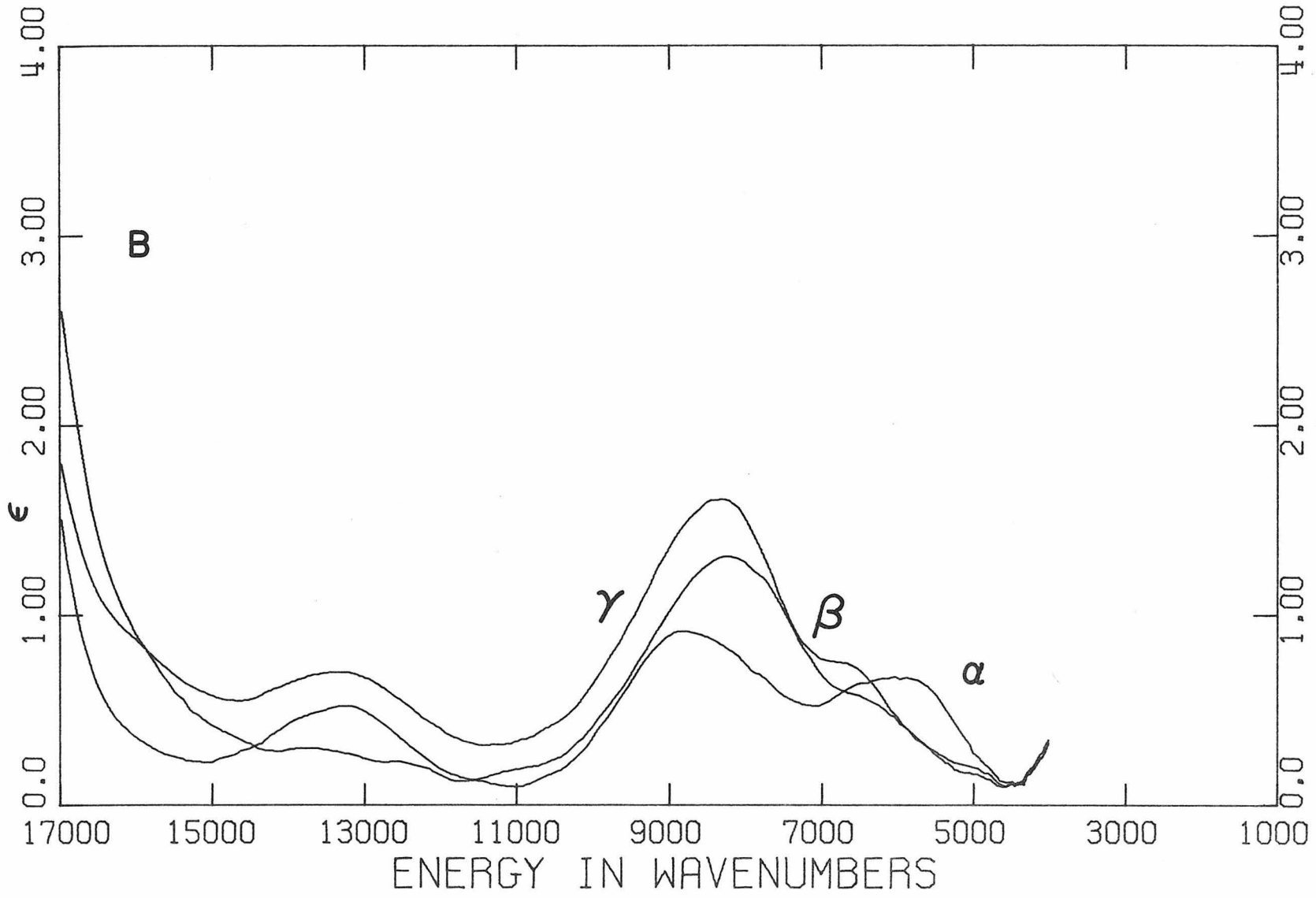
B
ε
4.00
3.00
2.00
1.00
0.0
γ
β
α
17000
15000
13000
11000
9000
7000
5000
3000
1000
ENERGY IN WAVENUMBERS

same crystal. X-ray diffraction data obtained on a precession camera confirmed that α = a, β = b and γ = c.

The room temperature, visible and near-infrared polarized absorption spectra of nickel olivine are presented in Figures 14a and b. The corresponding 77 K spectra are shown in Figures 15a and b. The room temperature, polarized absorption spectra of $Mg_{1.5}Ni_{0.5}SiO_4$ are shown in Figures 16a and b, and the corresponding 77 K spectra appear in Figures 17a and b. Two separate crystals were required to obtain all three polarization for both Ni_2SiO_4 and $Mg_{1.5}Ni_{0.5}SiO_4$. X-ray diffraction data obtained on a precession camera confirmed that α = a, β = b and γ = c.

DISCUSSION

Assignment of absorption spectra according to metal site

The polarized absorption spectra of olivine have been the subject of numerous investigations. Farrell and Newnham reported the spectra, but made no attempts to assign them[15]. Burns assigned bands at 11790 (Band I) and 9090 cm^{-1}(Band III) to be Fe^{+2} in the M_1 site and the intense feature polarized along c (γ) to Fe^{+2} in the M_2 site[7]. In a later work, Burns reported spectra of a series of olivines containing different magnesium to iron ratios[16]. Band I was observed in the range

FIGURE 13

The 77 polarized visible (a) and near-infrared (b) absorption spectra of $Mg_{1.62}Co_{0.38}SiO_4$. Crystal thicknesses were ~300μ. ϵ-values are extinction coefficients per cobalt atom. α = a, β = b, γ = c.

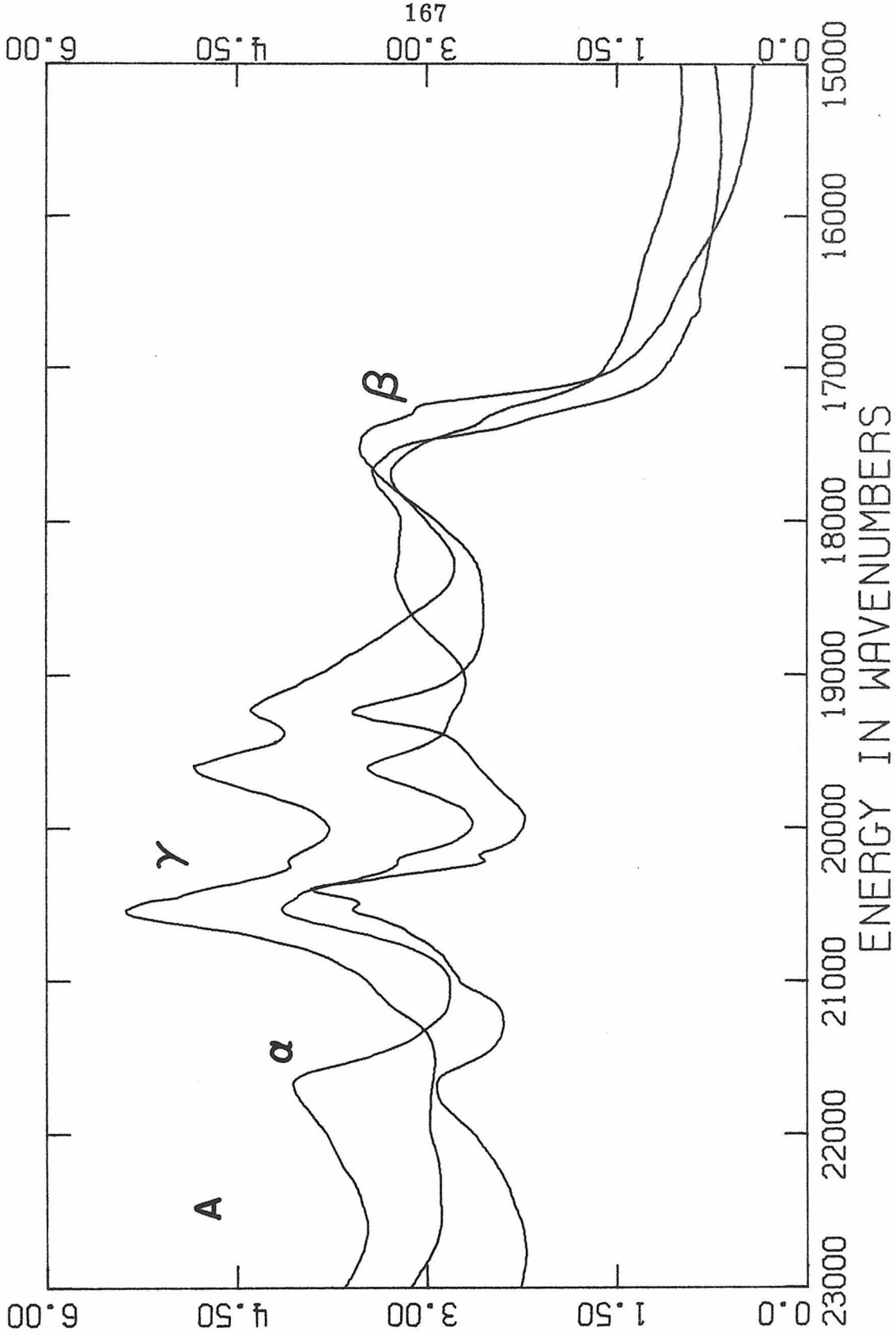
0.0
1.50
3.00
4.50
6.00
23000
22000
21000
20000
19000
18000
17000
16000
15000
ENERGY IN WAVENUMBERS
A
α
γ
β

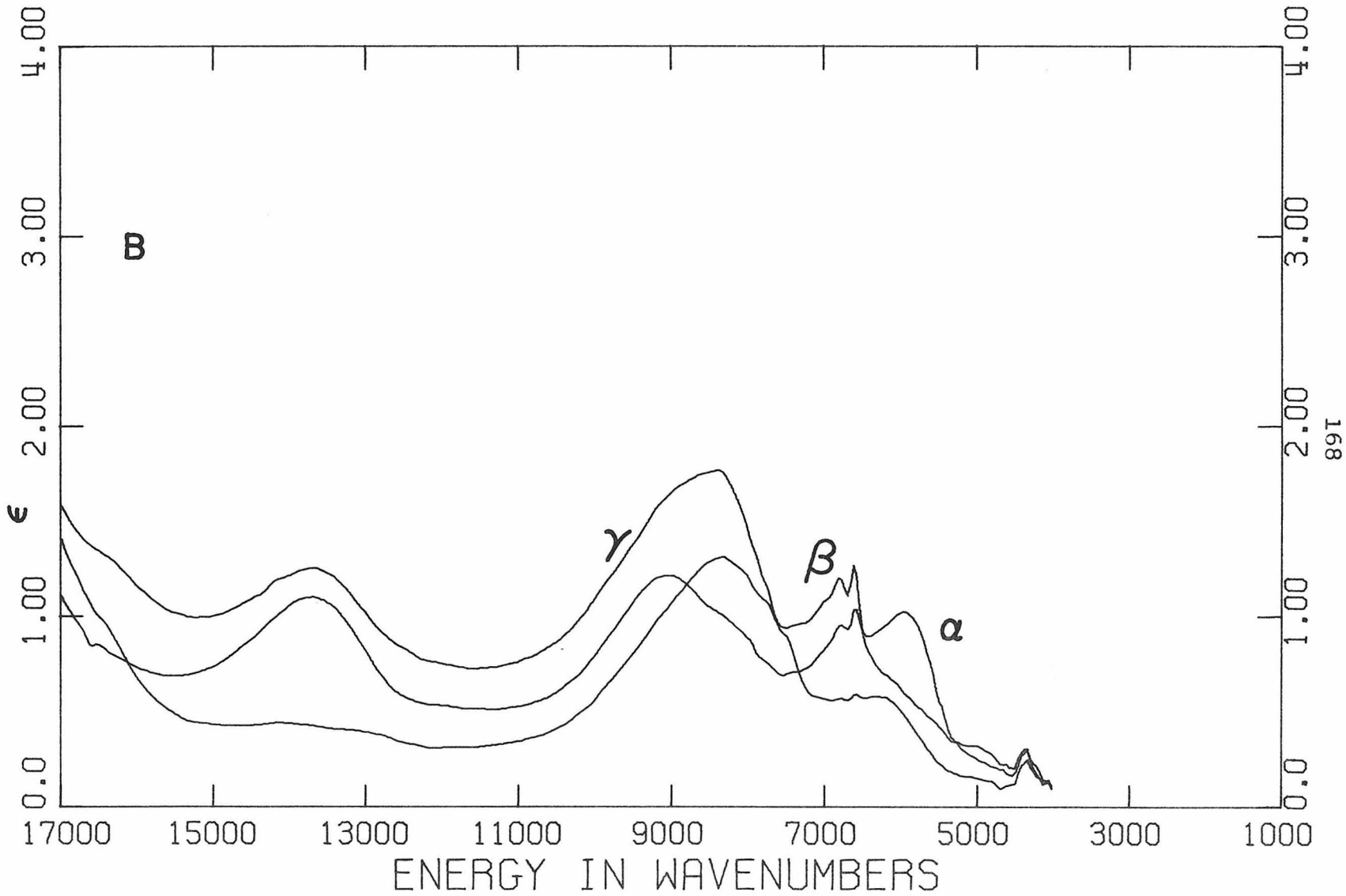
B
γ
β
α
ε
4.00
3.00
2.00
1.00
0.0
17000
15000
13000
11000
9000
7000
5000
3000
1000
ENERGY IN WAVENUMBERS

FIGURE 14

The room temperature, polarized visible (a) and near-infrared (b) spectra of Ni_2SiO_4. α = a, β = b, γ = c.

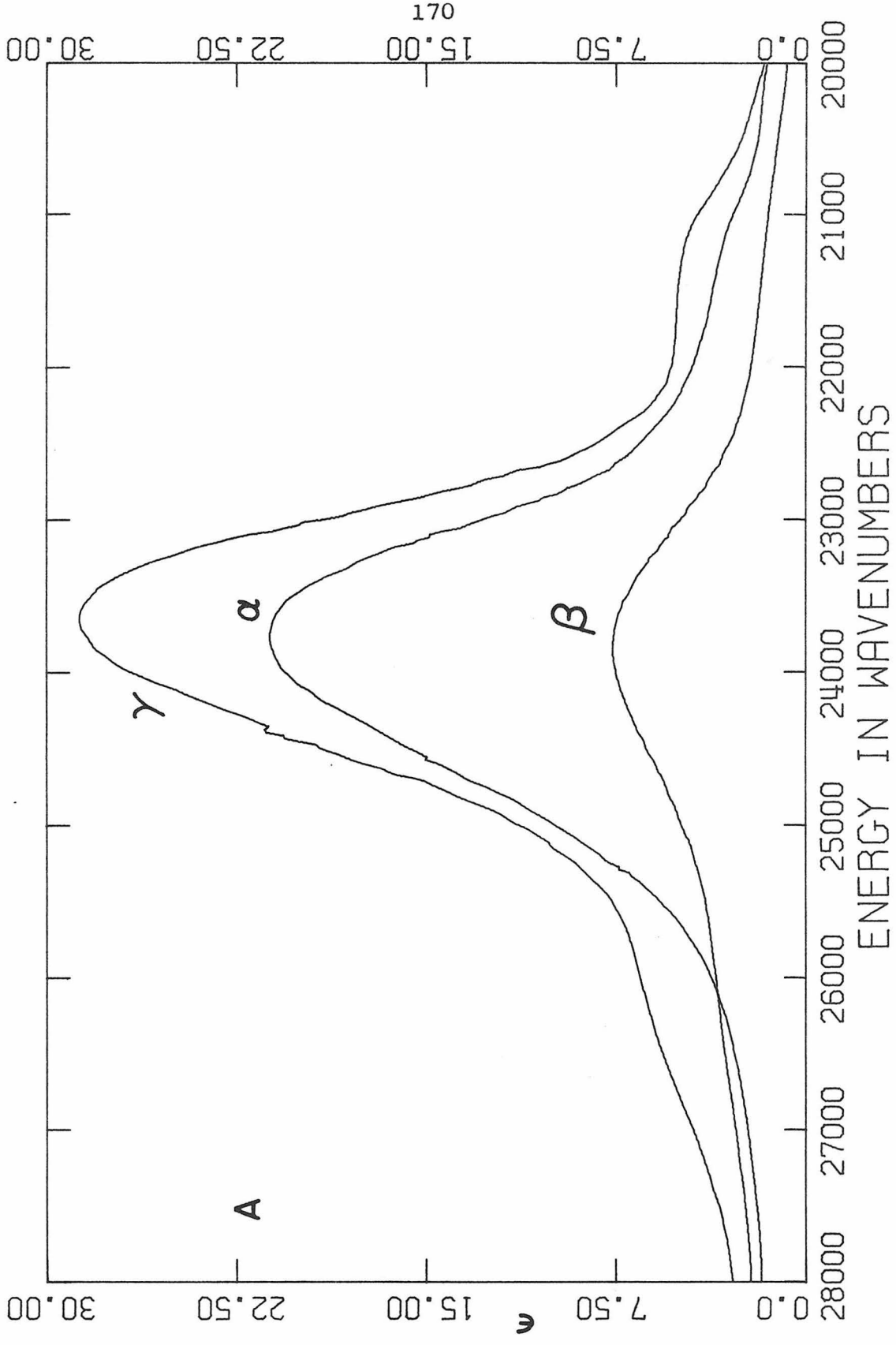
30.00
22.50
15.00
7.50
0.0
ε
A
γ
α
β
28000
27000
26000
25000
24000
23000
22000
21000
20000
ENERGY IN WAVENUMBERS

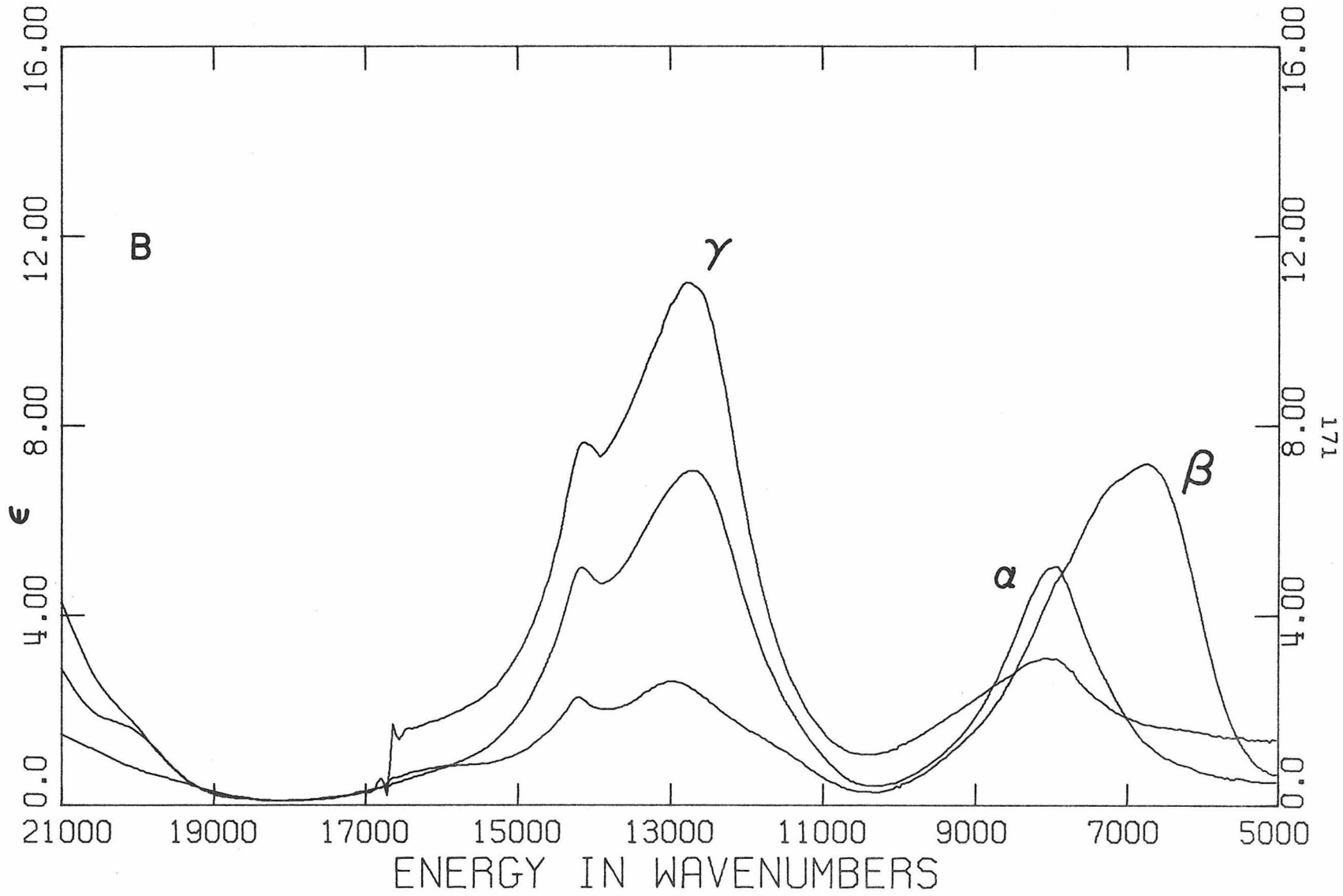
B
γ
β
α
ε
16.00
12.00
8.00
4.00
0.0
21000
19000
17000
15000
13000
11000
9000
7000
5000
ENERGY IN WAVENUMBERS

FIGURE 15

The 77 K polarized visible (a) and near-infrared (b) absorption spectra of Ni_2SiO_4. Crystal thicknesses of ~20 μ were required to keep the visible absorption band below an absorbance of 2. α = a, β = b, γ = c.

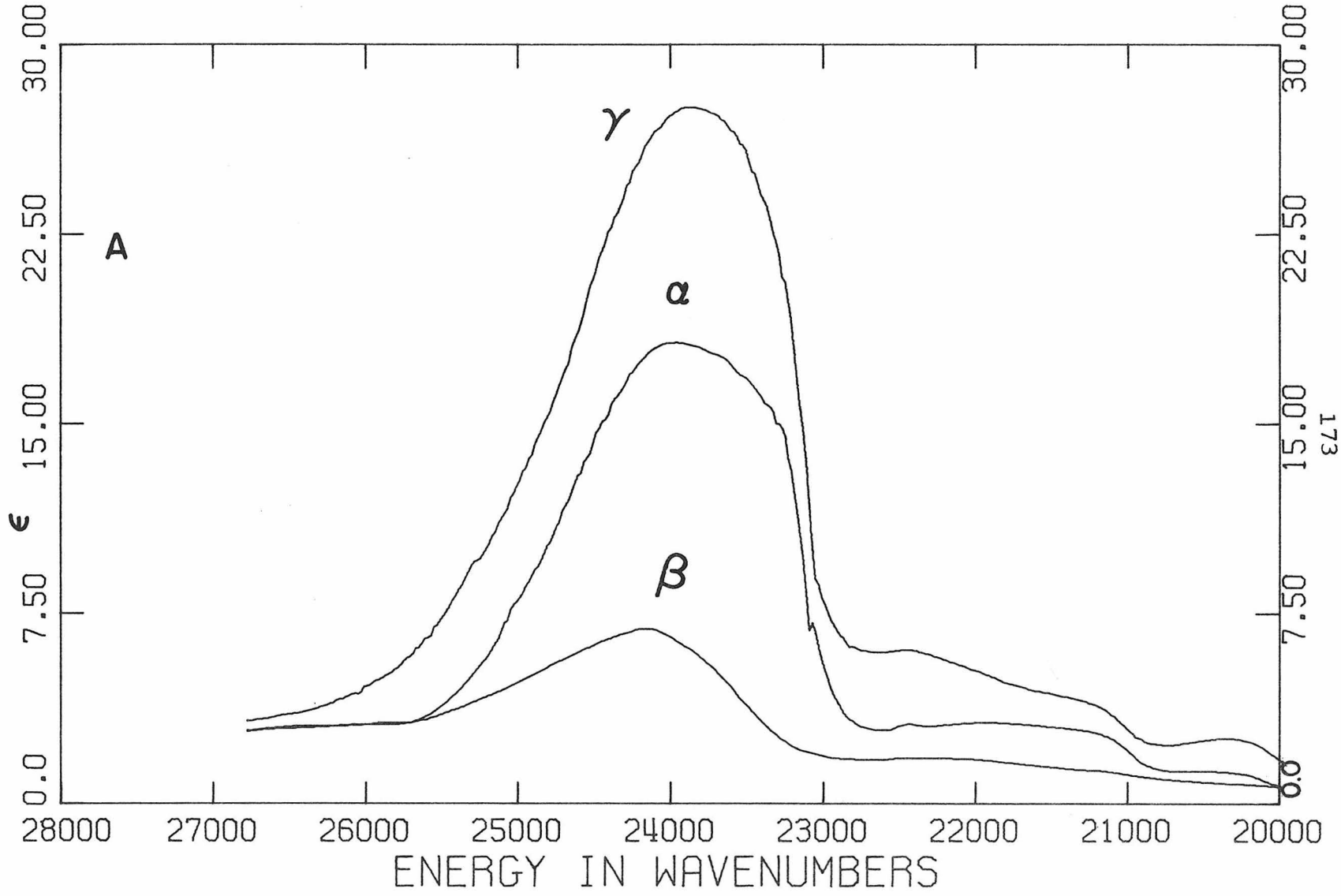
30.00
22.50
15.00
7.50
0.0
ε
A
γ
α
β
28000
27000
26000
25000
24000
23000
22000
21000
20000
ENERGY IN WAVENUMBERS

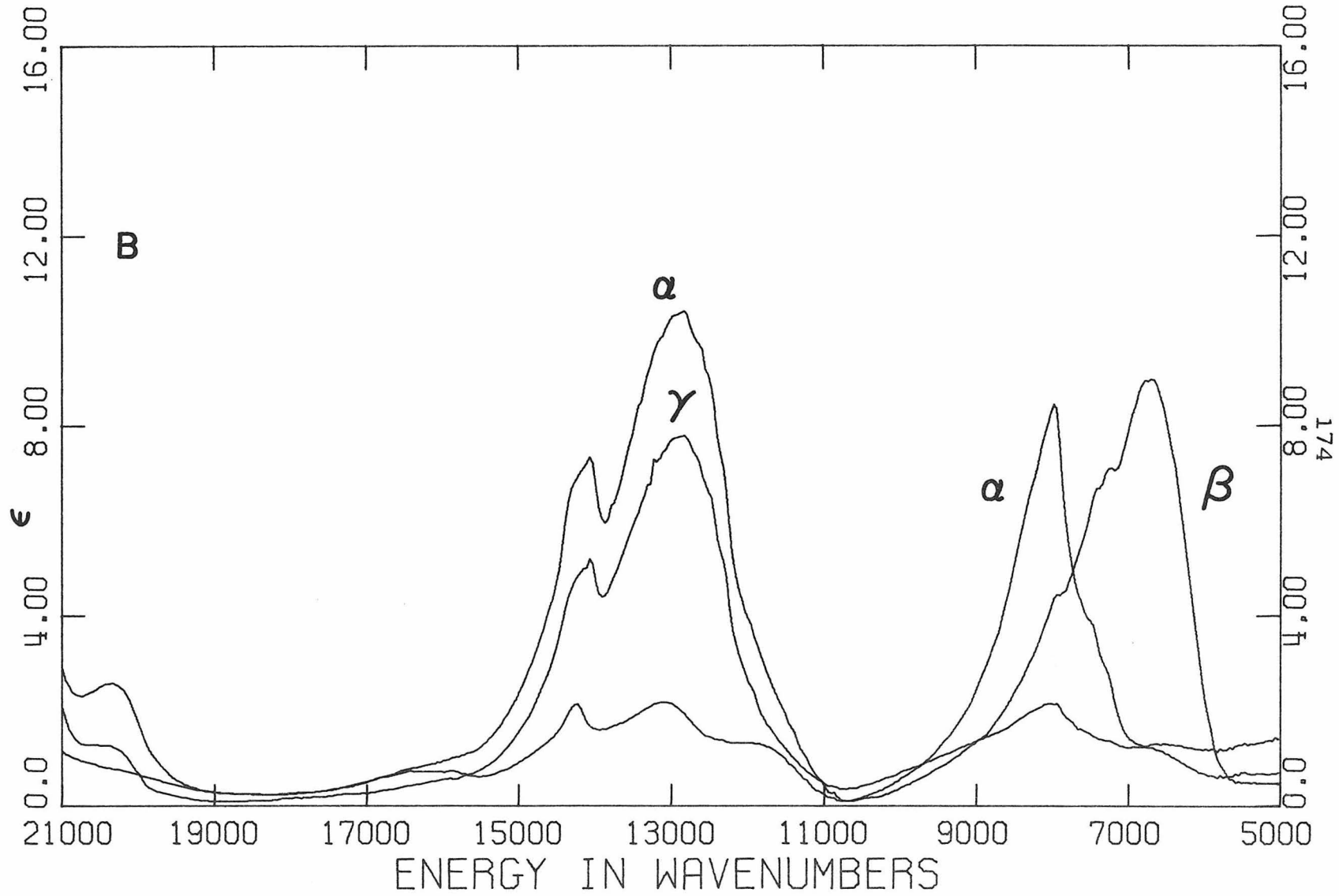
B
α
γ
α
β
ε
0.0
4.00
8.00
12.00
16.00
0.0
4.00
8.00
12.00
16.00
21000
19000
17000
15000
13000
11000
9000
7000
5000
ENERGY IN WAVENUMBERS

FIGURE 16

The room temperature, polarized near-infrared absorption spectra of $Mg_{1.5}Ni_{0.5}SiO_4$. α = a, β = b, γ = c.

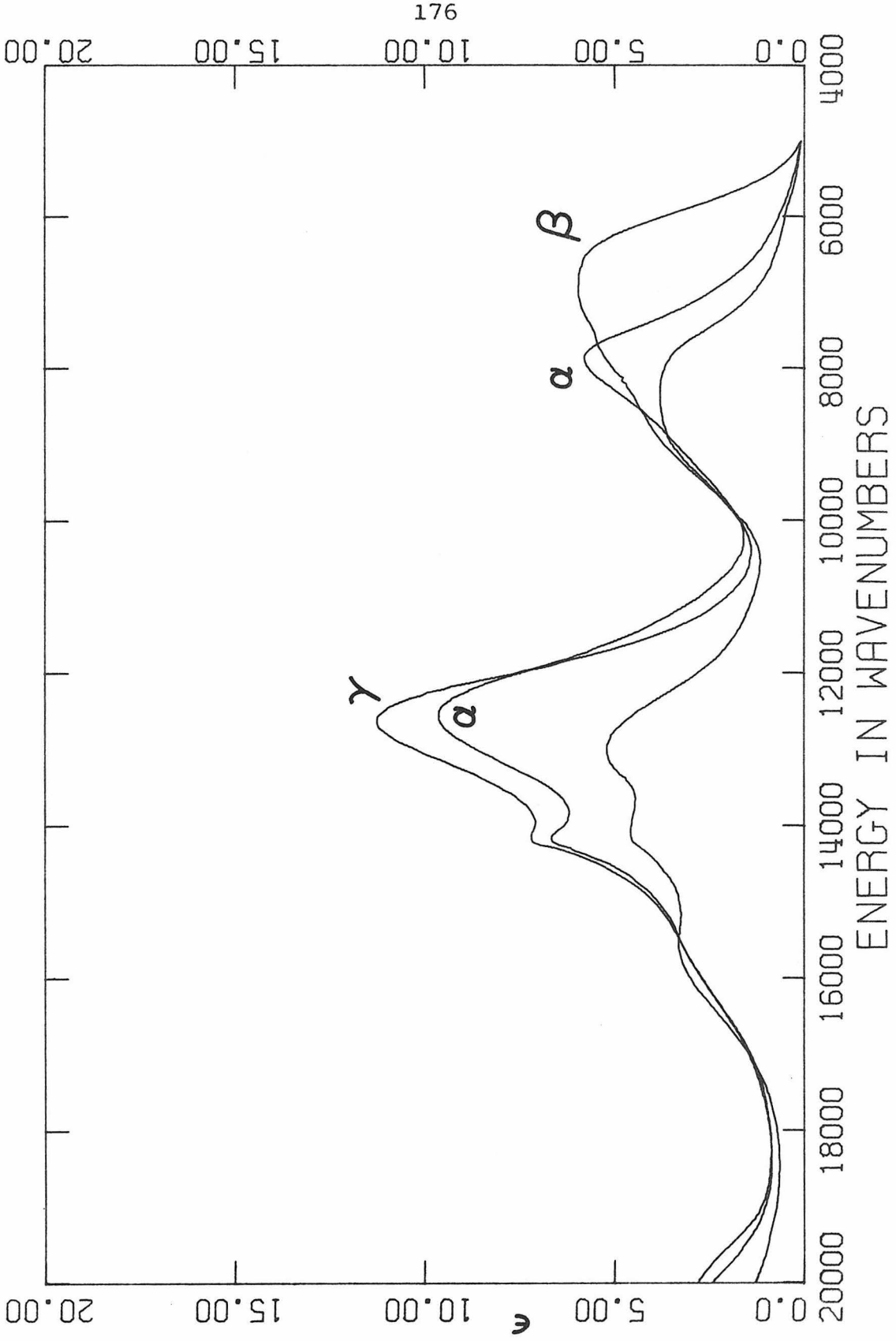
0.0
5.00
10.00
15.00
20.00
ε
20000
18000
16000
14000
12000
10000
8000
6000
4000
ENERGY IN WAVENUMBERS
γ
α
α
β

FIGURE 17

The 77 K polarized visible (a) and near-infrared (b) absorption spectra of $Mg_{1.5}Ni_{0.5}SiO_4$. Crystal thicknesses were ~40 μ. α = a, β = b, γ = c.

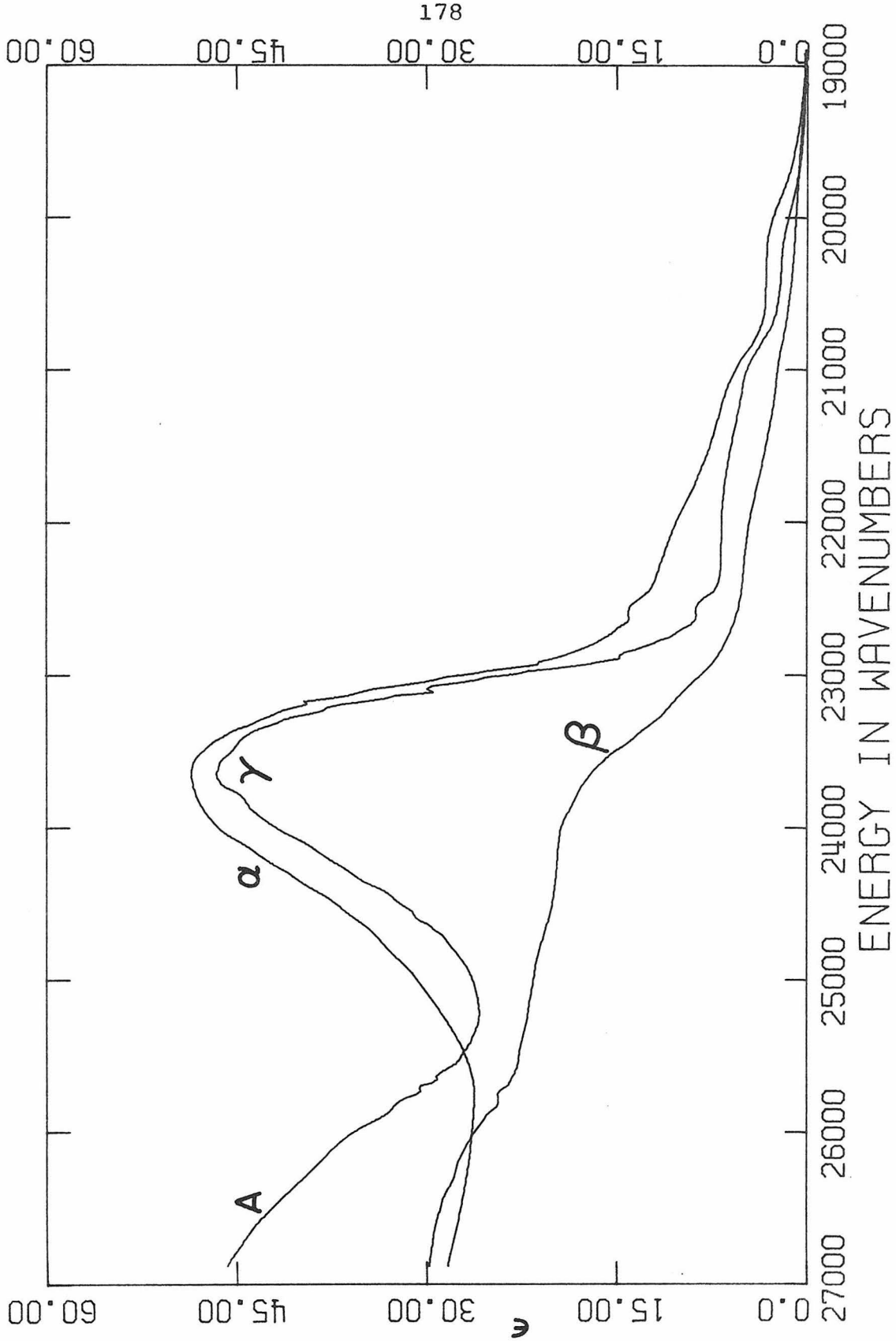
60.00
45.00
30.00
15.00
0.0
ε
A
α
γ
β
0.0
15.00
30.00
45.00
60.00
27000
26000
25000
24000
23000
22000
21000
20000
19000
ENERGY IN WAVENUMBERS

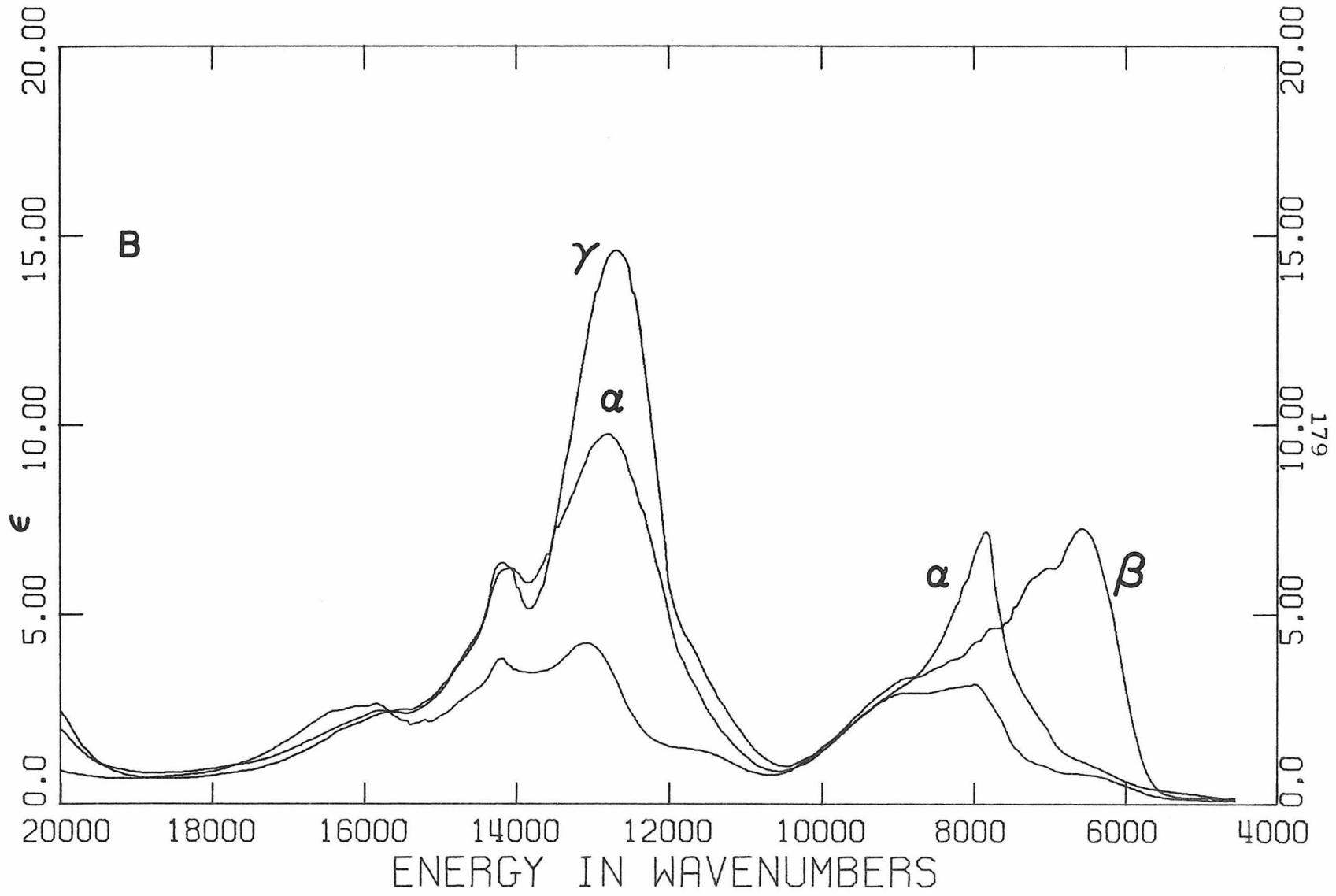
B
γ
α
α
β
ε
20.00
15.00
10.00
5.00
0.0
20000
18000
16000
14000
12000
10000
8000
6000
4000
ENERGY IN WAVENUMBERS

11680 to 10930 cm^{-1}, Band II showed a range of 9560 to 9280 cm^{-1}, and Band III had a range of 9200 to 8070 cm^{-1} for the series as the mole percent Fe_2SiO_4 increased from 8.4 to 97.9%. He cited composition dependent area ratios of the Gaussian resolved bands of the γ spectrum as further confirmation of his site assignment. Runciman, et al. assigned Bands II and III (at 9540 and 9100 cm^{-1}, respectively) to Fe^{+2} in the M_2 site and observed a weak shoulder at ~8000 cm^{-1} (Band IV), which was not assigned[17]. Burns' reply to Runciman, et al. included a spectrum of kirschteinite, an iron-rich monticellite with the stoichiometry $CaMg_{0.3}Fe_{0.7}SiO_4$[18]. The monticellites are calcic olivines which have been shown to have complete ordering of the octahedral sites with Ca^{+2} occupying the M_2 position[19], thus, Burns' spectrum should represent iron in the M_1 site. He reported bands at 10900 and 8700 cm^{-1} and no intense features in the γ-polarized spectrum, confirming that Band III was attributable to iron in the M_1 site[18].

The triphylites are phosphates which crystallize in the olivine structure[5]. They exhibit complete ordering of cations in the octahedral sites, with Li^+ occupying the M_1 site[20,21]. Hanke has compared the M_1 and M_2 sites of various olivine structures including $LiMnPO_4$ and Fe_2SiO_4[22]. The M_2 sites of these structures

are strikingly similar. The mean metal-oxygen distance is 0.01 Å longer in the phosphate, one set of $M\text{-}O_3$ lengths increases from 2.09 to 2.13 Å, and the $O_3\text{-}M\text{-}O_3$ angles change from 68.8° to 64.9° and 114.6° to 117.9°, thus the M_2 site of triphylite is slightly larger and somewhat more distorted than that of olivine. The polarized absorption spectra of triphylite (Figures 8 and 9) exhibit an intense band in $\alpha(c)$ at 9250 cm^{-1}, which corresponds to the energy of Band II in the iron-rich olivines[16]. In addition a shoulder is observed at ~7500 cm^{-1} in the α-polarized spectrum. Thus, Band IV is assigned to iron occupying M_2, and Burns' assignment of Bands I, II and III is confirmed.

Cobalt substituted triphylite ($LiCoPO_4$) was synthesized so that similar comparisons could be made for cobalt olivine. Several bands of the Co_2SiO_4 spectrum were assigned by Schmitz-DuMont and Friebel from reflectance studies on the systems $[Co,Mg]_2SiO_4$ and $Ca[Co,Mg]SiO_4$[23]. Specifically, bands at 6500 and 13300 cm^{-1} were assigned to Co^{+2} in M_2 and bands at 8250, 16000 and 21500 cm^{-1} to Co^{+2} in M_1 for Co_2SiO_4. As reflectance maxima do not necessarily represent absorption maxima, the TlCl pellet spectra of $LiCoPO_4$ and Co_2SiO_4 were compared to confirm Schmitz-DuMont and Friebel's assignments and sort out the complicated

visible energy region. Further, low temperature spectra were recorded to improve resolution in regions where heavy overlapping of bands was observed. Examination of Figures 4 and 5 reveal that bands at 21500 and ~9000 cm^{-1}, and possibly at 16300 cm^{-1}, can be identified with the M_1 site. The remaining spectral features are probably the result of d-d excitations of Co^{+2} in the M_2 site.

As attempts to crystallize $LiCoPO_4$ failed, crystals of cobalt-magnesium olivine, generously supplied by Dr. Jun Ito, were examined with polarized light and compared to the polarized Co_2SiO_4 spectra. The weak band at 21500 cm^{-1} in cobalt olivine has gained intensity with respect to the band at 20400 cm^{-1} upon lowering the total cobalt concentration, consistent with x-ray diffraction data which indicate Co^{+2} is preferentially located at the M_1 site[8]. As the absorption at 8800 cm^{-1} shows the same dependence on cobalt concentration, it must also be a transition associated with Co^{+2} in the M_1 site.

The reflection spectra of nickel monticellite and members of the $[Ni,Mg]_2SiO_4$ series were reported by Reinen[24]. Although he concluded nickel preferentially occupies M_1 and that 10 Dq is larger for M_1 and M_2, no band energies were specifically assigned with regards

to site. Nickel(II) has also been shown by Rajmani, et al. to prefer M_1 occupation[9]. In comparing the visible spectrum of $LiNiPO_4$ with that for Ni_2SiO_4 (Figures 6 and 7, respectively), it is clear that the prominent shoulder at ~26200 cm^{-1} is missing in the M_2 site spectrum. This band is therefore assigned to Ni^{+2} in the M_1 site. Increased intensity in the vicinity of 9500 cm^{-1} in Ni_2SiO_4 suggests that a transition in the Ni^{+2} d-manifold of the M_1 site occurs in this energy region. The main features of the Ni_2SiO_4 spectrum appear to be due to excitations of Ni^{+2} in the M_2 site, as they are also observed in $LiNiPO_4$.

The 26000 cm^{-1} band assignment could not be confirmed by the polarized absorption spectra of magnesium-nickel olivine, as the region is masked by an intense ultraviolet band, thought to be the result of trace levels of vanadium, reported in Ito's analyses. Reinen's reflectance spectra of the $[Mg,Ni]_2SiO_4$ series show that the 26000 cm^{-1} shoulder increases in intensity compared to the 24000 cm^{-1} band with decreasing nickel concentration, as expected for preferential population of the M_1 site. As absorption bands at 9000 and 16100 cm^{-1} are also more prominent in the single crystal spectra of magnesium-nickel olivine than in the

pure nickel sample, they are assigned as d-d transitions of Ni^{+2} in the M_1 site as well.

Polarization properties of the M_2 site

Burns has described the M_2 site as a trigonally distorted octahedron that can be regarded as approximately C_{3v}[16]. Runciman concluded that the observed polarization of Band II was in conflict with that predicted for a trigonal distortion and replaced the trigonal model with a C_{2v} description[17]. The crystal axes a, b and c were assigned the molecular axes .67y + .33z, x and .67z + .33y, respectively. Figure 18 illustrates the relationship between the crystal and molecular coordinate systems. As Runciman's assignment has been shown to be incorrect, the polarization properties of iron(II) in the M_2 site should be reexamined. The absorption spectrum of triphylite shows the 9300 and 7200 cm^{-1} bands are both polarized along $c \approx z(\alpha)$. As none of the energy level schemes of Figure 19 predict the observed polarizations, it is concluded that the simple site symmetry approximation must be modified to include the effects of spin-orbit coupling and possibly nearest neighbor interactions via the factor group antiferromagnetic coupling. The orbital splitting is assumed to remain the consequence of the approximate C_{2v} site symmetry.

FIGURE 18

ORTEP perspective views and projections of the M_2 site down the crystal axes. Molecular axes, according to Runciman, et al. are also shown for the projection views.

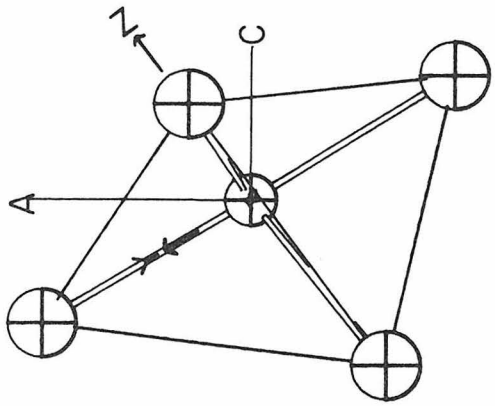
N
C
A

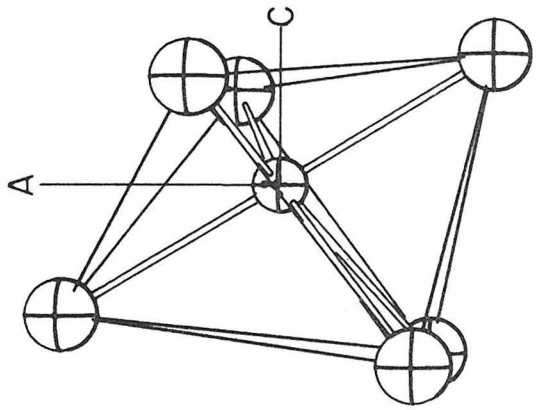
C
A

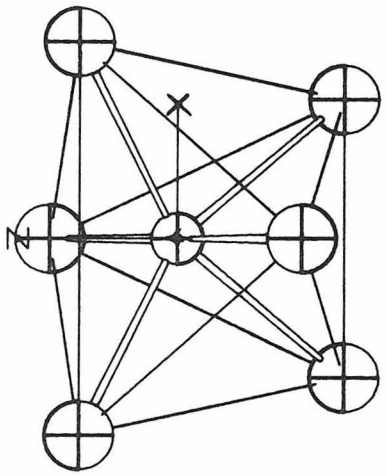
X
Z

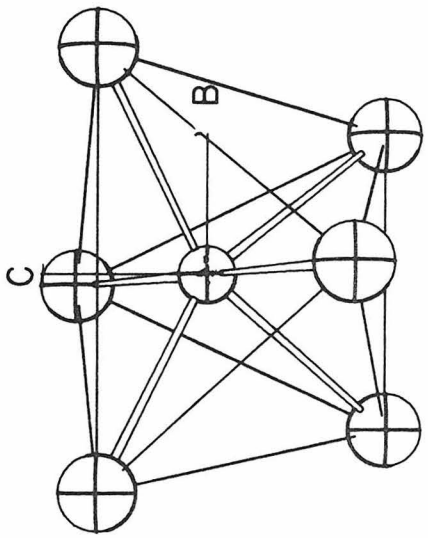
B
C

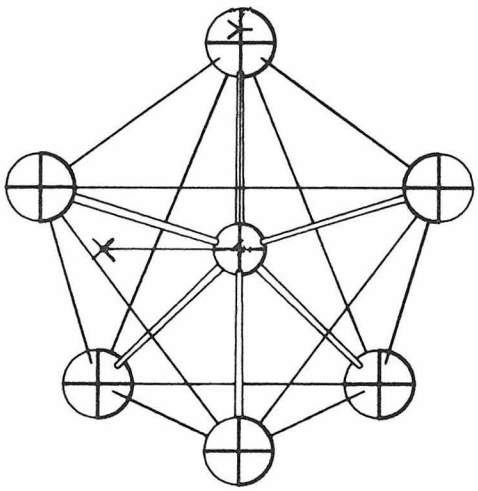
X
X

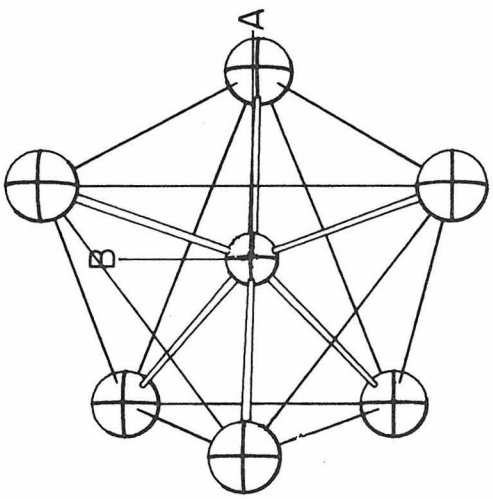
A
B

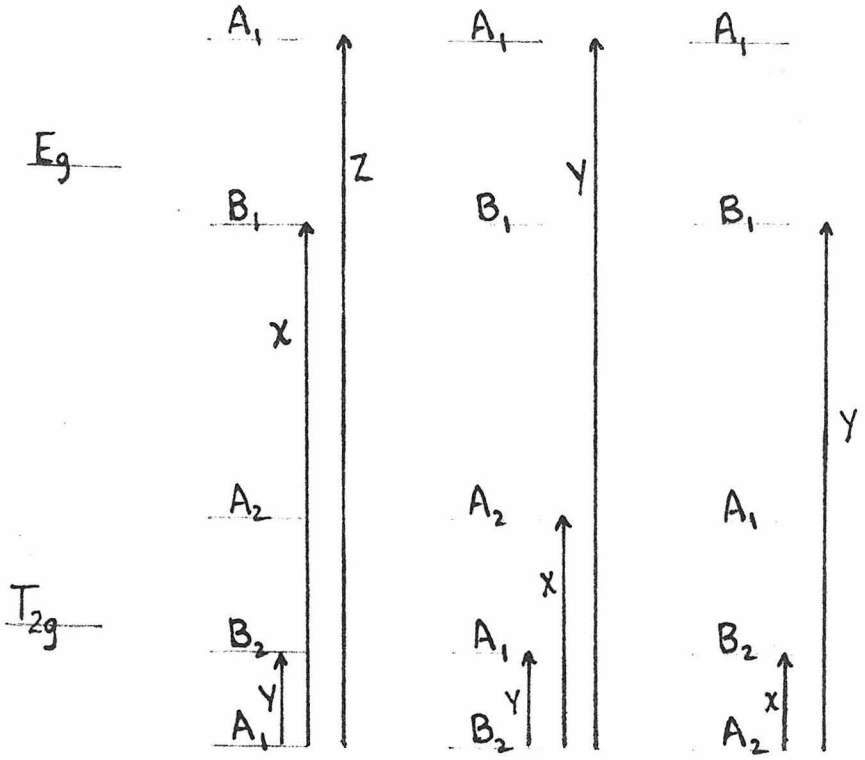

FIGURE 19

Polarization properties of the possible ground state configurations for C_{2v} symmetry.

Band assignments based on the C_{2v} site symmetry for Co^{+2} in M_2 are shown in Table I. As the ground state of octahedral Co^{+2} is triply degenerate, there are three possible ground states for Co^{+2} in C_{2v} symmetry. The polarization of the $^4T_{1g} \rightarrow {}^4A_{2g}$ (O_h) transition suggests the ground state of $Co^{+2}(M_2)$ is $^4A_2$. The visible energy region is complicated by the presence of doublet spin states. Although transitions to these states are expected to be less intense than spin-allowed excitations, Ferguson and coworkers have assigned prominent features just above 20000 cm^{-1} in cobalt-doped K_2MgF_4[25] and $CoCl_2 \cdot 6H_2O$[26] to transitions to the $^2T_{1g}$ term arising from the free ion ^2P. Increased intensities are explained by spin-orbit interactions with the nearby quartet spin states. Blunt has assigned bands at 18500, 18900 and 20400 cm^{-1} to quartet levels of rhombic (D_{2h}) Co^{+2} in MnF_2[27]. He concluded that the low symmetry field was the dominant perturbation for this case, as the $^2T_{1g}$ state near 20000 cm^{-1} was not observed.

The 6500 cm^{-1} band in the near-infrared is observed in all three polarizations. It has been assigned as the $^4A_2 \rightarrow {}^4A_1$ transition. As this excitation is electric dipole forbidden in C_{2v} symmetry, the observed intensity is thought to be derived from spin-orbit interaction

TABLE I

M_2 Site Band Assignments for C_{2v} Symmetry

Co^{+2}		Ni^{+2}	
Energy($cm^{-1}x10^3$)	Assignment	Energy($cm^{-1}x10^3$)	Assignment
20.4	$^2A_2$	23.65	$^3B_1$
19.5	$^4A_2$	-----	$^3B_2$
19.1		-----	$^3A_2$
17.5	$^4B_1$		
17.2	$^4B_2$	12.6	$^3B_1$
		-----	$^3B_2$
13.2	$^4B_1$	11.2	$^3A_2$
7.55	$^4B_1$	8.0	$^3A_2$
6.6	$^4A_1$	-----	$^3B_2$
5.9	$^4A_2$	6.75	$^3A_1$

with the ground state. The observed isotropy and splitting into two components at low temperature are consistent with this mechanism (all quartet states are split into two doubly degenerate Γ_5 representations in the C_{2v} double group).

There is no ambiguity of ground state assignments for Ni^{+2}, as the ground state is orbitally non-degenerate for octahedral symmetry. Table I also contains the Band assignments for Ni^{+2} in the M_2 site based on C_{2v} site symmetry. Bands at 8000 and 6750 cm^{-1} have been assigned as $^3A_2$ and $^3A_1$ states, respectively, on the basis of electric dipole polarizations. As the octahedral $^3T_{2g}$ parent state can also gain intensity from magnetic dipole interaction[28], these assignments may be reversed.

Ligand field calculations

The rhombic ligand field potential has the following form:

$$V_{C_{2v}} = r^2\left[\gamma^0_2 Y^0_2 + 1/\sqrt{2}\ \gamma^2_2 (Y^2_2 + Y^{-2}_2)\right] + r^4\left[\gamma^0_4 Y^0_4 + 1/\sqrt{2}\ \gamma^2_4 (Y^2_4 + Y^{-2}_4) + 1/\sqrt{2}\ \gamma^4_4 (Y^4_4 + Y^{-4}_4)\right], \quad (1)$$

where $\gamma^m_n = 4\pi/2n+1\ ze \sum_i Y^m_n(r_i, \theta_i, \varphi_i)$. Evaluation of equation 1 using the coordinate system of Figure 18 and assuming that r_i^{-n} can be replaced by the binomial approximation:

$$r_i^{-n} = (\bar{R} + \epsilon_i)^{-n} \cong \bar{R}^{-n}(1 - n\epsilon_i/\bar{R} + n(n+1)/2(\epsilon_i/\bar{R})^2 = \bar{R}^{-n}\delta_n^i, \quad (2)$$

yields the following expression for the rhombic potential:

$$V_{C_{2v}} = ze\langle r^2\rangle/\bar{R}^3[A(3z^2-r^2) + B(x^2-y^2)] + ze\langle r^4\rangle/\bar{R}^5[c(35z^4-30z^2r^2+3r^4) + d(7z^2-r^2)(x^2-y^2) + e(x^4-6x^2y^2+y^4)] \quad (3)$$

where $A = \sum_i \frac{1}{2}(3\cos^2\theta_i - 1)\delta_3^i$, $B = \sum_i 3/2\sin^2\theta_i\delta_3^i$, $c = \sum_i 1/32(35\cos^4\theta_i - 30\cos^2\theta_i + 3)\delta_5^i$, $d = \sum_i 5/8(\sin^2\theta_i)(7\cos^2\theta_i - 1)\delta_5^i$, and $e = \sum_i 35/32\ \sin^4\theta_i\delta_5^i$. For small rhombic distortions the octahedral contribution to the potential can be separated from the rhombic terms. Further, Stevens' operator equivalent method can be used to shorten computation time. The final form of the ligand field potential is:

$$V_{C_{2v}} = (AO_2^0 + BO_2^2)b_2 + (CO_4^0 + DO_4^2 + EO_4^4)b_4 \quad (4)$$

where $C = c + 7/64$, $D = d - 35/16$, $E = e - 105/64$, $b_2 = -2/21\ ze\langle r^2\rangle/\bar{R}^3$, $b_4 = 2/63\ ze\langle r^4\rangle/\bar{R}^5$, and O_n^m are the Stevens' operator equivalents according to Hutchings[29]. Diagonalization of the octahedral wavefunctions in this coordinate scheme yields the eigenfunctions $t_{2g}^a = -\frac{1}{2}(x^2-y^2) + \sqrt{3}/2(z^2) \equiv (z^2-x^2)$, $t_{2g}^b = (xy)$, $t_{2g}^c = (yz)$, $e_g^a = \sqrt{3}/2(x^2-y^2) + \frac{1}{2}(z^2) \equiv (y^2)$, and $e_g^b = (xz)$. The one electron values of the rhombic field are listed in Table II.

The multielectronic d^7 and d^8 configurations were

TABLE II

One Electron Values for the Rhombic Operator

$E\ (d_{z^2-x^2}) = (-3A - 3B)b_2 + (57C - 9D + 3E)b_4$

$E\ (d_{xy}) = 6Ab_2 + (12C - 12E)b_4$

$E\ (d_{yz}) = (-3A + 3B)b_2 - (48C + 12D)b_4$

$E\ (d_{xz}) = (-3A - 3B)b_2 + (-48C + 12D)b_4$

$E\ (d_{y^2}) = (3A + 3B)b_2 + (27C + 9D + 9E)b_4$

$\langle d_{z^2-x^2}|V_{rh}|d_{y^2}\rangle = \sqrt{3}(3A - B)b_2 + 3\sqrt{3}(-5C - D + E)b_4$

---

calculated by forming the strong field octahedral wavefunctions, adding the electron repulsion perturbation, mixing the two T_{1g} states for intermediate fields ($V_{oct} \cong e^2/r_{ij}$) and splitting the octahedral states with the rhombic operator. The results of these calculations are listed in Tables III, V and VII for iron, cobalt and nickel orthosilicates, respectively. Interaction between states in the rhombic field were assumed negligible.

The M_1 site has been assigned the effective site symmetry D_{4h}[16]. The tetragonal energies of Co(II) were reported by Ferguson, et al. for the strong field limit[25]. The coupling of the octahedral $^4T_{1g}$ states by the electron repulsion operator was included for the M_1 site. The values of the tetragonal energy levels for nickel and iron were derived from the d^1 and d^2 cases given

by Ballhausen by changing the sign of the Dq, Ds and Dt coefficients[30]. The results of the ligand field calculations on the M_1 site of olivine for Fe(II), Co(II) and Ni(II) are included in Tables III, IV and VI, respectively. The polarization properties of the M_1 site were masked by the more intense M_2 transitions, thus, the calculations were based on the tetragonally elongated octahedron observed crystallographically[22].

Iron(II) should have a $^5A_1$ ground state based on the observed z-polarization of the highest energy transition. The ligand field parameters were, therefore, adjusted for a calculated $^5A_1$ ground state. As there are more parameters than observed bands, the fit is somewhat misleading. The initial set of parameters was taken from the cobalt(II) and nickel(II) calculations and iterated to a reasonable fit with the observed near-infrared absorptions. The 7200 cm^{-1} band is predicted to be $^5B_1$ in C_{2v} symmetry and therefore, x-polarized (β). It is observed in α with the $^5A_1$ transition; however, the observed intensity drop of the 7200 cm^{-1} band in the 77 K spectrum suggests a vibronic interaction may account for the anomalous polarization.

The nickel(II) spectrum is fit quite well, particularly when magnetic dipole interactions are assumed responsible for the intensity of the lowest lying $^3A_2$

TABLE III

Ligand Field Calculations for Iron(II) Olivine

M_1 Site	Calculated* (cm^{-1})	Observed** (cm^{-1})
$^5B_{1g} = 10\ Dq + 3\ Ds - 5\ Dt$	10900	10900
$^5A_{1g} = 10\ Dq - Ds - 10Dt$	8700	8700
$^5B_{2g} = 3\ Ds - 5\ Dt$	3400	-----
$^5E_g = 0$		

LFSE = -3000 - 1600 = -4600 cm^{-1}

* Dq = 750 cm^{-1}, Ds = 800 cm^{-1}, Dt = -200 cm^{-1}

** Reference 18

M_2 Site	Calculated*** (cm^{-1})	Observed (cm^{-1})
$^5A_1 = -0.114\ b_2 + 11.995\ b_4 + 10\ Dq$	9210	9300
$^5B_1 = 0.264\ b_4 + 10\ Dq$	7020	7200
$^5A_2 = -2.172\ b_2 + 1.055\ b_4$	3350	-----
$^5A_1 = -1.001\ b_2 + 9.163\ b_4$	-100	-----
$^5B_2 = 0$		

LFSE = -2600 - 2000 = -4600 cm^{-1}

K_D = 1.0 (for 1200°)

$K_{D_{(obs)}}$ = 1.1-1.3****

*** Dq = 650 cm^{-1}, b_2 = -1600 cm^{-1}, b_4 = 120 cm^{-1}

**** Reference 9

TABLE IV.

Ligand Field Calculations for the M_1 Site of Cobalt(II) Olivine

	Calculated* (cm^{-1})	Observed (cm^{-1})
$^4A_{2g}$ = SQRT** - 6 Ds + 10 Dt	21630	21650
^4E_g = SQRT - 35/4 Dt	17830	18350
$^4B_{1g}$ = 15 Dq - 15/2 B + ½ SQRT - 2 Ds + 15 Dt	15450	-----
$^4B_{2g}$ = 5 Dq - 15/2 B + ½ SQRT - 2 Ds + 15 Dt	8350	8350
^4E_g = 5 Dq - 15/2 B + ½ SQRT - 2 Ds + 25/4 Dt	7390	----
^4E_g = -3 Ds + 5 Dt	1450	----
$^4A_{2g}$ = 0		

LFSE = -5680 - 1460 = -7140 cm^{-1}

* Dq = 710 cm^{-1}, B = 910 cm^{-1}, Ds = -290 cm^{-1}, Dt = 110 cm^{-1}

** SQRT = $(100\ Dq^2 + 180\ DqB + 225\ B^2)^{\frac{1}{2}}$

TABLE V

Ligand Field Calculations for the M_2 Site of Cobalt(II) Olivine

	Calculated* (cm^{-1})	Observed (cm^{-1})
$^4B_1$ = SQRT** + 0.677 b_2 - 4.693 b_4	19870	17500
$^4B_2$ = SQRT + 0.544 b_2 - 5.816 b_4	19440	17200
$^4A_2$ = SQRT + 0.055 b_2 - 10.665 b_4	17830	19100
$^4B_1$ = 15 Dq - 15/2 B + ½ SQRT + 0.425 b_2 - 8.553 b_4	13330	13200
$^4A_1$ = 5 Dq - 15/2 B + ½ SQRT + 0.425 b_2 + 2.275 b_4	7390	6660
$^4A_2$ = 5 Dq - 15/2 B + ½ **SQRT** + 0.670 b_2 - 11.936 b_4	6870	5900
$^4B_2$ = 5 Dq - 15/2 B + ½ SQRT + 0.181 b_2 - 10.538 b_4	5760	7550
$^4B_2$ = 0.977 b_2 + 2.415 b_4	2640	----
$^4B_1$ = 0.299 b_2 - 7.523 b_4	150	----
$^4A_2$ = 0		

LFSE = -5440 - 670 = -6110 cm^{-1} K_D = 3.6 (at 1250°) K_D = 4.6***

* Dq = 680 cm^{-1}, B = 910 cm^{-1}, b_2 = 2500 cm^{-1}, b_4 = 80 cm^{-1}

** SQRT = $(100\ Dq^2 + 180\ DqB + 225\ B^2)^{\frac{1}{2}}$ *** Reference 8

TABLE VI

Ligand Field Calculations for the M_1 Site of Nickel(II) Olivine

	Calculated* (cm^{-1})	Observed (cm^{-1})
$^3A_{2g} = 15\ Dq + 15/2\ B + \frac{1}{2}$ SQRT** + $\sin^2\theta$***(4 Ds + 5 Dt) + $\cos^2\theta$(-2 Ds + 15 Dt)	26750	26300
$^3E_g = 15\ Dq + 15/2\ B + \frac{1}{2}$ SQRT + $\sin^2\theta$(-2 Ds + 25/4 Dt) + $\cos^2\theta$(Ds + 10 Dt)	25810	-----
$^3A_{2g} = 15\ Dq + 15/2\ B - \frac{1}{2}$ SQRT + $\cos^2\theta$(4 Ds + 5 Dt) + $\sin^2\theta$(-2 Ds + 15 Dt)	15230	15800
$^3E_g = 15\ Dq + 15/2\ B - \frac{1}{2}$ SQRT + $\cos^2\theta$(-2 Ds + 25/4 Dt) + $\cos^2\theta$(Ds + 10 Dt)	14020	13000
$^3E_g = 10\ Dq + 35/4\ Dt$	9000	9000
$^2B_{2g} = 10\ Dq$	8000	-----
$^3B_{1g} = 0$		

$$LFSE = -9600 - 800 = -10400\ cm^{-1}$$

* $Dq = 800\ cm^{-1}$, $B = 970\ cm^{-1}$, $Ds = 576\ cm^{-1}$, $Dt = 114\ cm^{-1}$, $\theta = -43°$

** SQRT = $(100\ Dq^2 - 180\ DqB + 225\ B^2)^{\frac{1}{2}}$

*** $\theta = \frac{1}{2} \tan^{-1}(-12\ B/\ 9\ B - 10\ Dq)$

TABLE VII

Ligand Field Calculations for the M_2 Site of Nickel(II) Olivine

	Calculated* (cm^{-1})	Observed (cm^{-1})
$^3B_1 = 15\,Dq + 15/2\,B + \frac{1}{2}\,SQRT^{**} - (0.636 \sin^2\theta^{***} + 0.180 \cos^2\theta)\,b_2 - (4.818 \sin^2\theta + 3.343 \cos^2\theta)\,b_4$	23480	23650
$^3B_2 = 15\,Dq + 15/2\,B + \frac{1}{2}\,SQRT + (0.149 \sin^2\theta - 0.498 \cos^2\theta)\,b_2 - (1.39 \sin^2\theta + 10.48 \cos^2\theta)\,b_4$	23460	-----
$^3A_2 = 15\,Dq + 15/2\,B + \frac{1}{2}\,SQRT + (0.488 \sin^2\theta + 0.18 \cos^2\theta)\,b_2 - (1.961 \sin^2\theta + 8.79 \cos^2\theta)\,b_4$	22400	-----
$^3B_1 = 15\,Dq + 15/2\,B - \frac{1}{2}\,SQRT - (0.636 \cos^2\theta + 0.18 \sin^2\theta)\,b_2 - (4.818 \cos^2\theta + 3.303 \sin^2\theta)\,b_4$	12730	12600
$^3B_2 = 15\,Dq + 15/2\,B - \frac{1}{2}\,SQRT + (0.149 \cos^2\theta - 0.498 \sin^2\theta)\,b_2 - (1.39 \cos^2\theta + 10.48 \sin^2\theta)\,b_4$	12260	-----
$^3A_2 = 15\,Dq + 15/2\,B - \frac{1}{2}\,SQRT + (0.488 \cos^2\theta + 0.18 \sin^2\theta)\,b_2 - (1.961 \cos^2\theta + 8.79 \sin^2\theta)\,b_4$	11360	11200
$^3A_1 = 10\,Dq - 11.151\,b_4$	8040	6750
$^3B_2 = 10\,Dq + 0.170\,b_2 + 0.267\,b_4$	7100	----
$^3A_2 = 10\,Dq - 0.170\,b_2 - 0.491\,b_4$	6330	8000

$^3B_1 = 0$

LFSE = -8040 - 540 = -8580 cm^{-1} $K_D = 7.7$ (at 1280°) $K_{D(obs)} = 9.22$****

*Dq = 670 cm^{-1}, B = 900 cm^{-1}, b_2 = -2000 cm^{-1}, b_4 = -120 cm^{-1}, θ = -41°

SQRT=$(100Dq^2-180DqB+225B^2)^{\frac{1}{2}}$, *$\theta=\frac{1}{2}\tan^{-1}(-12B/9B-10Dq)$, ****Reference 9

and $^3A_1$ excited states. Ferguson has provided experimental justification for this assignment[28], but the apparent complete dominance by either magnetic or electric dipole interactions is quite unexpected for this transition.

In a crystal field calculation of $Mg_{1.8}Ni_{0.2}SiO_4$ based on reflectance spectra, Wood has reported values of 870 and 768 cm^{-1} for Dq for the M_1 and M_2 sites, respectively[31]. The discrepancies are most likely due to a neglect of ground state stabilization by the low symmetry fields and to shifts in the band positions due to compositional variations.

Although the observed energy splittings of rhombic Co(II) can be fit by the ligand field calculation, the ordering of states does not correlate. Blunt has observed considerable magnetic dipole character in the $^4T_{2g}$ band of Co(II) doped in MnF_2[27], which may account for some of the discrepancy between theory and spectra, as was observed for Ni(II). The highest manifold of excited states (components of the octahedral $^4T_{1g}(P)$ state) show considerable structure at low temperatures, assigned by Ferguson, et al. to spin-orbit coupling with the ^2P level in similar cobalt(II) systems[25,26]. Thus, inclusion of the spin-orbit coupling operator in the rhombic potential appears necessary to adequately

describe the visible spectrum of the Co(II) ion occupying the M_2 site of olivine.

The LFSE's for M_1 and M_2 of olivine, Co_2SiO_4 and Ni_2SiO_4 are listed in Tables III, IV or V, and VI or VII, respectively. Distribution coefficients (the equilibrium constants for cation exchange between the two sites) are calculated solely from the difference in LFSE of the two sites. In comparing this value to that calculated from site distribution data determined by x-ray diffraction methods, the agreement is remarkably good, even though entropy and cation size effects were ignored. The poorest correlation is found for nickel, where the observed value was admitted to be somewhat suspect because of zoning in the sample[9]. Such strong correlation suggests that ligand field stabilization dominates cation distribution in olivines.

Summary

The absorption bands of iron, cobalt and nickel olivines have been separated with respect to metal site on the basis of previous assignments, the absorption spectra of synthetic and natural triphylites, and the polarized spectra of magnesium-nickel and magnesium-cobalt olivines. The effective C_{2v} site symmetry proposed by Runciman, et al. has been shown to adequately describe the band splittings, but it fails to completely

describe the observed polarization properties particularly for Co(II). Ligand field calculations have resulted in values of B, Dq and the low symmetry radial parameters for both the M_1 and M_2 sites. Calculation of LFSE's and the ligand field contribution to the distribution coefficients of the cation exchange reactions from these parameters and comparison to K_D's calculated from x-ray diffraction data has led to the conclusion that ligand field stabilization is the major driving force for cation ordering in olivine.

BIBLIOGRAPHY

1. G. Gattlow, Zeit. Anorg. Allg. Chem., 333, 134(1964).
2. J. H. Fang and R. E. Newnham, Min. Mag., 35, 196(1965).
3. E. F. Farrell, J. H. Fang and R. E. Newnham, Amer. Mineral., 48, 804(1963).
4. W. L. Bragg and G. B. Brown, Zeit. Krist., 63, 538(1926).
5. D. Destenay, Mem. Soc. Roy. Sci. Liege, 10, 5(1950).
6. The crystal setting Pnma is used throughout the text, so that the a-axis always refers to the 10 Å axis, the b-axis is always the 6 Å axis, and the c-axis is always the 4.7 Å axis. References using other settings have been transformed into this system for consistency. Therefore, the axes referred to here as a, b and c may not coincide with those actually used in the cited work.
7. R. G. Burns, Mineralogical Applications of Crystal Field Theory, Cambridge University Press, Cambridge, 1970.
8. S. Ghose and C. Wan, Contrib. Mineral. Petrol., 47, 131(1974).
9. V. Rajmani, G. E. Brown and C. T. Prewitt, Amer. Mineral., 60, 292(1975).
10. R. P. Santoro, D. J. Segal and R. E. Newnham,

J. Phys. Chem. Solids, 27, 1192(1966).

11. E. Thielo, Naturwiss., 29, 239(1941).
12. F. Zambonini and L. Malossi, Zeit. Krist., 80, 442(1931).
13. Akimoto and H. Fujisawa, J. Geophys. Res., 73, 1467(1968).
14. G. Switzer, Amer. Mineral., 23, 811(1938).
15. E. F. Farrell and R. E. Newnham, ibid., 50, 1972(1965).
16. R. G. Burns, ibid., 55, 1608(1970).
17. W. A. Runciman, D. Sengupta and J. T. Gourley, ibid., 58, 451(1973).
18. R. G. Burns, ibid., 59, 625(1974).
19. H. Onken, Tschermak's Mineral. Petrogr. Mitt., 10, 34,(1965).
20. S. Geller and J. L. Durand, Acta Cryst., 13, 325(1960).
21. L. W. Finger and G. R. Rapp, Jr., Carnegie Inst. Wash. Yr. Bk., 68, 290(1970).
22. K. Hanke, Beitr. Mineral. Petrogr., 11, 535(1965).
23. C. Schmitz-DuMont and C. Friebel, Monat. Chem., 98, 1583(1967).
24. D. Reinen, Zeit. Anorg. Allg. Chem., 356, 182(1968).
25. J. Ferguson, T. E. Wood and H. J. Guggenheim, Inorg. Chem., 14, 177(1975).

26. J. Ferguson and T. E. Wood, ibid., 14, 184(1975).

27. R. F. Blunt, J. Chem. Phys., 44, 2317(1966).

28. J. Ferguson, H. J. Guggenheim, L. F. Johnson and H. Kamimura, J. Chem. Phys., 38, 2579(1963).

29. M. T. Hutchings, Adv. Solid State Phys., Vol. 16, 227(1964).

30. C. J. Ballhausen, Introduction to Ligand Field Theory, McGraw-Hill Book Co., New York, New York, 1962.

31. B. J. Wood, Amer. Mineral., 59, 244(1974).

PROPOSITIONS

ABSTRACTS TO PROPOSITIONS

1. Far-infrared spectral studies on silver(I), mercury (II) and copper(II) substituted azurin are proposed to elucidate the mechanism of tryptophan fluorescence quenching.

2. X-ray photoelectron spectral studies on hemoglobin and various derivatives are proposed to correlate the observed charge on iron to that deduced from resonance Raman data. Specific models of hemoglobin binding may then be formed.

3. Coherent anti-Stokes Raman spectroscopy is proposed as a method for obtaining resonance enhanced vibrational spectra of transition metal complexes in regions of d-d absorption. Initial experiments on vibronically active and photochemically important Cr(III) complexes are suggested.

4. A reexamination of the absorption spectra of cobalt(II) and nickel(II) substituted pyroxenes using recently grown single crystals is proposed to resolve the present conflict concerning site preferences of the transition metal cations. A rhombic ligand field analysis will be necessary to determine the contribution of ligand field stabilization energies to the observed site preferences.

5. A resonance Raman spectral study on low molecular weight flavodoxins is proposed to elucidate binding interactions between the flavin mononucleotide and the flavoprotein and the importance of these interactions on oxidation-reduction reactions.

PROPOSITION 1

Ultraviolet emmission studies of azurin (P. fluorescens) have shown that fluorescence attributed to tryptophan in the apoprotein is quenched some 60-70% upon binding to copper(II)[1,2]. Addition of Hg(II) ions to the apoproteins caused a similar quenching, whereas addition of Ag(I) and PMB (p-mercuribenzoate) had little effect on tryptophan fluorescence. As tryptophan analysis showed only one residue per mole of protein, incomplete quenching of fluorescence was interpreted to be the result of confirmational changes in the peptide backbone upon copper(II) incorporation rather than direct binding of copper(II) to the tryptophan. Grinvald, et al. have observed mono-exponential fluorescence decay for apoazurin (P. aeruginosa)[3]. The decay of holoprotein fluorescence was satisfactorily fit when a second exponential term was added to the decay function. Further, comparison of calculated and observed quantum yields indicated a majority of the holoazurin molecules are not fluorescent. It was concluded that apoazurin exists in one form, whereas holoazurin is an equilibrated system of at least two conformers, one exhibiting no fluorescence and therefore, containing strong copper-tryptophan

interactions.

It is proposed that far-infrared spectral studies of chemically modified azurins will help resolve the question of copper-tryptophan interaction. A band at 370 cm^{-1} in apoplastocyanin shifts to 345 cm^{-1} when the metal ions, Cu(I), Cu(II) or Co(II), are incorporated into the metal site (Part I, Chapter I). Further, resonance Raman spectral studies of the blue copper proteins indicate that the azurin blue site is similar to the plastocyanin site with respect to amide backbone coordination[4]. Thus, an analogous band near 370 cm^{-1} is expected in the far-infrared spectrum of azurin.

As silver(I) binds to apoazurin but does not quench tryptophan fluorescence, a shift in the helix deformation mode of silver(I)-substituted azurin would indicate no correlation between metal-amide backbone binding and fluorescence quenching and imply a strong metal ion-tryptophan interaction. Mercury(II) exhibits both two and four coordinate bonding, depending on the ligands involved. Finazzi-Agro and coworkers assumed tetrahedral coordination in the mercury(II)-azurin complex[1,2], which would certainly be confirmed by a shift in the helix defromation mode, analogous to the holoprotein results.

If two forms of azurin exist in equilibrium, as suggested by Grinvald, et al.[3], then the infrared spectrum should exhibit a temperature dependence resulting from the energetically favored form "freezing out" as the temperature is lowered. Similar infrared spectral studies could be performed on stellacyanin, as it also exhibits tryptophan fluorescence quenching upon Cu(II) binding[5].

BIBLIOGRAPHY

1. A. Finazzi-Agro, G. Rotilio, L. Avigliano, P Guerrieri, V. Boffi and B. Mondovi, Biochemistry, 9, 2009(1970).
2. A. Finazzi-Agro, C. Giovagndi, L. Avigliano, G. Rotilio and B. Mondovi, Eur. J. Biochem., 34, 20(1973).
3. A. Grinvald, J. Schlessinger, I. Pecht and I. Z. Steinberg, Biochemistry, 14, 1921(1975).
4. O. Siiman, N. M. Young and P. R. Carey, J. Amer. Chem. Soc., 96, 5583(1974); J. Amer. Chem. Soc., in press.
5. L. Morpugo, G. Rotilio, A. Finazzi-Agro and B. Mondave, Arch. Biochem. Biophys., 161, 291(1974).

PROPOSITION 2

Oxygen binding in hemoglobin has been the subject of countless physical studies spanning more than forty years, yet the actual mode of interaction has not been resolved. Griffith[1] and Pauling[2] proposed a low spin iron(II)-oxygen complex to account for the observed diamagnetism of oxyhemoglobin. Weiss suggested a low spin iron(III)-superoxide model with exchange coupling between unpaired electrons on the iron and superoxide would also fit the observed physical data[3]. As the oxygen-oxygen stretching frequency shows considerable sensitivity to bond order, the vibrational spectrum of hemoglobin appeared to be a direct method of determining the structure of the complex. However, strong absorption by aqueous solutions over much of the infrared and the inherent weak intensity associated with the stretching motion of a homonuclear diatomic molecule have made infrared investigations difficult. Although Barlow, et al. report a frequency of 1104 cm^{-1} for the O-O stretch from difference spectra of red blood cells[4], there is some question as to the validity of the assignment in light of the observation of the O-O stretch at the same frequency in cobaltiglobin[5]. Unfortunately, the visible spectral region

is dominated by intense porphyrin transitions, so that conventional Raman spectrum, which does not show interference from the aqueous solvent and is predicted to exhibit an allowed O-O stretch, is not observed. The resonance enhanced Raman spectrum of a series of hemoglobins has been reported[6]. Again, the principal absorptions are due to intra-ligand transitions within the porphyrin ring so that the observed resonance Raman spectrum contains only porphyrin vibrations. Spiro and Strekas have concluded, on the basis of vibrational frequency shifts, that iron in oxyhemoglobin has considerable iron(II) character. From the observed band positions of the porphyrin vibrational spectrum, carbon monoxyhemoglobin must also be assigned a similar iron(II) structure.

It is proposed that the x-ray photoelectron spectra (XPS) of a series of chemically modified hemoglobins, such as studied by Spiro and Strekas, will provide independent evidence concerning the charge on the iron atom. Recent successful studies on copper-sulfur binding in plastocyanin indicate that sampling techniques have improved to the point where meaningful XPS data may now be obtained for biological samples[7]. Seigbahn, et al. have shown that the core electron binding energies of iron are sensitive to

changes in chemical bonding, i.e., charge on the iron[8]. Thus, an x-ray photoelectron spectral study seems likely to yield useful information concerning the oxidation state of iron in oxyhemoglobin, particularly when compared to that predicted by resonance Raman data.

BIBLIOGRAPHY

1. J. S. Griffith, Proc. Roy. Soc., A 235, 23(1956).
2. L. Pauling, Nature, 203, 182(1964).
3. J. Weiss, ibid., 82(1964).
4. C. H. Barlow, J. C. Maxwell, W. J. Wallace and W. S. Caughey, Biochem. Biophys. Res. Commun., 55, 91(1973).
5. J. C. Maxwell and W. S. Caughey, Biochem. Biophys. Res. Commun., 60, 1309(1974).
6. T. G. Spiro and T. C. Strekas, J. Amer. Chem. Soc., 96, 338(1974).
7. E. I. Solomon, P. J. Clendening, H. B. Gray and F. J. Grunthaner, J. Amer. Chem. Soc., 97, 3878(1975).
8. K. Siegbahn, C. Nordling, A. Fahlman, R. Nordberg, K. Hamrin, J. Hedman, G. Johansson, T. Bergmark, S.-E. Karlsson, I. Lindgren and B. Lindberg, "ESCA; Atomic, Molecular and Solid State Structure by Means of Electron Spectroscopy" in Nova Acta Reg. Soc. Sci. Ups., Ser. IV, Vol. 20 (1967).

PROPOSITION 3

Since the advent of resonance Raman spectroscopy, there has been interest in applying the technique to transition metal d-d excitations. As those vibrations which are coupled to the electronic transition in question are the modes that are expected to be resonance enhanced[1], the technique should provide useful vibronic information concerning bands that exhibit little or no fine structure. Such information is particularly useful for photochemically active excited states of transition metal complexes. The technique should also provide information on the Jahn-Teller active vibrations of the dynamic or second-order effect[2]. Unfortunately, conventional resonance Raman methods have proved insufficiently sensitive to detect the weak signals generated by resonance enhancement from transition metal d-orbital excited states.

It is proposed that the technique coherent anti-Stokes Raman spectroscopy (CARS) is sufficiently sensitive to detect resonance enhanced vibrations of transition metal complexes. Coherent anti-Stokes emmission was first observed in benzene by Terheine[3]. The method received little attention until the

development of high-power tunable lasers. Recently, CARS spectra have been reported for gases[4] and solids[5], as well as liquids. The experimental arrangement consists of a high-power pulsed laser which pumps two tunable dye lasers. The first laser is set at a fixed frequency ν_p, while the second dye laser is scanned to lower frequencies ν_s. The two beams are focused and crossed at a small angle in the sample. At the crossing point a two photon excitation $2\nu_p$ occurs. Scattering of the sampling beam (at ν_s) by this virtual state results in the emission of an anti-Stokes coherent beam at frequency $2\nu_p - \nu_s \equiv \nu_{as}$. When the difference between ν_p and ν_s is equal to an allowed vibrational quantum, resonance occurs and the emitted anti-Stokes radiation intensifies, is detected by a visible light sensor, and plotted versus $\Delta\nu = \nu_p - \nu_s$ to yield a Raman spectrum. The emission intensity at resonance has been measured at 500 mw for a laser power of 1 kilowatt[6], thus, the experiment can be carried out in room light with no provisions make for screening background light levels other than separation and masking of the Rayleigh scattered pump laser beam. Further details of the experimental arrangement may be found in reference 7. The coherent anti-Stokes emission has been shown to be nine orders of magnitude

more efficient than conventional Raman scattering. This added sensitivity is expected to allow observation of the weak, resonance enhanced vibrations associated with d-electron excitations.

If one places ν_p with the band envelope of an electronic transition, a resonance enhanced Raman spectrum is predicted. Hudson and coworkers have observed the resonance enhanced Raman spectrum of a highly conjugated organic molecule by the CARS method[8,9]. Thus, CARS does hold promise as a method capable of yielding resonance enhanced Raman spectra of transition metal complexes.

A reasonable initial system is trans-$Cr(en)_2X_2^{+1}$. This series of complexes has several transitions in the visible region, which gain considerable intensity through vibronic-mixing[10]. Other chromium(III) complexes such as $Cr(NH_3)_5X^{+2}$ have photochemically active excited states in the red spectral region and, thus, also merit consideration.

BIBLIOGRAPHY

1. J. Tang and A. C. Albrecht, Raman Spectroscopy, Vol. 2, H. A. Szymanski, ed., Plenum Press, New York, New York, 1970, Chapter 2.

2. M. S. Child and H. C. Longuet-Higgins, Phil. Trans. Faraday Soc., A 254, 259(1961).

3. R. W. Terhune, Bull. Amer. Phys. Soc., 8, 359(1963).

4. P. R. Regnier and J. P. E. Teran, Appl. Phys. Lett., 23, 240(1973).

5. J. J. Wynne, Phys. Rev. Lett., 29, 650(1972).

6. R. F. Begley, A. B. Harvey, R. L. Byer and B. S. Hudson, J. Chem. Phys., 61, 2466(1974).

7. Molectron Corp., Applications Note No. 111, "Coherent Anti-Stokes Raman Spectroscopy(CARS)".

8. B. Hudson, Raman Newsletter, No. 81, 4(1975).

9. I. Chabay, G. Klauminzer and B. Hudson, in press.

10. P. Day and L. Dubicki, Inorg. Chem., 10, 2043(1971).

PROPOSITION 4

White, et al. have studied the diffuse reflectance spectra of nickel and cobalt orthopyroxenes in order to assign site preferences within the series $Mg_{1-x}M_xSiO_3$ where M = Co^{+2} and Ni^{+2} [1]. Orthopyroxene is a chain silicate which crystallizes in the space group Pbca[2]. There are two metal sites in the pyroxenes which lie in general crystallographic positions. The M_1 site is a distorted octahedron with a mean iron-oxygen distance of 2.1 Å, whereas the M_2 site is an extremely distorted octahedron exhibiting a mean iron-oxygen length of 2.22 Å. When calcium is present, an ordered structure analogous to the calcic olivine, monticellite, is found. Comparing $CaMg_xNi_{1-x}Si_2O_6$ and $CaMg_xCo_{1-x}Si_2O_6$ spectra to the corresponding magnesium pyroxene spectra, White and coworkers assigned cation preferences, nickel(II) to the M_2 site and cobalt(II) to the M_1 site. These results are in direct contradiction to the orderings predicted from ligand field theory by Burns[3]. Ghose, et al. reported the ordering Mn(II) > Zn(II) > Fe(II) > Co(II) for M_2 and Ni was observed to slightly prefer M_1[4].

As ligand field theory has successfully accounted for the cation orderings of olivine (Part II) and

cobalt(II) and nickel(II) doped $MgSiO_3$ have recently been successfully crystallized[5], it is proposed that the assignments of White, et al. be reexamined. A comparison of the reported assignments of Co(II) in $MgSiO_3$ and $CaMgSi_2O_6$ with those of cobalt(II)-olivine indicate several of the quartet levels may be incorrectly identified. Further, the octahedral ligand field analysis should be abandoned and replaced by a rhombic ligand field. As the C_{2v} site approximation has correctly predicted the observed ligand field band splitting and polarization for a natural iron(II) pyroxene[6], the analysis of the nickel and cobalt substituted pyroxenes should be simpler than observed in the olivine system, and may actually resolve some of the discrepancies between theory and experiments found in the olivines.

BIBLIOGRAPHY

1. W. B. White, G. J. McCarthy and B. E. Schutz, Amer. Mineral., 56, 72(1971).
2. S. Ghose, Zeit. Krist., 122, 81(1965).
3. R. G. Burns, Chem. Geol., 5, 275(1969).
4. S. Ghose, F. P. Okamura, C. Wan and H. Ohashi, EOS Transactions, A. G. U., 55, 4, 467(1974),

Abstract.

5. Personal communication relayed by Prof. G. R. Rossman from Dr. J. Ito, University of Chicago.

6. W. A. Runciman, D. Sengupta and M. Marshall, Amer. Mineral., 58, 444(1973).

PROPOSITION 5

Old yellow enzyme is a protein of great biochemical significance. Theorell isolated the enzyme from brewers bottom yeast in the mid-thirties, and soon discovered that the protein fraction lost all enzyme activity when separated from the accompanying yellow "impurity". Activity was restored by recombining the yellow fraction with the protein fraction. Thus, old yellow enzyme was the first example of a protein-cofactor complex which ceased enzymic function when the two components were separated and regained activity upon recombination[1]. The yellow cofactor has been identified as 6,7 dimethyl-9 (5'-phosphoribitolyl)-isoalloxazine or flavin mononucleotide (FMN). The enzyme has a molecular weight of ~110,000 and binds two FMN groups per mole. Although the activity of the enzyme is measured by the oxygen to peroxide oxidation, its biological function remains unknown.

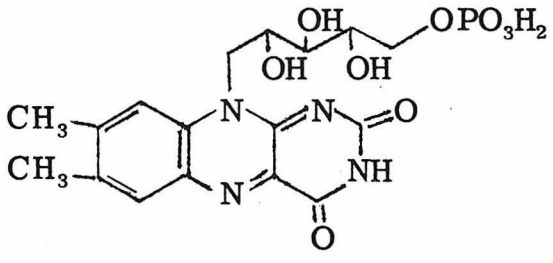

FMN

More recently, a series of low molecular weight flavoproteins, called flavodoxins, have been shown to

be electron carriers in low potential oxidation-reduction reactions[2]. They often reduce NADH, transferring electrons to molecular oxygen or cytochrome c. The flavodoxins isolated from Peptostreptococcus elsendii[2] (MW = 15000) and from Azotobacter vinelandii[3] (MW ≈ 35000) are typical members of this series. These flavodoxins appear to be one electron carriers as the FMN is easily reduced to a stable blue semiquinone form, but the second reduction proceeds only with great difficulty. Both bind one FMN group, which can be separated from the protein and recombined to yield an active enzyme. The FMN has been shown to be bound in part to the apoprotein by the phosphate group of the phosphoribitol moiety. The characteristic fluorescence of both the FMN and a tryptophan side chain on the protein are quenched when the complex is formed. The structure of Desulfovibrio vulgaris flavodoxin at 2 Å resolution shows the flavin ring sandwiched between a tyrosine ring and tryptophan ring[4]. Although the active site is fairly well known structurally, little information concerning protein-flavin interaction during binding and oxidation-reduction is known.

The flavin molecule has an absorption band at 446 nm with an absorption coefficient of ~6000, thus, it appears to be an excellent candidate for a resonance

Raman study. The reduced form has a broad band centered between 550 and 600 nm and is also sufficiently intense to observe resonance enhanced Raman vibrations. It is proposed that resonance Raman studies of the binding of FMN to the apoflavodoxins and also of the reduced flavin-protein complexes will yield information concerning the role of flavin-protein interaction in electron transport. Resonance Raman studies on hemoglobins[5], cytochrome c[6], rubredoxin[7], blue copper proteins[8], hemerythrin[9], and hemocyanin[10] have provided new information concerning those biological chromophores. Flavin mononucleotide has all the characteristics necessary for a successful resonance Raman experiment, thus, providing new information on FMN-flavodoxin interactions.

BIBLIOGRAPHY

1. Å. Åkeson, A. Ehrenberg, and H. Theorell, "Old Yellow Enzyme" in The Enzymes, Vol. 7, 2nd Edition, P. D. Boyer, H. Lardy and K. Myrbäck, eds., Academic Press, New York, New York, 1963, p. 477.
2. S. G. Mayhew in Flavins and Flavoproteins, H. Kamin, ed., University Park Press, Baltimore, Maryland, 1971, p. 185.
3. L. J. Andrews, M. L. MacKnight, J. Ryan and G. Tollin, Biochem. Biophys. Res. Commun., 55, 1165(1973).

4. K. D. Watenpaugh, L. C. Sieker and L. H. Jensen, Proc. Nat. Acad. Sci. (U. S. A.), 70, 3857(1973).

5. T. G. Spiro and T. C. Strekas, J. Amer. Chem. Soc., 96, 338(1974).

6. T. G. Spiro and T. C. Strekas, Biochim. Biophys. Acta, 351, 237(1974).

7. T. V. Long and T. M. Loehr, J. Amer. Chem. Soc., 92, 6384(1970).

8. V. Miskowski, S.-P. W. Tang, T. H. Moss, E. R. Shapiro and T. G. Spiro, Biochemistry, 14, 1244 (1975).

9. J. B. R. Dunn, A. F. Shriver and I. M. Klotz, Proc. Nat. Acad. Sci. (U. S. A.), 70, 2582(1973).

10. J. S. Loehr, T. B. Freeman and T. M. Loehr, Biochem. Biophys. Res. Commun., 56, 510(1974).